
Characterization of actin variants in *Dictyostelium discoideum*

Dissertation der Fakultät für Biologie der Ludwig-Maximilians-Universität München zur
Erlangung des akademischen Grades

„Doktor der Naturwissenschaften“

(Dr. rer. nat.)

vorgelegt von

Linda Sanftenberg

München, 2014

Eidesstattliche Erklärung

Ich versichere hiermit an Eides statt, dass die vorgelegte Dissertation von mir selbständig und ohne unerlaubte Hilfe angefertigt worden ist.

München, den 10.09.14

Linda Sanftenberg

Ort der Durchführung

Der experimentelle Teil der Dissertation wurde von Oktober 2011 bis Juni 2014 im Labor von Prof. Dr. Michael Schleicher am Institut für Anatomie und Zellbiologie der Ludwig-Maximilians-Universität München ausgeführt.

1.Gutachter: Prof. Dr. Michael Schleicher

2.Gutachter: Prof. Dr. Angelika Boettger

Eingereicht am: 10.09.14

Tag der mündlichen Prüfung: 17.11.14

Poster Presentations

Sanftenberg L, Gallinger J, Gallinger C, Joseph JM, Rieger D, Henze F,
Müller-Taubenberger A, Schleicher M,

Actin variants in *Dictyostelium discoideum*,

ASCB 53th international meeting, 2013, New Orleans, LA, USA

Sanftenberg L, Gallinger J, Gallinger C, Joseph JM, Rieger D, Henze F,
Müller-Taubenberger A, Schleicher M,

Actin variants in *Dictyostelium amoebae*,

Annual Meeting of the German Society for Cell Biology, 2014, Regensburg, Germany

Sanftenberg L, Gallinger J, Gallinger C, Joseph JM, Rieger D, Henze F,
Müller-Taubenberger A, Schleicher M,

Characterization of actin variants in *D. discoideum*,

Annual International *Dictyostelium* Conference, 2014, Potsdam, Germany

Table of contents

| | |
|---|-----------|
| Summary | 1 |
| Zusammenfassung | 3 |
| 1 Introduction | 5 |
| 1.1. <i>D. discoideum</i> as a model organism | 5 |
| 1.2. Structure and domains of actin | 6 |
| 1.3. The actin cytoskeleton | 7 |
| 1.4. The actinome of <i>D. discoideum</i> and its regulation | 11 |
| 1.5. The actin variants Act3, Act18 and Act31 in <i>D. discoideum</i> | 13 |
| 1.6. Aims of the thesis | 16 |
| 2 Materials and Methods | 17 |
| 2.1 Materials | 17 |
| 2.1.1 Instruments | 17 |
| 2.1.2 Computer programs | 18 |
| 2.1.3 Laboratory consumables | 19 |
| 2.1.4 Reagents | 19 |
| 2.1.5 Antibodies | 20 |
| 2.1.6 Vectors | 20 |
| 2.1.7 Bacterial strains | 20 |
| 2.1.8 Yeast strains | 21 |
| 2.1.9 <i>D. discoideum</i> strains | 21 |
| 2.2 Methods | 22 |
| 2.2.1 Molecular biological methods | 22 |
| 2.2.2 Biochemical methods | 22 |
| 2.2.2.1.1 SDS-polyacrylamide gel electrophoresis and western blotting | 22 |
| 2.2.2.1.2 Commassie and silver staining | 22 |
| 2.2.2.1.3 Actin preparation from rabbit skeletal muscle | 23 |
| 2.2.2.1.4 Labeling of actin with pyrene | 24 |
| 2.2.2.1.5 Flag-tagged protein expression using the baculoviral amplification system | 24 |
| 2.2.2.1.6 <i>In vitro</i> actin polymerization assay | 25 |
| 2.2.2.1.7 Low shear viscometry | 25 |
| 2.2.2.1.8 Gel filtration using the AEKTA 100 system | 26 |
| 2.2.2.1.9 Transmission electron microscopy | 26 |
| 2.2.2.1.10 Immunoprecipitation | 26 |
| 2.2.3 Cell biological methods | 27 |
| 2.2.3.1.1 Cell culture and transformation of <i>D. discoideum</i> | 27 |
| 2.2.3.1.2 Live-cell microscopy of <i>D. discoideum</i> | 27 |
| 2.2.3.1.3 Immunofluorescence microscopy | 28 |
| 2.2.3.1.4 Induction of nuclear and cytoplasmic rods | 28 |
| 2.2.3.1.5 Growth and germination | 28 |
| 2.2.3.1.6 Phagocytosis measurements | 29 |
| 2.2.3.1.7 Analysis of phototaxis and development | 29 |

| | | |
|----------|---|-----------|
| 3 | Results | 30 |
| 3.1 | The actinome of <i>D. discoideum</i> | 30 |
| 3.1.1 | Phylogeny of the <i>D. discoideum</i> actinome | 30 |
| 3.1.2 | Sequence motifs | 32 |
| 3.1.3 | Structural homologies | 33 |
| 3.2 | Flag-tagged actin variants | 35 |
| 3.2.1 | Nucleating activities of Flag-actin variants | 35 |
| 3.2.2 | Influences of Flag-actin variants on actin filaments | 38 |
| 3.2.3 | Depolymerization of F-actin | 40 |
| 3.2.4 | Sedimentation assays | 42 |
| 3.2.5 | Phalloidin stabilized F-actin | 43 |
| 3.2.6 | FPLC-analysis of Flag-actin variants | 45 |
| 3.2.7 | Purified Flag-actin variants in a transmission electron microscope | 46 |
| 3.2.8 | Interaction studies with severin | 48 |
| 3.3 | GFP-actin variant overexpressors | 49 |
| 3.3.1 | Expression of the fusion proteins | 49 |
| 3.3.2 | Analyzing the F-actin cytoskeleton | 54 |
| 3.3.2.1 | Localization studies of actin variants in <i>D. discoideum</i> using fluorescence microscopy | 54 |
| 3.3.2.2 | The Triton-insoluble cytoskeleton and differential spin downs for the detection of additional cytoskeletal components | 55 |
| 3.3.3 | Rod formation in GFP-actin overexpressors | 57 |
| 3.3.3.1 | Nuclear actin rods | 57 |
| 3.3.3.2 | The role of Act16, Act3, Act18 and Act31 in cytoplasmic rods | 58 |
| 3.3.4 | Germination and viability of spores | 60 |
| 3.3.5 | Growth rates in <i>D. discoideum</i> mutants | 62 |
| 3.3.6 | The role of Act16, Act3, Act18 and Act31 in phagocytosis | 63 |
| 3.3.7 | Phototaxis and development of GFP-actin mutants | 65 |
| 3.3.8 | The <i>in vivo</i> effects of GFP-Act16, GFP-Act3, GFP-Act18 and GFP-Act31 | 70 |
| 4 | Discussion | 71 |
| 4.1 | Evolution of the actinome | 71 |
| 4.2 | The influence of Flag-tagged actin variants on <i>in vitro</i> actin dynamics | 72 |
| 4.3 | GFP-Act16, GFP-Act3, GFP-Act18, GFP-Act31 and their cellular functions in <i>D. discoideum</i> | 75 |
| 5 | References | 79 |
| | List of figures | 86 |
| | List of tables | 88 |
| | Acknowledgements | 89 |

Summary

The actin cytoskeleton in eukaryotic cells is crucial for a wide range of cellular functions including cell shape changes, cell motility, cell division or intracellular transport. As *Dictyostelium discoideum* harbors a relatively large actinome composed of 33 actin genes and eight genes that code for actin related proteins, this social amoebae serves as an excellent model organism to study the actin system. The main objective of this study was to get an overview of the huge variety of actin variants in *D. discoideum*. Conventional actin is encoded by 17 distinct genes (Act8 group), whereas the protein sequences of the other 16 actin variants can be almost identical with conventional actin or differ rather drastically. To cover a broad range of relative similarities we studied Act3 (97% identity), Act18 (88% identity) and Act31 (37% identity). As a reference we used Act16, a member of the Act8 group.

Although the amino acid sequences of the compared actin variants show different levels of similarity, the alignment of the sequence motifs and the computed ribbon models suggest that structure and fundamental functions of the compared proteins are strongly conserved.

We used Sf9 cells to express the actin variants Flag-Act16, Flag-Act3, Flag-Act18 and Flag-Act31. The conducted *in vitro* experiments showed that Flag-Act16 and Flag-Act3 promote the polymerization of short actin filaments, whereas Flag-Act18 and Flag-Act31 do not affect actin polymerization. Cosedimentation assays indicated that Flag-Act16, Flag-Act3 and Flag-Act31 are associated with polymerized actin, whereas Flag-Act18 cannot be detected together with actin filaments. Flag-Act16 and Flag-Act31 are not able to form filaments without conventional actin, not even in the presence of stabilizing phalloidin. Patches of assembled Flag-Act3 and Flag-Act18 monomers occurred when we added phalloidin. Gel filtration assays propose a tetrameric structure of Flag-Act16. Furthermore, denatured aggregates of Flag-Act3 are detectable, whereas an ordered oligomerization of Flag-Act18 and Flag-Act31 can be excluded. Images taken at the electron microscope suggest that none of the tested Flag-tagged actin variants is able to form stable actin filaments without conventional actin. Additionally, the formation of the actin network is not disturbed by the Flag-tagged variants. Protein interaction studies showed that the actin-binding protein severin binds Flag-Act16, Flag-Act3, Flag-Act18 and Flag-Act31 in a Ca²⁺-dependent manner.

In vivo studies were performed using GFP-Act16, GFP-Act3, GFP-Act18 and GFP-Act31 overexpressing cells of *D. discoideum*. Immunofluorescence studies and biochemical approaches showed that GFP-Act16 and GFP-Act3 are colocalizing with endogenous actin in the cell cortex, and partially in the cytoplasm. In contrast, GFP-Act18 and GFP-Act31 seem to be soluble proteins without interactions with the actin cytoskeleton. A most peculiar behavior is the stress-induced appearance of GFP-Act16 and GFP-Act3 in nuclear actin rods. GFP-Act18 and GFP-Act31 expressing cells are able to form nuclear rods, but these actin variants are not part of the rods. The tested GFP-actin variant overexpressors do not form typical needle-shaped cytoplasmic rods, but GFP-Act16 and GFP-Act3 are part of crescent-shaped aggregates within the cytoplasm.

As the viability of GFP-actin variant overexpressing spores is reduced in all mutants, we assume a disturbed activation of the actin cytoskeleton due to the excess of GFP-actin variant monomers, which could sequester actin binding proteins that are not available anymore for constitutively synthesized actins during germination. The size and shape of the tested spores is not affected as well as the overexpression of the GFP-actin variants has no influence on cytokinesis. GFP-Act16 and GFP-Act3 are accumulated in the phagocytic cup, whereas GFP-Act18 and GFP-Act31 are not enriched in this actin driven structure. During the 24 hours developmental cycle, smaller fruiting bodies of GFP-Act18 overexpressing cells and their increased density per area are conspicuous. In parallel, the expression of the aggregation marker glycoprotein A (CsA) is reduced in GFP-Act18 cells, which could restrict the formation of stable intercellular contacts.

Taken together, these data suggest that Act16 and Act3 are part of the F-actin network, whereas less related isoforms like Act18 and Act31 could even exhibit cytoskeleton-independent subcellular functions.

Zusammenfassung

Das Aktinzytoskelett in Nicht-Muskelzellen ist äußerst wichtig für eine Vielzahl zellulärer Funktionen wie die Dynamik der Zellform, der Zellmigration, der Zellteilung oder auch des intrazellulären Transports. Da *Dictyostelium discoideum* ein relativ großes Aktinom besitzt, bestehend aus 33 Aktinogenen und acht Genen, die für aktinverwandte Proteine codieren, bietet sich diese soziale Amöbe als ausgezeichneter Modellorganismus an, um ausgewählte Komponenten des Aktinsystems zu untersuchen. Ziel dieser Arbeit war es, sich einen Überblick über die enorme Vielfalt der Aktinvarianten in *D. discoideum* zu verschaffen. Konventionelles Aktin wird über 17 verschiedene Gene (Akt8 Gruppe) codiert, wohingegen die 16 übrigen Aktinvarianten mehr oder weniger große Unterschiede zu konventionellem Aktin aufweisen. Die wichtigsten Aktine dieser Arbeit waren: Akt16, ein Mitglied der Akt8 Gruppe konventionellen Aktins (100% Referenz), Akt3 (zu 97% identisch), Akt18 (zu 88% identisch) und Akt31 (zu 37% identisch).

Obwohl die Aminosäuresequenzen der verglichenen Aktinvarianten verschiedene Stufen an Ähnlichkeit zueinander aufweisen, verdeutlichen der Abgleich der Sequenzmotive und die berechneten 3D Modelle, dass die Strukturen und grundlegenden Funktionen der verglichenen Proteine stark konserviert sind.

Wir nutzten Sf9 Zellen, um die Aktinvarianten Flag-Akt16, Flag-Akt3, Flag-Akt18 und Flag-Akt31 zu exprimieren. *In vitro* Versuche zeigten, dass Flag-Akt16 und Flag-Akt3 die Polymerisation kurzer Aktinfilamente fördern, wohingegen Flag-Akt18 und Flag-Akt31 sich nicht auf die Aktinpolymerisation auswirken. Versuche zur Cosedimentation deuteten darauf hin, dass Flag-Akt16, Flag-Akt3 und Flag-Akt31 mit polymerisiertem Aktin verbunden sind, dies gilt nicht für Flag-Akt18. Flag-Akt16 und Flag-Akt31 können keine Aktinfilamente ohne konventionelles Aktin ausbilden, auch nicht unter Verwendung von stabilisierendem Phalloidin. Jedoch konnten unter Einfluss von Phalloidin Stücke aneinandergfügter Flag-Akt3 und Flag-Akt18 Monomere nachgewiesen werden. Gelfiltrationsmessungen deuten auf eine tetramere Struktur von Flag-Akt16 hin. Des Weiteren sind denaturierte Aggregate von Flag-Akt3 nachweisbar, wohingegen eine geordnete Oligomerisierung von Flag-Akt18 und Flag-Akt31 ausgeschlossen werden kann. Elektronenmikroskopische Aufnahmen lassen vermuten, dass keine der untersuchten Flag-Aktinvarianten stabile Filamente ohne konventionelles Aktin hervorbringt. Die Ausbildung des Aktinnetzwerks wird von den Flag-Aktinvarianten nicht gestört. Proteininteraktionsstudien zeigten, dass das aktinbindende Protein Severin Ca^{2+} -abhängig an Flag-Akt16, Flag-Akt3, Flag-Akt18 und Flag-Akt31 bindet.

In vivo Experimente wurden unter Einsatz von GFP-Akt16, GFP-Akt3, GFP-Akt18 und GFP-Akt31 überexprimierenden Zellen von *D. discoideum* durchgeführt. Studien zur Immunfluoreszenz und biochemische Ansätze zeigten, dass GFP-Akt16 und GFP-Akt3 gemeinsam mit endogenem Aktin im Zellcortex und teilweise im Zytoplasma lokalisieren. Hingegen scheinen GFP-Akt18 und GFP-Akt31 lösliche Proteine des Zytoplasmas zu sein. Besonders auffällig ist das stressinduzierte Auftreten von GFP-Akt16 und GFP-Akt3 in intranukleären, stäbchenförmigen Proteinaggregaten („nuclear rods“). GFP-Akt18 und GFP-Akt31 Zellen bilden zwar nuclear rods aus, beide Aktinvarianten sind aber nicht Teil dieser Strukturen. Die untersuchten GFP-Aktin Überexpressoren bilden nicht die typischen nadelförmigen cytoplasmatischen Aktinbündel, jedoch sind GFP-Akt16 und GFP-Akt3 Teil halbmondförmiger Aggregate innerhalb des Zytoplasmas.

Da die Keimfähigkeit aller GFP-Aktin überexprimierenden Sporen reduziert ist, gehen wir von einer gestörten Aktivierung des Aktinzytoskeletts aus, welche durch den Überschuss an GFP-Aktin Monomeren entsteht. Aktinbindeproteine könnten dadurch abfangen werden, die folglich nicht mehr den konstitutiv synthetisierten Aktinen während der Keimung zur Verfügung stehen. Größe und Form der untersuchten Sporen waren nicht verändert. Die Zytokinese selbst ist bei keiner GFP-Aktin Mutante verändert. GFP-Akt16 und GFP-Akt3 reichern sich in Phagozytosen an, wohingegen GFP-Akt18 und GFP-Akt31 hier nicht konzentriert vorliegen. Während des 24 Stunden dauernden Entwicklungszyklus fallen kleinere Fruchtkörper der GFP-Akt18 Überexpressoren und deren erhöhte Dichte auf. Zugleich ist die Expression des Markerproteins für Zellaggregation Glycoprotein A verringert, so dass die Ausprägung stabiler Kontakte zwischen den einzelnen Zellen begrenzt ist.

Zusammenfassend weisen diese Daten darauf hin, dass Akt16 und Akt3 Teile des F-Aktinnetzwerks sind, wohingegen weniger nah verwandte Isoformen wie Akt18 und Akt31 möglicherweise sogar Funktionen unabhängig vom Zytoskelett besitzen.

1. Introduction

1.1 *Dictyostelium discoideum* as a model organism

The eukaryotic soil amoeba *Dictyostelium discoideum* (*D. discoideum*) is an excellent model organism to study cellular processes. Dictyostelia belong to the phylum mycetozoa and are described as social organisms (Raper, 1935). Cellular dynamics as growth, germination, cell adhesion, phagocytosis, development and phototaxis can be analyzed easily, as well as the required signaling processes. Moreover, the high motility of *D. discoideum* facilitates insights into the actin cytoskeleton and its regulatory machinery. The extraordinary life cycle classifies the amoeba as a linker between unicellular and multicellular organisms due to its transition from autonomous single cells to higher organized organisms. Usually the professional phagocyte lives on forest soil and feeds on bacteria, but upon starvation it undergoes a specific developmental program, which leads to the aggregation of about 10^5 single cells induced and mediated by a cyclic adenosine monophosphate (cAMP) gradient. The movement of an organism in response to a chemical stimulus is called chemotaxis. Later on, these aggregates can form slug-shaped bodies, which migrate towards light sources.

The slug rises from the underlying substratum during culmination and forms a fruiting body consisting of a basal disk, stalk and a spore head, completing the life cycle. The spores of the fruiting body are useful to endure harsh environmental periods as starvation, heat or frost. Under favorable conditions germination into amoebae is induced. The entire developmental cycle can be completed within 24 hours under laboratory conditions (Chisholm & Firtel, 2004).

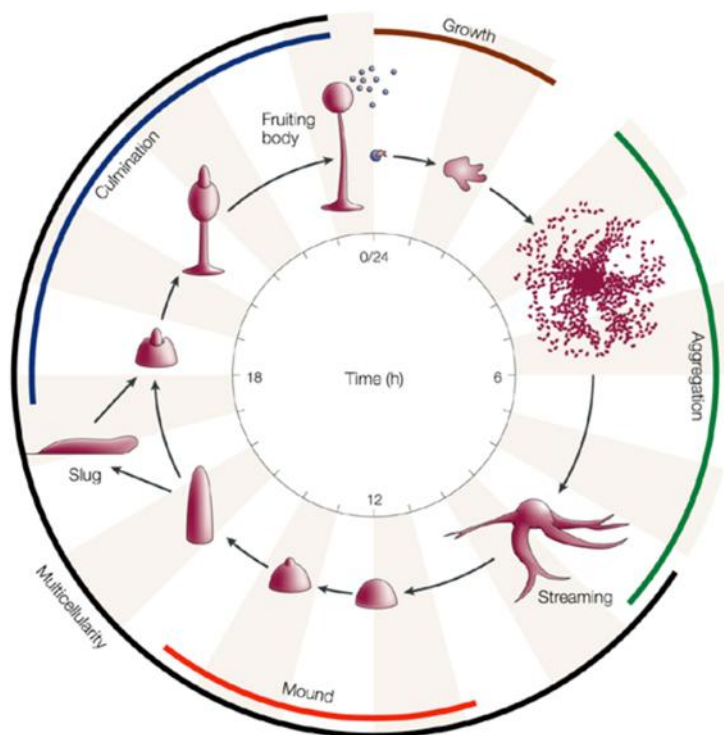


Figure 1: Life cycle of *D. discoideum* (Chisholm & Firtel, 2004). Single, vegetative cells start the developmental cycle to form a mature fruiting body, by developing a multicellular organism induced via cAMP. Directional streaming of the cells into multicellular aggregates is characteristic for this part of morphogenesis. The resulting multicellular organism is called mound, respectively tipped mound in the next phase of the cycle. The arising finger forms the adjacent slug, which culminates into a fruiting body. The head of the fruiting body incorporates the elliptical spores.

With a total size of 34Mb the genome of *D. discoideum* contains about 12.000 genes and has therefore the extent of the *Drosophila* genome. The availability of the completely sequenced genome was an enormous help towards our understanding of actins and actin-related proteins (ARPs; Eichinger et al., 2005). As a founder of a large protein family, any sequenced genome can be used to study actin. We selected the recently unraveled *D. discoideum* genome since it contains 33 genes that code for *bona fide* actin. In contrast, the genome of the budding yeast contains only one single gene that codes for actin, mouse harbors 35, and the plant *Arabidopsis thaliana* contains 10 actin genes. As a conclusion the number of actin genes does not tell us very much about the complexity of an organism. Elimination of redundant genes during evolution can only be avoided if they represent a selective advantage and it is still unclear why evolution allows this seemingly luxurious feature (Schleicher & Jockusch, 2008). The haploid genome of *D. discoideum* is easily susceptible to manipulation via recombinational methods and facilitates analyzing the functions of single protein isoforms. We used the wild type strain AX2 in this work that can grow in the simplified axenic media AX and HL5 (Schwalb & Roth, 1970). Consequently, laboratory culture is easy and inexpensive, highly accessible for biochemical, molecular and cell biological studies. To sum up, *D. discoideum* is a prime organism to analyze the activities of single molecules in their cellular environment.

1.2 Structure and domains of actin

Despite of their different protein sequences, actin turned out to be a structural homolog of proteins like hexokinases, the Hsp70 family, other sugar kinases and prokaryotic cell cycle proteins such as MreB, FtsA and StbA (Doolittle & York, 2002). It is assumed that convergent evolution with high pressure towards structure and function is the reason for analogies (Csete & Doyle, 2002). Actin has a molecular mass of 42kDa and exhibits a characteristic structure of five structural motifs and four domains. The five conserved actin sequence motifs are the phosphate binding loop 1 (Ph1), connecting motif 1 (C1), phosphate binding loop 2 (Ph2), adenosine binding loop (AD), connecting motif 2 (C2) (Bork et al., 1992).



Figure 2: Sequential arrangement of the five actin motifs. Illustration of the order of appearance of the five actin motifs from the amino-terminus (N) to the carboxy-terminus (C): phosphate binding loop 1 (Ph1=light blue), connecting motif 1 (C1=red), phosphate binding loop 2 (Ph2=orange), adenosine binding loop (AD=green), connecting motif 2 (C2=dark blue).

Domain I and domain II are two structurally similar globular domains connected by a flexible hinge that forms the core of actin. Most important for the actin dynamic is the interface between the two domains, which forms an adenosine triphosphate (ATP) binding pocket. Domain I as well as domain II are composed of two subdomains in each case 1 (Ia), 2 (Ib), 3 (IIa) and 4 (IIb). The barbed end of an actin filament is defined by the subdomains 1 and 3, opposed by the pointed end composed by subdomain 2 and 4 (Carrier, 1990). The structural similarity suggests that duplication of one ancestral domain could have formed the two domains of G-actin (Bork et al., 1992).

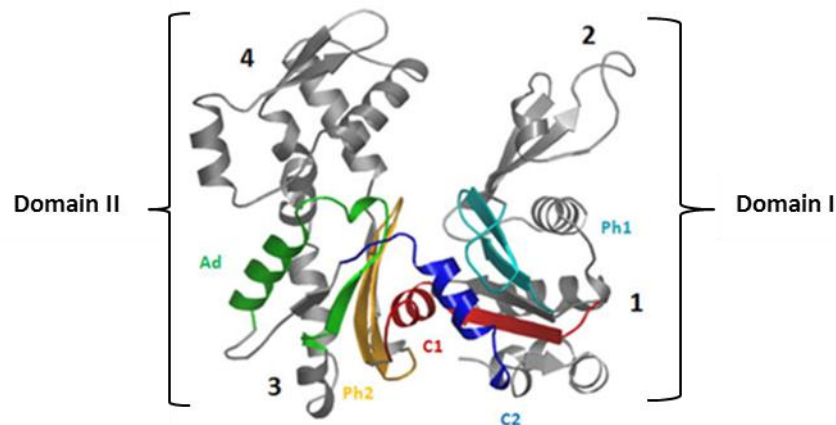


Figure 3: Typical G-actin structure in the ADP-state. The computed ribbon model of Act8 (P07830) of *D. discoideum* in the ADP-state (Joseph et al., 2008) shows that the ATP-binding pocket is exposed between the domains I and II. The four subdomains are marked (1-4) as well as the five structural motifs (Ph1= light blue, C1=red, Ph2=orange, Ad=green and C2=dark blue).

1.3 The actin cytoskeleton

The cytoskeleton in eukaryotic cells plays an important role in cell shape, structure, migration, cytokinesis, intracellular transport and provides one of the machineries for actively moving organelles within the cytoplasm. A complex and dynamic network of protein filaments is therefore spread throughout the cell consisting of microfilaments (diameter~7nm), intermediate filaments (diameter~10nm) and microtubules (diameter~24nm). Actin belongs to the microfilament system, is highly conserved and an abundant protein making up to 5-10% of the total cell protein (Pollard & Earnshaw, 2004).

Actin is present in two states, as monomeric globular actin (G-actin) and as polymeric, filamentous actin (F-actin). Two helical, interlaced F-actin strands build a right handed helix and form an actin filament. The addition of physiological salts like Mg^{2+} or K^+ to a G-actin pool above critical concentration induces polymerization *in vivo*.

The polymerization process of actin is marked by three distinct phases: first, G-actin forms short, unstable dimers and trimers during the so called lag-phase. Polymerization is energetically unfavorable until there is a nucleus of a certain length (typically a trimer). This stable seed elongates during the second phase into a filament by the addition of actin monomers to both of its ends. The growth of the filament leads to a decrease of G-actin until an equilibrium with the filament is reached. In the third phase, which is called the steady state phase, ATP-loaded monomers are preferentially added at the barbed/plus end of the filament and ADP-actin monomers dissociate from the pointed/minus end. This happens until the minimal concentration of G-actin required for addition of monomers (critical concentration) is lower at the plus end (about $0.1\mu\text{M}$) than at the minus end (about $0.8\mu\text{M}$). After incorporation of ATP-loaded actin into a filament, phosphate is released shortly after addition, and ADP-actin remains in the chain. The polarity is based on the structural asymmetry of the G-actin monomers and on the growing plus end that is marked by newly added ATP-actin, whereas the minus end consists of ADP-actin. Released ADP-actin monomers undergo nucleotide exchange to generate ATP-actin monomers that can be used for new rounds of polymerization. This ATP-hydrolysis-driven, directional filament growth is called actin treadmilling (Alberts et al., 2004).

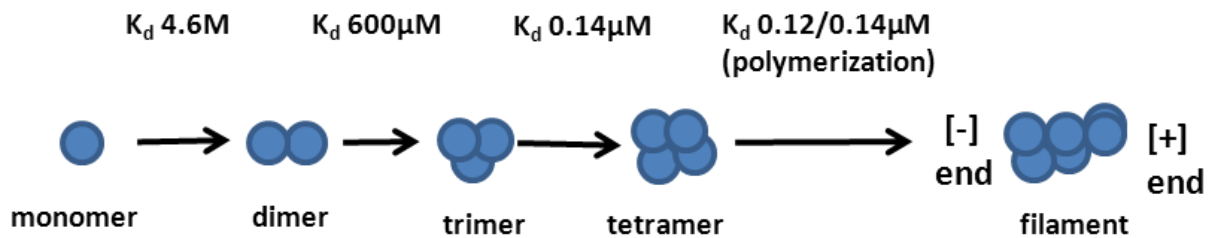


Figure 4: The process of actin polymerization (after Gallinger, 2013). The calculated dissociation constants demonstrate that the formation of actin dimers and trimeric nuclei is kinetically unfavorable (Sept & McCammon, 2001). Consequently, spontaneous actin polymerization *in vivo* is highly inefficient and requires nucleation factors that help to overcome this lag-phase. Once a nucleus is formed, addition of further actin molecules is accelerated by more than three orders of magnitude.

Actin-binding proteins are able to fulfill a large variety of tasks including the control of actin assembly and disassembly, as well as regulating filament branching and bundling to help arranging actin filaments into higher ordered structures. While actin monomer binding proteins control the amount and availability of monomers for polymerization, proteins that bind F-actin are involved in barbed and pointed end capping, filament severing and filament crosslinking. Among others, the ATP/G-actin binding proteins ARP2/3, WASP and formin induce the nucleation of F-actin, whereas profilin and thymosin control the pool of G-actin monomers via sequestering (Schüler et al., 2006). Profilin promotes the ADP/ATP exchange of the actin monomers, and thus ensures the delivery of ATP-actin for incorporation into growing filaments by actin polymerizing machineries (Dickinson et al. 2002). β -thymosin binds G-actin stoichiometrically and prevents G-actin even above its critical concentration from assembling to F-actin (Lodish et al., 2000). Gelsolin, cofilin or severin bind ADP/G-actin within the polymerized filament to disassemble the actin network. A severing protein cuts the filament and remains bound at the plus end of the resulting fragments, where it prevents the addition or exchange of actin subunits, an activity called capping. The minus ends of fragments remain uncapped and are rapidly shortened. Thus severing promotes the turnover of actin filaments by creating new minus ends and causes disintegration of the actin network. All of the mentioned severing proteins are regulated in a Ca^{2+} -dependent manner (Lodish et al., 2000). Capping at the plus end to block the addition and loss of actin subunits is also observed under the influence of Cap32/34 in *D. discoideum*. This heterodimeric protein consists of two subunits (32kDa and 34kDa) that can be inhibited by phosphatidyl bisphosphate, an important component in signal transduction during chemotaxis (Haus et al., 1991). The resulting lowered viscosity is a prerequisite to allow the flow of cellular contents during movement of the cell. Besides nucleation, ARP2/3 is also operating as a minus end capping protein, like tropomodulin. ARP2/3 inhibits both monomer addition and dissociation at the pointed ends of actin filaments and increases the critical concentration for polymerization at the pointed end. The high affinity of the ARP2/3 complex for pointed ends and its abundance in amoebae suggests that *in vivo* all pointed ends of actin filaments are capped by the ARP2/3 complex (Mullins et al., 1998). Furthermore ARP2/3 is important to allow dendritic branching that is found at the leading edge of motile cells (Pollard & Borisy, 2003). Besides the mentioned interactors, numerous other actin binding proteins are of great importance to the cell in the integration of structure and signaling between the cytoskeletal elements and the maintenance of cell integrity.

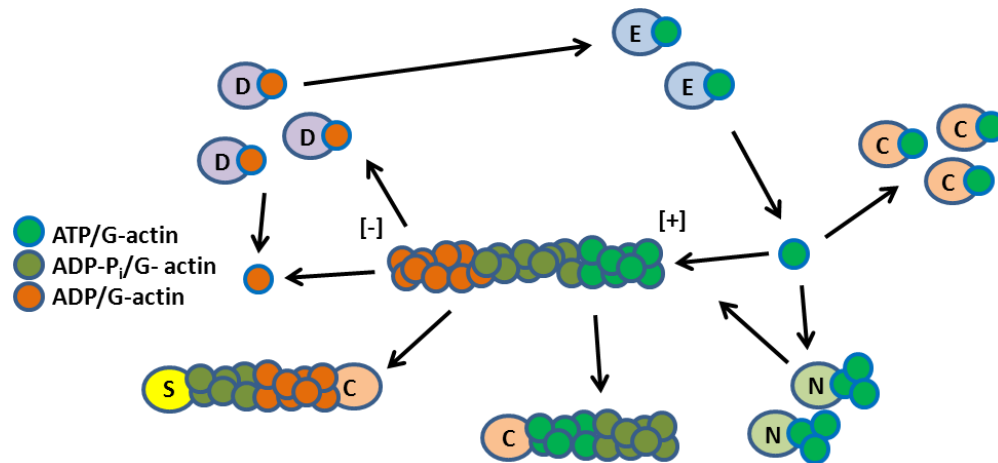


Figure 5: Actin binding proteins. Different actin binding proteins regulate the actin polymerization kinetics and stability of the microfilament network. Nucleation is mediated e.g. via ARP2/3, WASP or formins (N). These proteins are specific for binding ATP/G-actin monomers, like profilin (E) moderating nucleotide exchange. Severing and capping of ADP-P_i/G-actin is procured by gelsolin, fragmin or vilin (S), if lower viscosity is required in the cytoplasm. Thymosins (C) can bind ATP/G-actin subunits and ADP/G-actin monomers to induce capping/sequestration. For disassembly of the F-actin network the actin-depolymerization factor ADF/cofilin (D) binds ADP/G-actin and therefore communicates severing and depolymerization (after Winder & Ayscough, 2005).

If actin dynamics in human cells are disturbed, many diseases including muscular, neurological, immunological, vascular diseases and even cancer can occur (Cleuren & Boonstra, 2012). Also nemaline myopathies are caused by dysfunctions of the actin protein. The mutation of Val163Leu in ACTA1 (actin gene expressed in the human skeletal muscle) leads often to the intranuclear rod myopathy (IRM). This genetic defect results in the accumulation of rod-shaped protein aggregates in the nuclei and cytoplasm of human muscle cells (Domazetovska et al., 2007; Kaimaktchiev et al., 2006; Sparrow et al. 2003; Vandebrouck et al., 2010). Mutations in actin, nebulin, cofilin, troponin and tropomyosin could be ascertained in the affected patients, whereas the exact composition, formation and biophysics of these rod-shaped structures are yet unknown. One possible explanation for the presented disease pattern could be cell death, induced via harmed chromatin within the cells due to the stiff rod-shaped aggregates in the nucleus (Sparrow et al., 2003).

1.3 The actinome of *D. discoideum* and its regulation

To fulfill all the required functions and dynamics, the regulation of the actin cytoskeleton is not only controlled by actin binding proteins. Also posttranslational modifications on different actin isoforms play important roles in the modification of the actin network. Acetylation, acylation, serine/threonine/tyrosine-phosphorylation and ubiquitinylation of actin are possible. One can assume that a developmentally regulated expression of actin genes requires a similarly regulated expression of enzymes that catalyze posttranslational modifications (Schleicher & Jockusch, 2008). The discovery of ARPs made this picture even more complex. Due to its huge variety of actin genes, the *D. discoideum* genome provides a very good basis to study the actinome for potential cellular targets and conserved sequence motifs (Joseph et al., 2008). The actinome is comprised of 41 actins and ARPs. Seven potential pseudogenes are part of the *D. discoideum* genome, as well as eight ARPs. ARPs vary in presence and copy in different organisms and show altered degrees of similarity with actin (Muller et al., 2005). A few of them have preserved the actin structural fold, and are assumed to have originated from a common ancestor parallel to the actin isoforms. First identified in *Saccharomyces cerevisiae* (*S. cerevisiae*), the ARPs are named on decreasing order according to their relative identity with the conventional actin sequences, where ARP1 is the most similar and ARP10 the least similar (Poch & Winsor, 1997).

To get an overview of the actinome presented in *D. discoideum*, the genetic organization was analyzed using multiple sequence alignments and profile-hidden Markov models from the 'Pfam' protein family database. Altogether 33 actins and 8 ARPs have been identified (Joseph et al., 2008). 95% of the cellular actin consists of the Act8 group of conventional actin, which contains 17 distinct genes coding for identical amino acid sequences. The range of differences in the amino acid sequences in the other 17 actin genes varies from a single substituted residue (0.3%) for example in Act10, up to 295 (78%) non-identical amino acids in Act33 (Joseph et al., 2008).

| No. | Protein | Gene | dictyBase ID | Uni-Prot ID |
|-----|----------|-------|--------------|-------------|
| 1 | Act3 | act3 | DDB0220458 | P07829 |
| 2 | Act8 | act8 | DDB0216213 | P07830 |
| 3 | Act10 | act10 | DDB0220457 | Q54GX7 |
| 4 | Act17 | act17 | DDB0185125 | Q554S6 |
| 5 | Act18 | act18 | DDB0220459 | P07828 |
| 6 | Act22 | act22 | DDB0220460 | Q553U6 |
| 7 | Act23 | act23 | DDB0220461 | Q55EU6 |
| 8 | Act24 | act24 | DDB0220462 | Q54HF1 |
| 9 | Act25 | act25 | DDB0220463 | Q54HF0 |
| 10 | Act26 | act26 | DDB0220464 | Q55CU2 |
| 11 | Act27 | act27 | DDB0229353 | Q54HE9 |
| 12 | Act28 | act28 | DDB0229354 | Q54HE7 |
| 13 | Act29 | act29 | DDB0229355 | Q54L54 |
| 14 | Act31 | act31 | DDB0234013 | Q55DY5 |
| 15 | Act32 | act32 | DDB0234014 | Q55DS6 |
| 16 | Act33 | act33 | DDB0234012 | Q54JL1 |
| 17 | Filactin | Fia | DDB0220465 | Q54PQ2 |
| 18 | Arp1 | arpA | DDB0220489 | Q54I79 |
| 19 | Arp2 | arpB | DDB0185179 | O96621 |
| 20 | Arp3 | arpC | DDB0219936 | P42528 |
| 21 | Arp4 | arpD | DDB0233063 | Q54UQ7 |
| 22 | Arp5 | arpE | DDB0234009 | Q54E71 |
| 23 | Arp6 | arpF | DDB0234010 | Q54KZ7 |
| 24 | Arp8 | arpG | DDB0234011 | Q54JV5 |
| 25 | Arp11 | arpH | DDB0233828 | Q54JY2 |

| Identical actins of the Act8 group | | |
|------------------------------------|-------|------------|
| 1 | Act1 | DDB0220444 |
| 2 | Act2 | DDB0185124 |
| 3 | Act4 | DDB0220448 |
| 4 | Act5 | DDB0220447 |
| 5 | Act6 | DDB0185126 |
| 6 | Act7 | DDB0220445 |
| 7 | Act8 | DDB0216213 |
| 8 | Act9 | DDB0220456 |
| 9 | Act11 | DDB0220449 |
| 10 | Act12 | DDB0216214 |
| 11 | Act13 | DDB0220454 |
| 12 | Act14 | DDB0220455 |
| 13 | Act15 | DDB0185015 |
| 14 | Act16 | DDB0185127 |
| 15 | Act19 | DDB0220446 |
| 16 | Act20 | DDB0220450 |
| 17 | Act21 | DDB0220451 |

Figure 6: The actinome of *D. discoideum* (after Joseph et al., 2008). According to their actin sequence profile 41 actin genes have been identified. The Act8 group comprises 17 genes coding for the same amino acid sequences (right panel). The remaining 17 actin genes share high homologies to conventional actin but are different in their protein sequences (left panel No.1-17). The eight ARPs are characterized by the conserved actin motif, but the further protein sequences differ to variable extents (left panel No.19-25).

1.4 The actin variants Act3, Act18 and Act31 in *D. discoideum*

To cover a broad range of relative similarities to conventional actin we studied Act3 (97% identity to conventional actin), Act18 (88% identity to conventional actin) and Act31 (37% identity to conventional actin). As a reference we used Act16, a member of the Act8 group.

A

| | | |
|-----------|---|-----|
| Act16 1 | LDG EDVQALVIDNGSGMCKAGFAGDDAFRAVFFSIVGRPEHFGVMVGMGQKDSIVGDEAC | 60 |
| Act3 1 | ES EDVQALVIDNGSGMCKAGFAGDDAFRAVFFSIVGRPEYFGVMVGMGQKDSIIIGDEAC | 60 |
| Act16 61 | KRILLILKYPIEHGIVTNWDDMEKIWHHTFYNELRVAFEEHFVLLTEAPLNFKANREK | 120 |
| Act3 61 | SRKILLILKYPIEHGIVTNWDDMEKIWHHTFYNELRVAFEEHFVLLTEAPLNFKANREK | 120 |
| Act16 121 | FQIMFETFNTPAMYVAIQAVLSLYASGRTTGIVMDSGGDGVSHTVPIYEGYALPHAILRLD | 180 |
| Act3 121 | FQIMFETFNTPAMYVAIQAVLSLYASGRTTGIVMDSGGDGVSHTVPIYEGYALPHAILRLD | 180 |
| Act16 181 | LAGRDLTDYMMKILTERGYSFTTTAEREIVRDIKEKLAYVALDFEALMTAASSSALEK | 240 |
| Act3 181 | LAGRDLTDYMMKILTERGYSFTTTAEREIVRDIKEKLAYVALDFEALMTAASSSALEK | 240 |
| Act16 241 | VELPDGQVITIGNERFRCPEALFQPSFLGME SAGIHETTYSIMKCDVDIRKDLVGNVVI | 300 |
| Act3 241 | VELPDGQVITIGNERFRCPEALFQPSFLGME SAGIHETTYSIMKCDVDIRKDLVGNVVI | 300 |
| Act16 301 | SGGTHMFFGIADRMNKELTALAPSTMKIKIIPAPPERKYSVWIGGSILASLSTFQQMWISK | 360 |
| Act3 301 | SGGTHMFFGIADRMNKELTALAPSTMKIKIIPAPPERKYSVWIGGSILASLSTFQQMWISK | 360 |
| Act16 361 | EEYDESGPSIVHRKCF* | 377 |
| Act3 361 | EEYDESGPSIVHRKCF* | 377 |

B

| | | |
|-----------|---|-----|
| Act16 1 | LDG EDVQALVIDNGSGMCKAGFAGDDAFRAVFFSIVGRPEHFGVMVGMGQKDSIVGDEAC | 60 |
| Act18 1 | EREEVQALVIDNGSDMCKAGFAGDDAFRAVFCIVGRPEYFGVMVGMGQKDSIIIGDEAH | 60 |
| Act16 61 | KRILLILKYPIEHGIVTNWDDMEKIWHHTFYNELRVAFEEHFVLLTEAPLNFKANREK | 120 |
| Act18 61 | SRKILLILKYPIEHGIVTNWDDMEKIWHHTFYNELRVAFEEHFVLLTEAPLNFKANREK | 120 |
| Act16 121 | FQIMFETFNTPAMYVAIQAVLSLYASGRTTGIVMDSGGDGVSHTVPIYEGYALPHAILRLD | 180 |
| Act18 121 | FQIMFETFNTPAMYVAIQAVLSLYASGRTTGIVMDSGGDGVSHTVPIYEGYALPHAILRLD | 180 |
| Act16 181 | LAGRDLTDYMMKILTERGYSFTTTAEREIVRDIKEKLAYVALDFEALMTAASSSALEK | 240 |
| Act18 181 | LAGRDLTDYMMKILTERGYSFTTTAEREIVRDIKEKLAYVALDFEALMTAASSSALEK | 240 |
| Act16 241 | VELPDGQVITIGNERFRCPEALFQPSFLGME SAGIHETTYSIMKCDVDIRKDLVGNVVI | 300 |
| Act18 241 | VELPDGQVITIGNERFRCPEALFQPSFLGME SAGIHETTYSIMKCDVDIRKDLVGNVVI | 300 |
| Act16 301 | SGGTHMFFGIADRMNKELTALAPSTMKIKIIPAPPERKYSVWIGGSILASLSTFQQMWISK | 360 |
| Act18 301 | SGGTHMFFGIADRMNKELTALAPSTMKIKIIPAPPERKYSVWIGGSILASLSTFQQMWISK | 360 |
| Act16 361 | EEYDESGPSIVHRKCF* | 375 |
| Act18 361 | EEYDESGPSIVHRKCF* | 375 |

Table 1: Actin variants analyzed in this study (dictybase.org, NCBI Blast).

| | Act16 | Act3 | Act18 | Act31 |
|--|---|--|---|--------------|
| Dictybase Gene ID | DDB_G0272248 | DDB_G0289487 | DDB_G0289489 | DDB_G0269476 |
| Identity with <i>D. discoideum</i> conventional actin (P07830) | 100% | 97% | 88% | 39% |
| Identity with human beta-actin (P60709) | 95% | 92% | 83% | 39% |
| Identity with rabbit muscle actin (P68135) | 91% | 89% | 80% | 38% |
| location of the gene | Chromosome 2 | Chromosome 5 | Chromosome 5 | Chromosome 1 |
| number of amino acids | 376aa | 376aa | 380aa | 355aa |
| Number of identified ESTs | 60 | 3 | 4 | 3 |
| predicted molecular function | nucleotide binding; structural constituent of the cytoskeleton; protein binding; ATP binding; myosin binding | nucleotide binding; structural constituent of the cytoskeleton; protein binding; ATP binding; myosin binding | nucleotide binding; structural constituent of the cytoskeleton; ATP binding; myosin binding | unknown |
| predicted cellular component | phagocytic cup; cytoplasm; cytoskeleton; actin filament; actin cytoskeleton; pseudopodium; cell leading edge; early phagosome; phagolysosome; phagocytic vesicle; cell pole | phagocytic cup; cytoplasm; cytoskeleton; actin cytoskeleton; early phagosome; phagolysosome; phagocytic vesicle; cell pole | cytoplasm; cytoskeleton; actin cytoskeleton | unknown |

1.6 Aims of the thesis

Given that *D. discoideum* comprises 41 actins and ARPs, several approaches should be performed to get an overview over this huge actinome. It is still unclear why such a multitude of genes is kept active within the genome of *D. discoideum*, where other organisms vary their proteomes simply via splicing or posttranslational modifications. Accordingly, we assumed that the actin variants which are not part of the Act8 group are not necessary for the cytoskeleton itself, but are rather regulators of its dynamical features or subunits in larger protein complexes. Therefore, we aimed at the functions of the actin variants Act3, Act18 and Act31 in the microfilament system *in vitro* and *in vivo*. Act16 as a member of the Act8 group served as a control.

First, the *in vitro* characterization of the selected actin variants should be performed. For this purpose the baculoviral amplification system (Sf9 cells) should be used to express N-terminal Flag-tagged actin variants. To analyze the role of Flag-Act16, Flag-Act3, Flag-Act18 and Flag-Act31 in actin dynamics, actin polymerization assays have to be performed using fluorometric approaches, low shear viscometry, spin down assays and the transmission electron microscopy. Additionally, oligomerization of the Flag-tagged actin variants should be checked via FPLC-gelfiltration and immunoprecipitation studies could reveal potential binding partners of the actin variants.

The *in vivo* assays should be performed using green fluorescent protein-actin variant (GFP-actin variant) overexpressing cells of *D. discoideum*. To determine if the actin variants are part of the microfilament system, immunofluorescence and spin down assays were to be performed. Furthermore, phenotypical characterization should be carried out with the analysis of growth, germination, phagocytosis, development and phototaxis. Additionally, we were interested in the role of GFP-Act16, GFP-Act3, GFP-Act18 and GFP-Act31 concerning the formation of actin bundles, like nuclear and cytoplasmic rods. In all *in vivo* assays the influence of the N-terminal GFP-tag had to be compared to the results to GFP-overexpressing wild type cells from *D. discoideum* (AX2-GFP cells).

2. Materials and Methods

2.1 Materials

2.1.1 Instruments

| | |
|-------------------------------------|---------------------------|
| AEKTA purifier 100 | GE Healthcare |
| BioDocAnalyze | Biometra |
| Dounce homogenizer | Braun/Wheaton |
| fluorescence spectrometer LS55 | Perkin Elmer |
| Gene pulse electroporator Xcell | BioRad |
| Gelsystem MiniPROTEAN | BioRad |
| PCR-Thermocycler Tpersonal | Biometra |
| pH-meter pH720 | Inolab WTW series |
| plasma cleaner | Diener, Ebhausen |
| Power supplies | Biorad, Biometra, Consort |
| Protein Transfer Transblot Semi-Dry | BioRad |
| Protein Transfer TF 77XP | Serva |
| Shaker Orbital Incubator SI500 | Memmert |
| Shakers for Dictyostelium cultures | Kühner |
| Thermomixer | Eppendorf |
| Tabletop Film Processor Curix 60 | Agfa |
| Vortex Genie 2 | Bender & Hobein |
| Waterbath | GFL, Kühner |

Microscopes

| | |
|--|------------|
| Binocular microscope Stereo Discovery.V8 | Carl Zeiss |
| LSM 510 confocal microscope | Carl Zeiss |
| JEM-1200 EX II Electron microscope | JEOL |

Objectives

| | |
|---|------------|
| Achromat S 0.63x FWD 115mm | Carl Zeiss |
| 40x LD A-Plan 0.50 Ph2 | Carl Zeiss |
| 63x Neofluar 1.4 oil immersion objective | Carl Zeiss |
| 100x Neofluar 1.3 oil immersion objective | Carl Zeiss |

Centrifuges

| | |
|--------------------------------|-----------|
| GS-6KR | Beckman |
| J2-21M/E | Beckman |
| J6-HC | Beckman |
| Microcentrifuge 5415 D, 5417 R | Eppendorf |
| Optima LE-80K | Beckman |
| Optima TL ultracentrifuge | Beckman |

Rotors

| | |
|---------------------|---------|
| JA-10, JA-15, JA-20 | Beckman |
| Ti35, Ti45, Ti70 | Beckman |
| TLA 100.3 | Beckman |

2.1.2 Computer programs

| | |
|----------------------------|---|
| Adobe Creative Suite 2 | Adobe Systems |
| ApE plasmid editor v1.10.4 | M. Wayne |
| AxioVision | Carl Zeiss |
| BioDoc Analyze | Biometra |
| BioEdit 7.0.9.0 | Tom Hall |
| ClustalX2 | European Molecular Biology Laboratory |
| FL Winlab | Perkin Elmer |
| LSM 5, 4.2 SP1 | Carl Zeiss |
| Microsoft Office | Mircosoft Corporation |
| Multalin 5.4.1 | Florence Corpet |
| NCBI | National Center for Biotech Information |
| OpenAstexViewer | Carl Zeiss |
| Pfam 22.0 | Trust Sanger Institute |
| Swissmodel Expasy | Swiss Institute of Bioinformatics |
| Treeview 1.6.6 | Java |
| Unicorn 5.20 | GE Healthcare |
| Uniprot | European Bioinformatics Institute |
| Weblogo2.0 | University of California, Berkley |
| ZEN | Carl Zeiss |

2.1.3 Laboratory consumables

| | |
|--|-------------------------|
| 1.5ml centrifuge tubes | Eppendorf |
| Amersham Hyperfilm ECL | GE Healthcare |
| Cell culture plates, 24 wells | Starlab Int. |
| Cell culture dishes, Ø 100mm x 20mm | Greiner bio-one |
| 100Carbon Support Films-grids Cu 200 | QUANTIFOIL |
| Dialysis tubings Type 8, 20, 27 | Biomol |
| Gel-blotting paper 3MM Chr | Whatman |
| GFP-Nano-Trap | Chromotek |
| High Pure Plasmid Isolation Kit | Roche |
| High Pure PCR Product Purification Kit | Roche |
| High precision cuvettes 10mm | Hellma |
| Nitrocellulose transfer membrane Protran | Whatman |
| Parafilm | American National Can |
| PCR tubes Thermo Tube 0.2ml | Peqlab |
| Phusion High-Fidelity DNA-Polymerase | New England Biolabs |
| Petri dishes Ø 92mmx 16mm | Sarstedt |
| Pipettes 10ml, 25ml | Sarstedt |
| Pipette tips | Biozym, Gilson, Starlab |
| Plasmid DNA Purification Maxi Kit | Machery Nagel |
| 600 mesh Cu ²⁺ -grids | Plano |
| Restriction Enzymes | New England Biolabs |
| Sterile filter, Filtropur S 0.2 | Sarstedt |
| Tubes 15ml, 50ml | Sarstedt |
| Ultracentrifuge tubes 1.5ml | Beckman |

2.1.4 Reagents

Standard laboratory chemicals were mainly purchased from Biomol, Biorad, Fluka, Invitrogen, Merck, Peqlab, Roche, Roth, Serva or Sigma-Aldrich and had the degree of purity 'p.a.' unless otherwise mentioned. Media and buffers used in this study were prepared with de-ionised water (Millipore), sterilized either by autoclaving or passing through a micro-filter (pore size 0.2µm).

2.1.5 Antibodies

Primary antibodies

| | |
|---|-------------------------|
| Actin, <i>D. discoideum</i> (Act-1) | Simpson et al. (1984) |
| Actin, <i>D. discoideum</i> (224-236-1) | Westphal et al. (1997) |
| Contact site A glycoprotein (33-294-17) | Bertholdt et al. (1985) |
| Filactin (4S-59-4) | Israel (2002) |
| Flag-tag (6F7) | Chromotek |
| GFP (K3-184-2) | Noegel et al. (2004) |
| Severin (102-200-1) | Andre et al. (1989) |

Secondary antibodies

| | |
|--|---------------|
| Goat-anti-mouse IgG Cy3-conjugated | Invitrogen |
| Anti-mouse IgG horseradish peroxidase-linked (ECL) | GE Healthcare |

2.1.6 Vectors

| | |
|--|-----------------------------|
| pDEX-(g418)-GFP-act16 (Mo-1) | Annette Müller-Taubenberger |
| pDEX-(blastocidin)-GFP-act3 (#614_2) | Annette Müller-Taubenberger |
| pDEX-(blastocidin)-GFP-act18 (#681_43) | Annette Müller-Taubenberger |
| pDEX-(blastocidin)-GFP-act31 (#668_1) | Annette Müller-Taubenberger |
| pFastBac1 | Invitrogen |

Constructs generated in this study

| | |
|-----------------|-----------|
| pFastBac1 Act16 | Sall/KpnI |
| pFastBac1 Act3 | Sall/KpnI |
| pFastBac1 Act18 | Sall/KpnI |
| pFastBac1 Act31 | Sall/KpnI |

2.1.7 Bacterial strains

| | |
|--------------------------|-------------------------|
| E.coliDH5 α | Invitrogen |
| E.coliDH10Bac | Invitrogen |
| E.coliDH10Bac FLAG-Act16 | Present study |
| E.coliDH10Bac FLAG-Act3 | Present study |
| E.coliDH10Bac FLAG-Act18 | Present study |
| E.coliDH10Bac FLAG-Act31 | Present study |
| <i>K. aerogenes</i> | Williams & Newell, 1976 |

2.1.8 Yeast strains

S. cerevisiae YSC-II

Sigma -Aldrich

2.1.9 *D. discoideum* strains

| Strain name | Resistance | Source |
|--------------------|-------------------|-----------------------------|
| AX2 | / | laboratory wild type |
| AX2-GFP | G10 | Meino Rohlfs |
| Cherry-cofilin | G10 | Hellen Ishikawa-Ankerhold |
| GFP-Act16 | G10 | Annette Müller-Taubenberger |
| GFP-Act3 | B10 | Annette Müller-Taubenberger |
| GFP-Act18 | B10 | Annette Müller-Taubenberger |
| GFP-Act31 | B10 | Annette Müller-Taubenberger |

2.2 Methods

2.2.1 Molecular methods

To generate various GFP- and Flag-tagged protein constructs standard molecular biological methods were used. Polymerase chain reactions (PCRs) were performed with Phusion High-Fidelity DNA-Polymerase (New England Biolabs) according to the manufacturer's manual. Extraction and purification of DNA from Tris-borate-EDTA agarose gels were performed using the High Pure PCR Product Purification Kit (Roche). PCR products were cloned into the appropriate plasmids using standard restriction enzyme mediated cloning techniques. Plasmid DNA was obtained from *E.coli* by using standard alkaline lysis miniprep or by using the silica-based mini- and maxiprep kits (Roche, Macherey Nagel). Chemically competent *E. coli* cells were prepared according to the CaCl₂ method (Dagert & Ehrlich, 1979). The correctness of the DNA sequences inserted into the respective expression vectors was controlled by sequencing using specific primers (Eurofins MWG Operon, Ebersberg).

2.2.2 Biochemical methods

2.2.2.1 SDS-polyacrylamide gel electrophoresis and western blotting

Standard discontinuous SDS-page was used to separate protein mixtures (Laemmli, 1970). Afterwards transfer buffer (25mM Tris; pH8.5, 190mM glycine, 20% methanol, 0.02% SDS) transmitted these proteins onto a nitrocellulose membrane via semi-dry western blotting. Nonfat milk powder in NCP buffer (10mM Tris; pH7.3, 150mM NaCl, 0.05% Tween20) blocked the membranes, before incubation steps with the appropriate primary and secondary antibodies followed. The Enhanced Chemiluminescence System (ECL) was used for developing the membranes finally.

2.2.2.2 Coomassie Blue and silver staining

To detect proteins after electrophoretic separation on polyacrylamide gels, staining with Coomassie Brilliant Blue R250 was performed. If sensitivity in the low nanogram range was needed, we conducted silver staining. This is compatible with downstream processing such as mass spectrometry analysis after protein digestion. The sequential phases of silver staining were protein fixation (40% ethanol, 10% acetate; 30 minutes) then sensitization (30% ethanol, sodium thiosulfate, 0.83M sodium acetate, 0.125 % freshly added glutaraldehyde; 30 minutes). After washing three times with ddH₂O (10 minutes each), the gels were stained in silver impregnation (0.25% silver nitrate, 0.015% freshly added formaldehyde; 30 minutes). Gels were rinsed with ddH₂O and exposed to developing solution (23.5mM sodium carbonate, 0.015% freshly added formaldehyde) until the desired grade of staining intensity was reached. The reaction was stopped by addition of an aqueous EDTA solution.

2.2.2.3 Actin preparation from rabbit skeletal muscle

In the present thesis rabbit muscle actin was used as a control in many assays. Routine actin purification methods were used to obtain actin essentially as described (Spudich & Watt, 1971). The upper and back thigh muscles of a rabbit were detached, chilled and ground twice. A high salt extraction buffer (0.5M KCl, 0.1M K_2HPO_4) was applied for 10-15 minutes on a stirrer to remove myosin. Next, the mixture was centrifuged (4.000g, 4°C, 10 minutes) and reextracted. Until the pellet swelled, stirring in cold distilled water for 10 minutes and centrifugational steps were repeated again and again. Afterwards the pellet was incubated with cold acetone for about 30 minutes, filtered and dried overnight. For subsequent actin preparations the acetone powder was stored at -20°C.

Regularly, 10g acetone powder were extracted with 200ml G-actin buffer (2mM Tris; pH 8.0, 0.2mM ATP, 0.5mM DTT, 0.2mM $CaCl_2$, 0.01% NaN_3) at 4°C for 30 minutes, followed by filtration through nylon sets and reextraction for 15 minutes. Past centrifugation of the filtrate (30.000g, 30 minutes, 4°C) actin polymerization was induced by adding 50mM KCl, 2mM $MgCl_2$ and 1mM ATP dissolved in 100mM NaOH, and the mixture was incubated at 4°C for two hours, respectively overnight. Up to 0.8M solid KCl was slowly added to remove tropomyosin. To accumulate F-actin, centrifugation at 150.000g for three hours at 4°C was performed and the supernatant was discarded. Homogenization was executed by a douncer. To achieve depolymerization, F-actin was dialyzed against G-buffer for two-three days with a total of about six buffer changes. Again the remaining F-actin fraction was separated by centrifugation at 150.000g and 4°C for three hours, then 65% from the top supernatant were further purified using a Sephacryl S300 gel filtration column (2.5x45cm; Pharmacia). The actin concentrations of the different fractions were determined by measuring the optical density at 290nm (1mg/ml pure actin: $OD_{290nm}=0.65$). Adjacent falling ball viscometry verified the quality. Freshly prepared rabbit muscle actin can be stored on ice for up to three weeks for most applications and was dialyzed against freshly prepared G-buffer before usage.

2.2.2.4 Labeling of actin with pyrene

Actin was labeled for *in vitro* polymerization assays with N-(1-pyrenyl) iodoacetamide (pyrene; Kouyama & Mihashi, 1981). After the first ultracentrifugation step during actin preparation, the F-actin pellet was dialyzed against P-buffer (1mM NaHCO₃; pH7.6, 0.1mM CaCl₂, 0.2mM ATP, 0.1mM β-mercaptoethanol) for two-three days with a total of about six buffer changes. 65% of the top supernatant was used, after centrifugation at 150.000g for three hours at 4°C. In parallel, 100mM KCl and 1mM MgCl₂ were added to promote actin polymerization, while a three-five fold molar excess of pyrene dissolved in DMSO was dropwise stirred into the actin solution. Given that pyrene is light sensitive, the following working steps had to be performed under protection of light. The solution was mixed gently overnight by turning end-over-end in a 50ml tube at room temperature before F-actin was pelleted again at 150.000g. G-buffer was supplemented to the pellet of F-actin for homogenization and dialysis to effect depolymerization. A further centrifugational step at 150.000g for three hours at 4°C was undertaken, before the pyrenylated G-actin was further purified via gel filtration as described in 2.2.3.3. By using the respective extinction coefficients ($OD_{290nm}=2.6 \rightarrow 100\mu M$ actin; $OD_{344nm} \rightarrow 100\mu M$ pyrene; micromolar concentration pyrene/micromolar concentration actin = % of pyrene-labeled actin) the percentage of labeled actin could be calculated when the concentrations of actin and pyrene were measured at the photometer. 60-90% of the actin fraction should be successfully labeled. Before usage the aliquots were dialyzed against G-buffer. Storage at -80°C.

2.2.2.5 Flag-tagged protein expression using the baculoviral amplification system

To ensure correct expression, folding and oligomerization of the selected actin variants, the eukaryotic Bac-to-Bac baculoviral expression system was utilized to express recombinant protein constructs. First of all, the appropriate nucleotide sequence with an N-terminal Flag-tag was cloned into the pFastBac1 vector. Thereupon, DH10Bac cells were transformed with 300ng of the newly cloned pFastBac1 construct. DH10Bac cells contained the baculoviral shuttle vector (bacmid) with a mini-attTn7 target site and a helper plasmid that encoded certain transposition proteins. The transposition of the mini-Tn7 element on the pFastBac1 donor plasmid to the mini-attTn7 target site on the bacmid was supported by the special transposition proteins. If the recombination was successful, the lacZ gene on the bacmid was disrupted, which allowed a blue/white screening in the presence of X-Gal and IPTG. After isolation of the bacmid via miniprep, immortalized Sf9 insect cells could be transfected and cultivated at 28°C. For this purpose 200μl Sf-900 II SFM medium (Invitrogen), 10μl cellfectin (Invitrogen) and 30-100μg bacmid DNA were mixed and incubated for 45 minutes at room temperature. Afterwards the mix was added to 2ml of Sf9 cells (density 5×10^5 cells/ml) which were placed in wells of a 6-well-plate and incubated at 28°C for five hours.

The transfection mixture was removed, before SFM medium supplemented with 5% fetal bovine serum and gentamycin (0.1mg/ml) was added. The virus (P0 virus) was harvested after 72 hours of incubation at 28°C, sterile-filtered and stored at 4°C. The virus was amplified by generating P1 and P2 generations. For protein expression >97%, viable Sf9 cells were infected at a density of 2×10^6 cells/ml with P2 virus at a ratio of about 1/10 (10ml P2 virus+ 90ml cells), and incubated as a shaking culture at 110rpm at 28°C for 48-72 hours. Cells were harvested by centrifugation (2000g, 15 minutes, 4°C) and pellets of a 100ml culture were resuspended in 5ml lysis buffer (15mM Hepes, pH 7.4; 30mM NaCl, 1mM EGTA, 1mM DTT, 0.1mM magnesium-ATP, one Complete Protease Inhibitor cocktail tablet (Roche) per 20ml buffer, 2% glycerol, 1% Triton-X100). The lysates were centrifuged at 30.000g for 10 minutes at 4°C and the supernatant was incubated at 4°C under gentle end-over-end mixing for 90 minutes with 100µl Anti-Flag M2 Affinity Gel (Sigma) for lysates of a 100ml culture. The matrix was washed in washing buffer (15mM Hepes, pH7.4; 30mM NaCl, 1mM DTT, 0.1mM magnesium-ATP, one Complete Protease Inhibitor cocktail tablet (Roche) per 20ml buffer, 2% glycerol), with 10-30 column volumes in a Poly-Prep Chromatography column (Biorad). For elution, the column outlet was closed and 200µl elution buffer (wash buffer containing 100µg Flag-peptides; Sigma) were used to elute the protein from 100µl Anti-Flag M2 Affinity Gel for 60 minutes. The eluate was collected and the concentration was determined by SDS-page analysis. The purified protein was subsequently used in further experiments or stored at -80°C.

2.2.2.6 *In vitro* actin polymerization assay

A Perkin Elmer fluorometer was used for fluorometric actin polymerization assays by the application of pyrenylated actin. 20x increase of fluorescence could be obtained if actin polymerizes and the environment of pyrene-actin changes. A convenient signal occurred already with about 10% pyrenylated actin. The polymerization-induced fluorescence was captured at 386nm using an excitation wavelength of 365nm and 8nm slit widths. Polymerization was induced by application of polymerization buffer (10mM imidazole, pH7.2; 3mM MgCl₂, 1mM Na-ATP, 0.2mM CaCl₂). G-actin, Flag-tagged actin variants and different buffering conditions (e.g. elution buffer or 100mM KCl) were mixed and preincubated for about one-two minutes prior to addition of polymerization buffer and recording. Filament-disrupting measurements were performed with prepolymerized actin samples.

2.2.2.7 Low shear viscometry

Low shear viscometry assays were carried out in a falling ball viscometer (MacLean-Fletcher & Pollard, 1980). Polymerization of the incubated actin proteins was started by the addition of polymerization buffer. The mixture was briefly vortexed, immediately filled into the capillary and allowed to polymerize for 15 minutes. The viscosity of the solution was measured by recording the time a mini steel ball took to pass a certain distance.

2.2.2.8 Gel filtration using the AEKTA 100 system

The gel filtration column Superose 6 10/300GL (GE Healthcare) provides the appropriate range of pore sizes for the selected Flag-actin constructs. The column was equilibrated with IEDANBP buffer (10mM imidazole, 1mM EGTA, 1mM DTT, 0.02% NaN₃, 50mM NaCl, 1mM benzamidine, 1mM PMSF; pH 7.3). The flow rate was set between 0.1-0.5ml/min. Before starting size analysis the column was calibrated using protein molecular weight standards in a range between 12.4–450kDa (Serva). The void volume (V₀) was identified with Dextran blue 2000 (GE Healthcare). Usually 0.2mg purified protein was injected, 0.5ml fractions were collected and analyzed by SDS-page.

2.2.2.9 Transmission electron microscopy

First the grids were cleaned using a plasma cleaner. About 10µl of the protein samples (50µg/ml, respectively 25µg/ml) were pipetted onto a parafilm, the grids were placed on the sample drops with their carbon coated side and incubated for one-two minutes. Afterwards the grids were washed in a drop of H₂O two times. By using a filter paper superfluous fluid was removed and the grids were placed in a 2% uranyl acetate solution, incubated for two minutes and dried. Images were taken on a CM20 electron microscope (JEOL) at 70kV and 10.000x magnifications.

2.2.2.10 Immunoprecipitation

The GFP-Nano-Trap system (Chromotek) was used to identify proteins interacting with the cloned GFP-actin variants (Zolghadr et al., 2012). 5x10⁷ cells of the relevant *D. discoideum* strains were harvested and opened in lysis buffer (25mM HEPES; pH7.4, 50mM NaCl, 1mM EDTA, 1mM EGTA, 1mM DTT, 5mM benzamidine, 1µM PMSF, one Complete Protease Inhibitor cocktail tablet (Roche) per 20ml buffer, 5% Glycerol, 1% Triton X-100). The lysate was centrifuged for 15-30 minutes at 10.000g and 4°C. Afterwards the supernatant was incubated with 15-20µl packed GFP-Trap agarose beads equilibrated in lysis buffer. The following incubation via end-over-end mixing at 4°C took 60-90 minutes. As described in the manufacturer's protocol the beads were washed, and the GFP-tagged proteins with their potential interaction partners were eluted by boiling in SDS-sample buffer. Proteins were separated by SDS-page and silver stained (O-Connel & Stults, 1997). Bands of interest were cut out from the gel and analyzed via MALDI-TOF mass spectrometry (ZfP, LMU Munich).

2.2.3 Cell biological methods

2.2.3.1 Cell culture and transformation of *D. discoideum*

The wild type strain of *D. discoideum* AX2, or mutant cells derived from it, were cultured axenically in either AX medium (14.3g peptone, 7.15g yeast extract, 50mM glucose, 3.5mM Na₂HPO₄, 3.5mM KH₂PO₄ in 1l H₂O) or HL5 medium (5g yeast extract, 10g proteose peptone, 50mM glucose, 8.5mM KH₂PO₄, made up to 1l with H₂O; pH7.5). Cells can be brought up in culture dishes, in shaking cultures at 150rpm or on lawns of non-pathogenic *Klebsiella aerogenes*. To cultivate the mutants the media were supplemented with the appropriate antibiotics. For long time storage, spores of mature fruiting bodies were brought up on Soerensen phosphate agar plates (10g Bacto-agar, dissolved in 1l Soerensen buffer), and were resuspended in Soerensen phosphate buffer (14.6mM KH₂PO₄, 2mM Na₂HPO₄; pH6.0).

Afterwards the spores were shock-frozen in liquid nitrogen and stored at -80°C.

For transformation, electroporation was used with the appropriate plasmids. 2x10⁷ cells were extensively washed in cold Soerensen buffer and electroporation buffer (50mM sucrose, 10mM KH₂PO₄; pH6.1) and resuspended in 1ml cold electroporation buffer. In the presence of 25µg DNA, the cells were electroporated in a 4mm electroporation cuvette using a Gene Pulser XCell (Biorad), applying the standard settings (square wave, V=1.0kV, 1ms pulse length, two pulses, five seconds pulse interval). After gentle shaking (50rpm, room temperature, 15 minutes) in a cell culture dish 2µM CaCl₂ and 2µM MgCl₂ were added. The cells were incubated in HL5 medium after additional 15 minutes, and the cells were allowed to recover for about 24 hours before the respective antibiotic (either 10µg/ml gentamicin or blasticidin) was applied to select the transformants.

Single clones were amplified via spreader dilution with non-pathogenic *K. aerogenes* on SM agar plates (9g agar, 10g peptone, 50mM glucose, 1g yeast extract, 4mM MgSO₄, 16mM KH₂PO₄, 5.7mM K₂HPO₄ in 1l with H₂O; pH6.5). The overexpression of fluorescently labeled proteins was checked via live-cell microscopy.

2.2.3.2 Live-cell microscopy of *D. discoideum* amoebae

After cells were transferred onto coverslips and allowed to settle down, they were washed twice with Soerensen buffer. Confocal images were taken by the usage of an inverted laser scanning microscope (LSM) 510 confocal microscope (Zeiss) equipped with a 40x LDA-Plan 0.50 Ph2, a 63x Neofluar 1.4 or a 100x Neofluar 1.3 oil immersion objective. For excitation, the 488nm argon ion laser line and the 543nm helium neon laser lines were used. Emission was collected using a 510-525nm band-pass and a 585-615nm band pass filter.

For recording of phagocytosis at the LSM 510 confocal microscope (Zeiss), cells were incubated with a suspension of heat-killed *S. cerevisiae* cells (Sigma-Aldrich) labeled with tetramethyl rhodamine isothiocyanate (TRITC; Sigma) in Soerensen buffer for 20 minutes, and recorded at intervals of 10 seconds.

2.2.3.3 Immunofluorescence microscopy

Indirect immunofluorescence studies were used to investigate subcellular localization of proteins. In advance, cover slips were washed with 3.6% HCl and rinsed with H₂O. 5x10⁶ cells/ml were harvested, washed twice in Soerensen buffer and allowed to settle on the coverslips for 15 minutes. Subsequently, the medium was removed and the cells were fixed with methanol (-20°C for 10 minutes). Afterwards, the coverslips were washed several times with phosphate buffered saline (PBS; 137mM NaCl, 2.7mM KCl, 8.1mM Na₂HPO₄, 1.5mM KH₂PO₄; pH7.4) supplemented with 100mM glycine. After washing the samples with phosphate buffered glucose (PBS + 0.5% BSA, 0.045% fish gelatin), they were incubated with the primary antibody overnight at 4°C. The next day, preparations were washed with PBG and incubated for 60 minutes with the secondary adequate antibody, which was fluorescence-dye labeled (e.g. goat-anti-mouse IgG Cy3-conjugated). TOPRO (Invitrogen) was used to stain the DNA. At last the coverslips were quickly rinsed with H₂O, embedded in gelvatol mounting medium (0.14M NaCl, 0.01M KH₂PO₄ /Na₂HPO₄ pH7.2, 5.7M polyvinyl alcohol, 0.5mM glycerol, 0.9mM DABCO) and stored in the dark at 4°C. Confocal microscopy data were acquired on an inverted LSM 510 confocal microscope (Zeiss) with a 63x or 100x oil immersion objectives with a numerical aperture of 1.4 and 1.3, respectively. Excitation of fluorophores was achieved with the 488nm argon ion laser line, the 543nm and 633nm helium laser lines, and emission was collected using 510-525nm band-pass, 585-615nm band-pass or 650nm long-pass filters.

2.2.3.4 Induction of nuclear and cytoplasmic rods

D. discoideum cells were exposed to 5% dimethylsulfoxide (DMSO) in HL5 medium to induce nuclear protein rod formation, respectively 10mM sodium azide (NaN₃) dissolved in HL5 medium, to provoke the formation of cytoplasmic protein rods.

Both applications were carried out at 28°C for one hour. Cells with induced nuclear rods were treated consecutively as described in immunofluorescence microscopy (2.2.2.4), whereas cytoplasmic rods were imaged under live-cell conditions (2.2.2.3).

2.2.3.5 Growth and germination

To determine any differences in growth of AX2 mutants, *D. discoideum* cells were brought up to densities below 5x10⁶ cells/ml. After washing the cells in Soerensen buffer, they were adjusted to a density of 5x10⁴ cells/ml. 30ml of cell suspension were shaken at 150rpm, 21°C in 100ml Erlenmeyer flasks without any supplementary antibiotics. Densities of cell cultures were determined two times daily.

100 spores were plated together with the non-pathogenic feeding bacterium *K. aerogenes* on SM agar plates. The viability of spores was investigated by counting the number of plaques after 96 hours.

2.2.3.6 Phagocytosis measurements

Phagocytosis of yeast by *D. discoideum* cells was measured through fluorescence spectroscopy. Cells were grown to 6×10^6 cells/ml, harvested, washed, resuspended in Soerensen buffer and adjusted to a density of 2×10^6 cells/ml. 12ml of this solution were shaken at 150rpm and 21°C in a 25ml Erlenmeyer flask for one hour. TRITC-labeled yeast cells ($120 \mu\text{l}$ of 10^9 cells/ml) were added. Samples of 1ml were withdrawn every 10 minutes and added to $100 \mu\text{l}$ of trypan blue solution (20mg/ml dissolved in 20mM sodium citrate containing 150mM NaCl), which quenched the fluorescence of non-internalized yeast cells. After three minutes of agitated incubation, cells were spun and the supernatant was removed carefully. After resuspension in Soerensen buffer, fluorescence was measured in a fluorometer using 544nm light for excitation.

To check the ability of phagocytosing bacteria, single clones from *D. discoideum* cells were picked from the edges of colonies growing on plated non-pathogenic *K. aerogenes* and transferred to the middle of new non-pathogenic *K. aerogenes* lawns on SM agar plates. The diameter of the developing plaque was measured daily.

2.2.3.7 Analysis of phototaxis and development

Using a sterile inoculation loop, cells were transferred onto water agar plates from the edges of colonies growing on non-pathogenic *K. aerogenes* lawns to test the phototaxis efficiency of different cell lines. The plates were stored in a darkly colored box with a 2mm wide opening for the entry of light. After incubation at 21°C for 48 hours, the tracks of the migrating slugs could be visualized by transferring them onto a nitrocellulose membrane and final amido black staining.

The 24 hours cell cycle was induced in washed 5×10^6 cells/ml. Wild type and mutant cells were transferred onto nutrient free phosphate agar plates to document developmental stages by time-lapse photography. Pictures were taken every 10 minutes for 24 hours.

3. Results

3.1 The actinome of *D. discoideum*

3.1.1 Phylogeny of the *D. discoideum* actinome

The bacterial actin murein cluster e proteins (MreB) have been known for a long time to be cell shape determinants and are present in gram-positive and gram-negative bacterial cells (Wachi et al., 1987). They also contain five conserved sequence motifs to determine the three dimensional fold similar to that of actin, including the nucleotide binding pocket (Carballido-Lopez, 2006). Furthermore, MreB filaments are generated by actin-like polymerization and show similar dynamics. Although just 15% identity exists between MreB and conventional actin, they are assumed to be structural and functional homologues of actin (Bork et al., 1992). As MreB and actins are putative descendants from a common ATP-binding ancestor, MreB (*E.coli*; E0J6V5) was used as outgroup for the phylogenetic tree of the *D. discoideum* actinome. All 17 conventional actin genes are represented by Act8. The ARPs are displayed in green, the actin variants are shown in dark blue. Phylogenetic analyses illustrated that Act3 is closely related to conventional actin (11 different amino acids), whereas Act18 contains more mutations (45 different amino acids). Act31 has evolved independently (224 different amino acids) and is more closely related to the protein sequences of the ARPs (Eichinger et al., 2005).

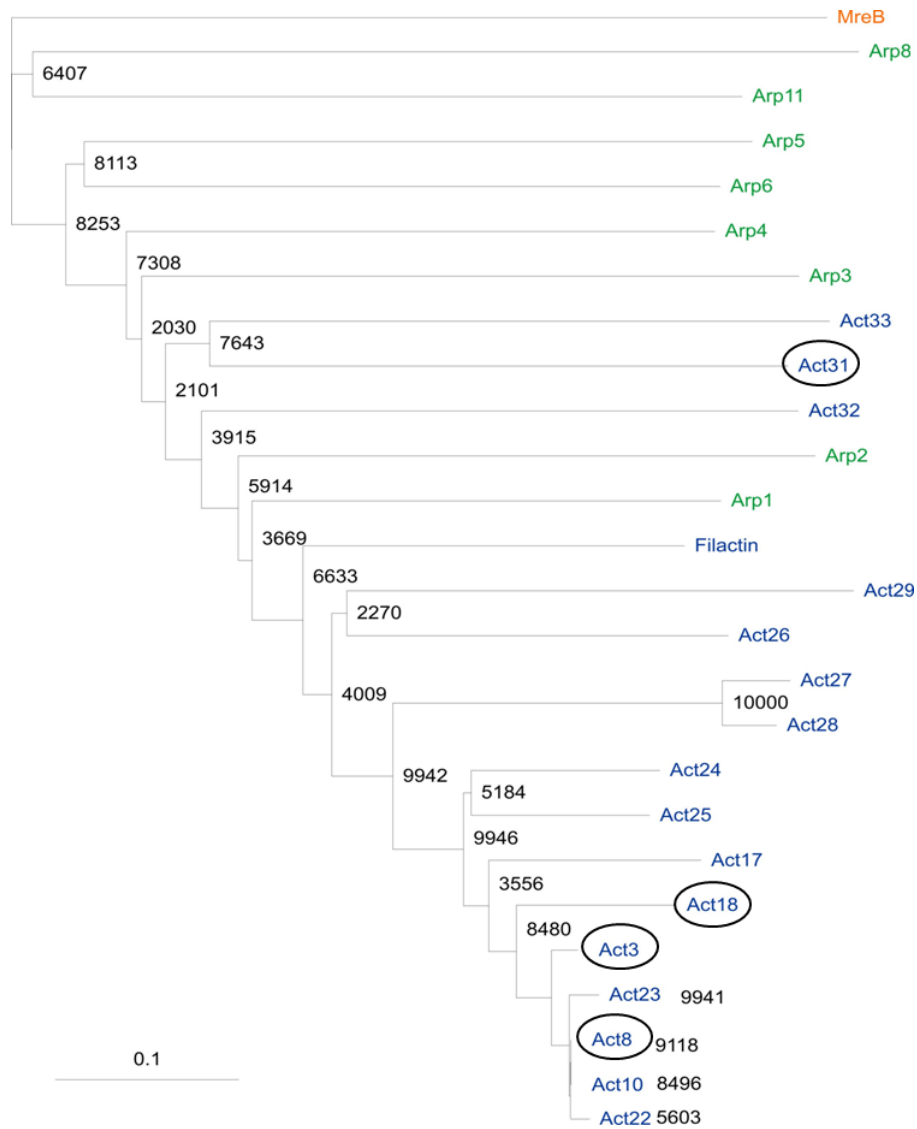
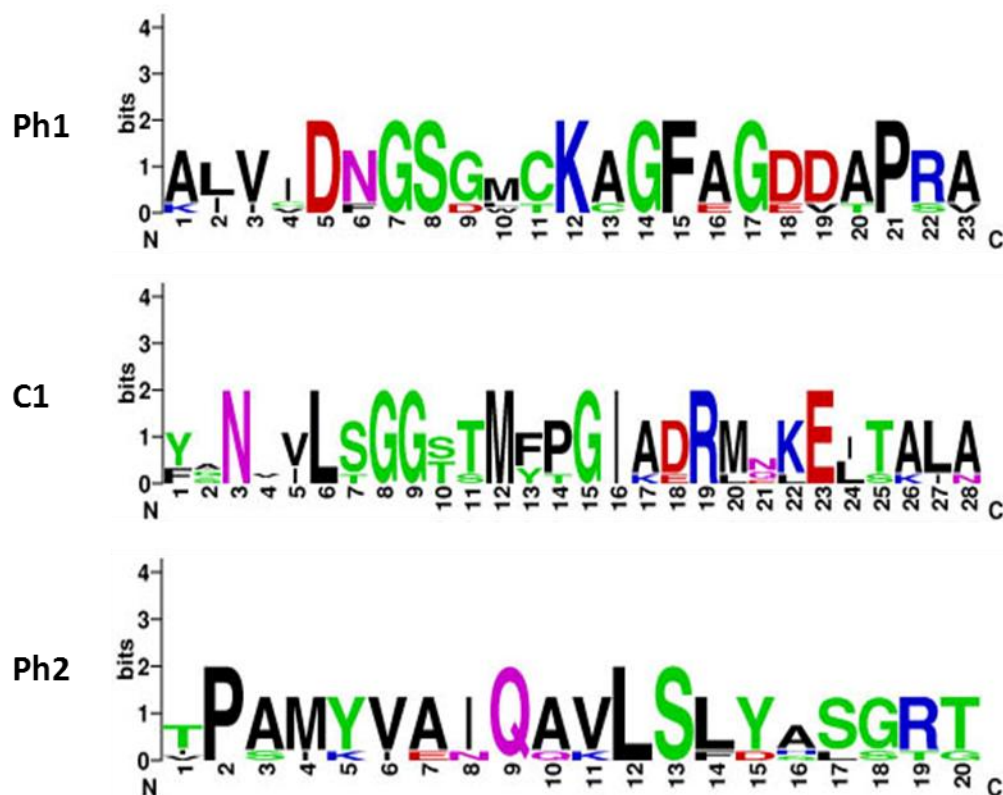


Figure 8: Phylogenetic tree of the *D. discoideum* actinome. ClustalX2 was used for tree construction and 1000 trees were generated. For tree visualization Treeview 1.6.6 was used. Act8 represents the 17 conventional actin isoforms. Labels at the branch nodes are bootstrap values, calculated at the basis of 10.000 bootstrap trials. 0.1 amino acid substitution per site is shown by the branch length and corresponds to the scale bar. Actin variants of interest in this thesis are highlighted (black eclipses). Act3 showed the closest relation to Act8 due to gene duplication events, whereas Act18 exhibited more amino acid substitutions. Due to its strong phylogenetic relation to the ARPs, Act31 is called ‘orphan ARP’.

3.1.2 Sequence motifs

As the function of a protein in general is determined by its surface, five sequence motifs are seen as characteristic for all actins. Via protein sequence alignments the motifs (i) phosphate binding motif 1 (Ph1), (ii) connecting motif 2 (C2), (iii) phosphate motif 2 (Ph2), (iv) adenosine motif (Ad), and (v) the connecting motif 1 (C1) could be identified in human β -actin (P60709), rabbit muscle actin (P68135), and the *D. discoideum* actins Act16 (DDB_G0272248), Act3 (DDB_G0289487), Act18 (DDB_G0289489) and Act31 (DDB_G0269476). The amino acids were colored according to their chemical properties; polar amino acids (G, Y, C, S, T) are shown in green, amidated amino acids are visualized in pink (N, Q), basic amino acids are displayed in blue (K, R, H), acidic amino acids are depicted in red (D, E) and hydrophobic amino acids (A, V, L, I, P, W, F, M) can be seen in black. Big letters indicate a high level of conservation of the respective residue, whereas smaller letters display amino acids which are more variable. A constantly high degree of conservation could be observed for all five sequence motifs in the compared actins, independent from the chemical properties of the amino acids.



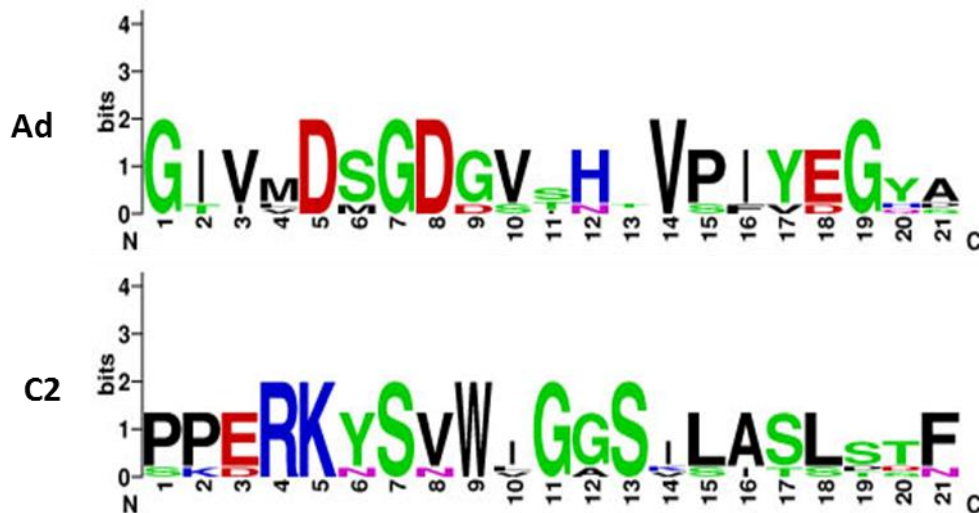


Figure 9: Motif logos of human β -actin, rabbit actin, and the *D. discoideum* actins Act16, Act3, Act18 and Act31. Sequence logos were designed using Weblogo 2.0. The sequence logos show the five structural motifs: Ph1, C1, Ph2, Ad and C2. The single amino acids are colored according to their chemical properties (polar amino acids=green, amidated amino acids=pink, basic amino acids=blue, acidic amino acids=red and hydrophobic amino acids=black). Big letters indicate a high level of conservation of the particular residue, whereas smaller letters display amino acids which are more variable. A constant high degree of conservation could be observed between all compared actins.

3.1.3 Structural homologies

We created the putative three dimensional ribbon models of human β -actin (P60709), rabbit muscle actin (P68135), Act16 (DDB_G0272248), Act3 (DDB_G0289487), Act18 (DDB_G0289489) and Act31 (DDB_G0269476) bioinformatically. Act8 (P07830) of *D. discoideum* in the ADP-state was used as a template. High similarities between the compared actins were obvious.

The supposed structures were organized like conventional actins with domain 2 at the left and domain 1 at the right which both could be subdivided further into a total of four subdomains (see also figure 3).

Despite the differences in primary structures all actins exhibit the typical domain structure of G-actin, including the ATP-binding pocket. As expected, Act31 showed the strongest deviation in its tertiary structure, whereas Act16 is identical to Act8, because it belongs to those 17 gene products with identical amino acid sequences.

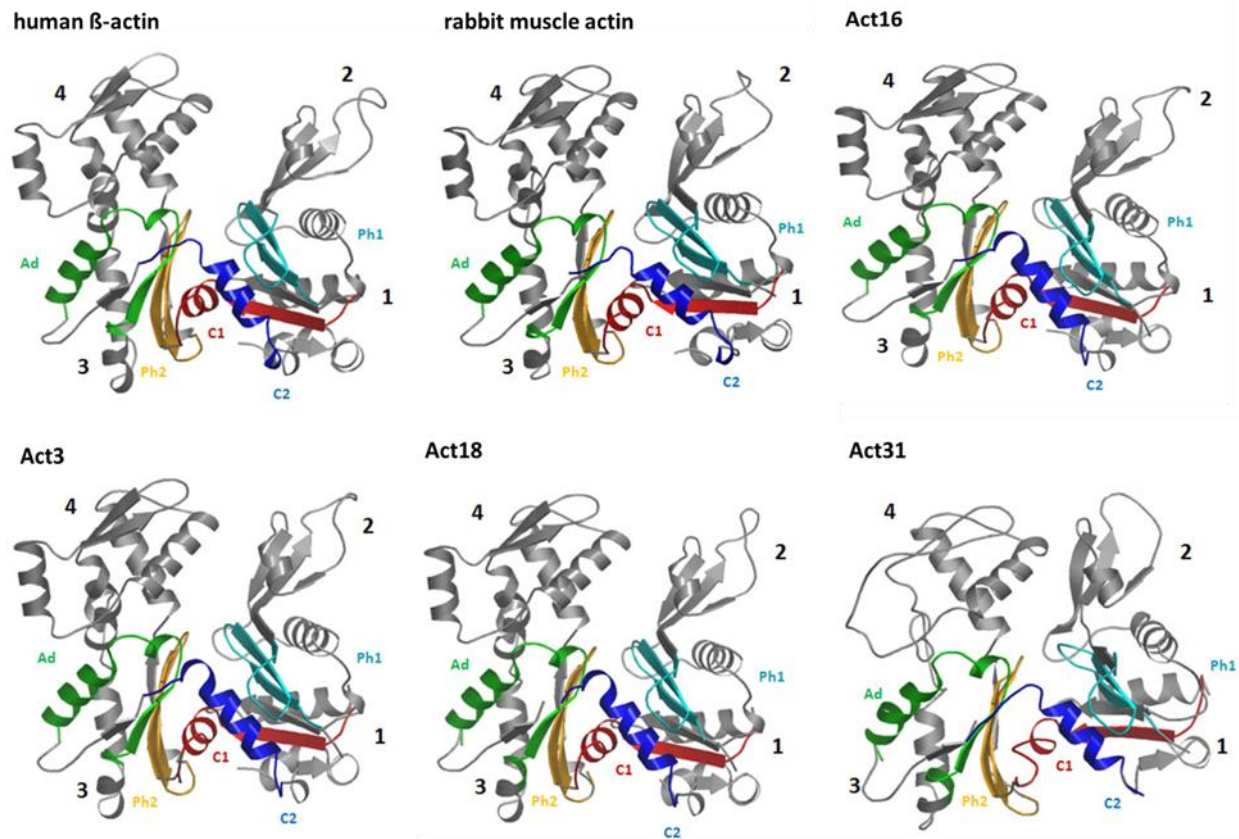


Figure 10: Ribbon-models of human β -actin, rabbit actin, and the *D. discoideum* actins Act16, Act3, Act18 and Act31. Modeling was done using Swiss Model Expaty and OpenAstexViewer to show structural homologies among the actin variants. The ribbon-model of the *D. discoideum* Act8 (P07830) in the ADP state (Joseph et al., 2008) was used as a template. The four domains were marked (1-4) as well as the five structural motifs (Ph1= light blue, C1=red, Ph2=orange, Ad=green and C2=dark blue). The typical domain structure of G-actin and the ATP-binding pocket could be observed in all compared actins.

3.2 Flag-tagged actin variants

To analyse actin dynamics *in vitro*, we expressed Flag-tagged Act16, Act3, Act18 and Act31 using the baculoviral expression system of *Spodoptera frugiperda* (Sf9) cells. As posttranslational modifications, correct folding and oligomerization of recombinant proteins are possible, this eukaryotic protein expression system was useful to amplify the recombinant proteins. Supplementary to the proper biological activity and function, the high yields in protein expression was a significant advantage.

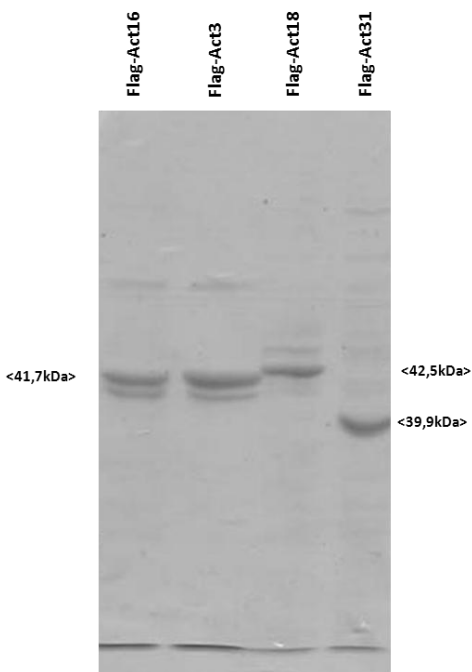


Figure 11: Flag-tagged actin variants purified from Sf9 cells.

Flag-Act16 and Flag-Act3 had a molecular weight of 41.7kDa, whereas Flag-Act18 could be detected at 42.5kDa. Flag-Act31, exhibited a molecular mass of 39.9kDa. All variants were stable towards proteolytic degradation and could be obtained to comparable amounts.

3.2.1 Nucleating activities of Flag-actin variants

To investigate the impact on actin polymerization, the purified Flag-tagged actin variants were examined in fluorometric approaches. Fluorescence spectroscopy assays make use of G-actin covalently labeled with a fluorescent dye (pyrene-actin), which increases the fluorescence spectrum when it is polymerized into F-actin. Polymerization buffer induced the formation of actin filaments in 2 μ M rabbit actin (10% pyrenylated) that served as reference. The fluorescence spectrometer LS55 (365nm excitation) was used to measure the developing fluorescence signal. When we incubated 0.5 μ M Flag-Act16, respectively 0.5 μ M Flag-Act3, with 2 μ M rabbit actin under polymerizing conditions, the formation of F-actin was promoted and the lag-phase was drastically shortened. Potential effects caused by the elution buffer could be excluded, as the incubation of 2 μ M rabbit actin with an adequate volume of elution buffer had no influence on actin dynamics.

We tested the effect of different concentrations of Flag-Act16 and Flag-Act3 on actin dynamics and incubated 0.1 μ M, 0.3 μ M, 1 μ M, respectively 2 μ M of the Flag-tagged actins with 2 μ M rabbit actin under polymerizing conditions. It was obvious that with increasing concentrations of Flag-Act16 or Flag-Act3, the lag-period of F-actin formation was gradually shortened.

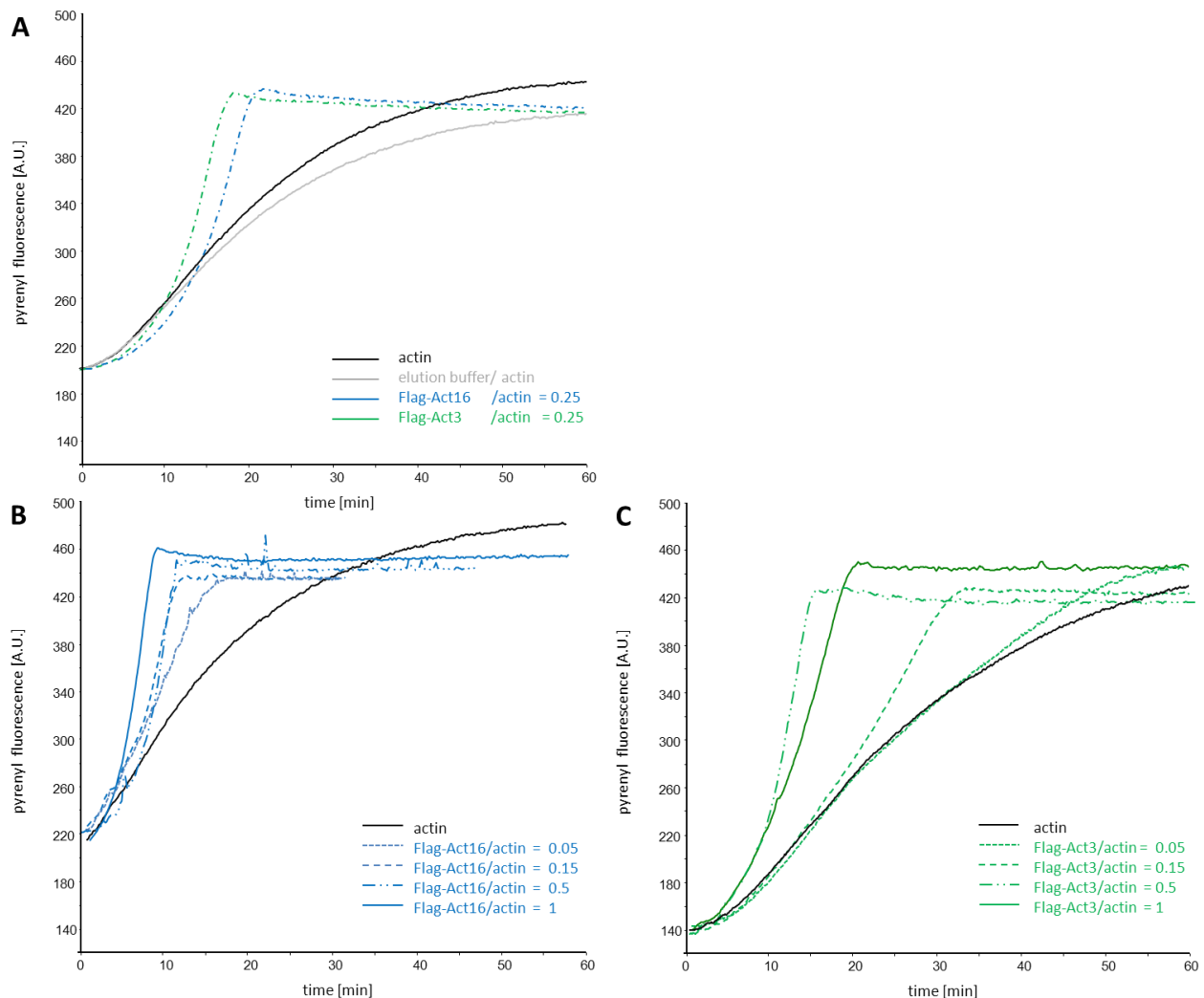


Figure 12: Fluorometric analysis of the influence of Flag-Act16 and Flag-Act3 on actin polymerization.

We incubated Flag-Act16, respectively Flag-Act3, with rabbit actin under polymerizing conditions. As pyrene-labeled actin raises the fluorometric signal during polymerization, we measured the signals with the fluorescence spectrometer LS55 (365nm excitation). A) Incubation of Flag-Act16, respectively Flag-Act3, with rabbit actin provoked a shortened lag-phase during actin polymerization. Effects caused by the elution buffer could be excluded. B) Adding increasing concentrations of Flag-Act16 to rabbit actin, the lag-period was gradually reduced. C) Adding increasing concentrations of Flag-Act3 to rabbit actin induced a stepwise shortening of the lag-phase.

We also checked Flag-Act18 and Flag-Act31 for potential nucleating activities and incubated 0.1 μ M, 0.2 μ M and 0.5 μ M Flag-Act18, respectively Flag-Act31, with 2 μ M rabbit actin under polymerizing conditions. No significant effects on actin polymerization could be determined by adding Flag-Act18, respectively Flag-Act31.

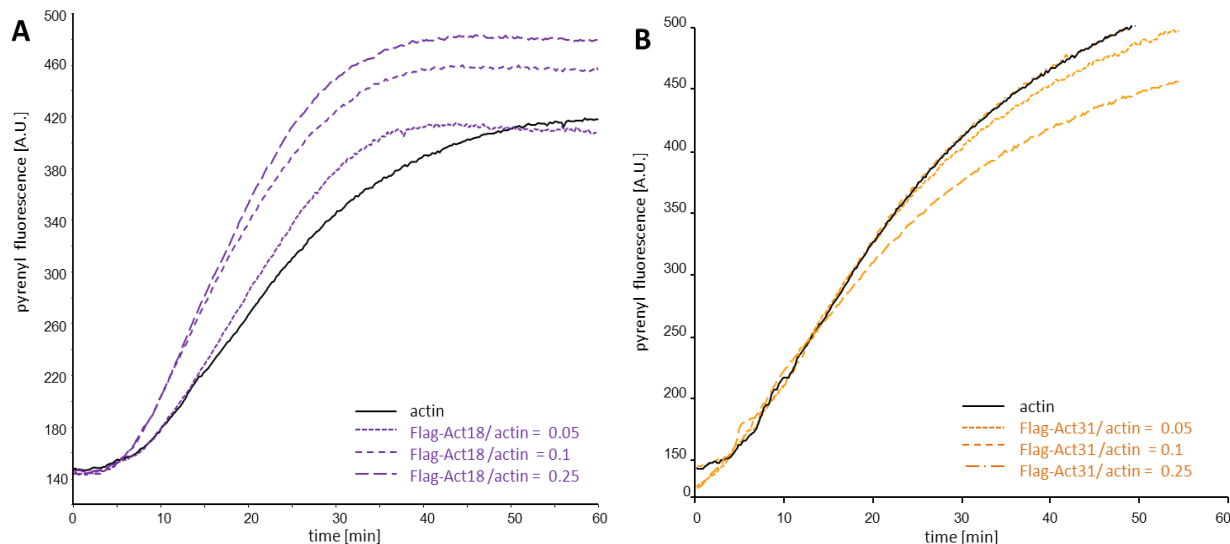


Figure 13: Fluorometric analysis of the influence of Flag-Act18 and Flag-Act31 on actin polymerization.

We incubated Flag-Act18, respectively Flag-Act31 with rabbit actin under polymerizing conditions. As pyrene-labeled actin raises the fluorometric spectrum during polymerization, we measured the signals with the fluorescence spectrometer LS55 (365nm excitation). A) Incubation of Flag-Act18 with rabbit actin did not show any influence on rabbit actin polymerization. B) Adding Flag-Act31 to rabbit actin did not change the actin dynamics *in vitro*.

The addition of salts at physiological concentrations to a solution of G-actin increases the rate of ATP-hydrolysis by a factor of 100. Consequently, a tight coupling between actin monomer interactions and ATP-hydrolysis is assumed. The ATPase activity per actin monomer under non-polymerizing conditions is independent of the total monomer concentration, as every single actin subunit has an intrinsic ATPase activity. The stimulation of the actin ATPase activity seen after addition of salts might be due to changes in ionic conditions and conformational changes occurring during subsequent incorporation of the actin monomers into the filaments (Pollard & Weeds, 1984). To test possible salt influences we added 100mM KCl to different actin polymerization arrays, whereby we incubated 2 μ M rabbit actin with 0.5 μ M, 1 μ M and 2 μ M Flag-Act16, respectively Flag-Act3, under polymerizing conditions. The polymerization of 2 μ M rabbit actin was used as reference. Surprisingly, the nucleating activity of Flag-Act16 and Flag-Act3 was abolished by the addition of physiological salt concentrations. Consequently, the lag-phase of the rabbit actin correlated with the measured lag-phases of polymerizing rabbit actin plus Flag-Act16, respectively plus Flag-Act3.

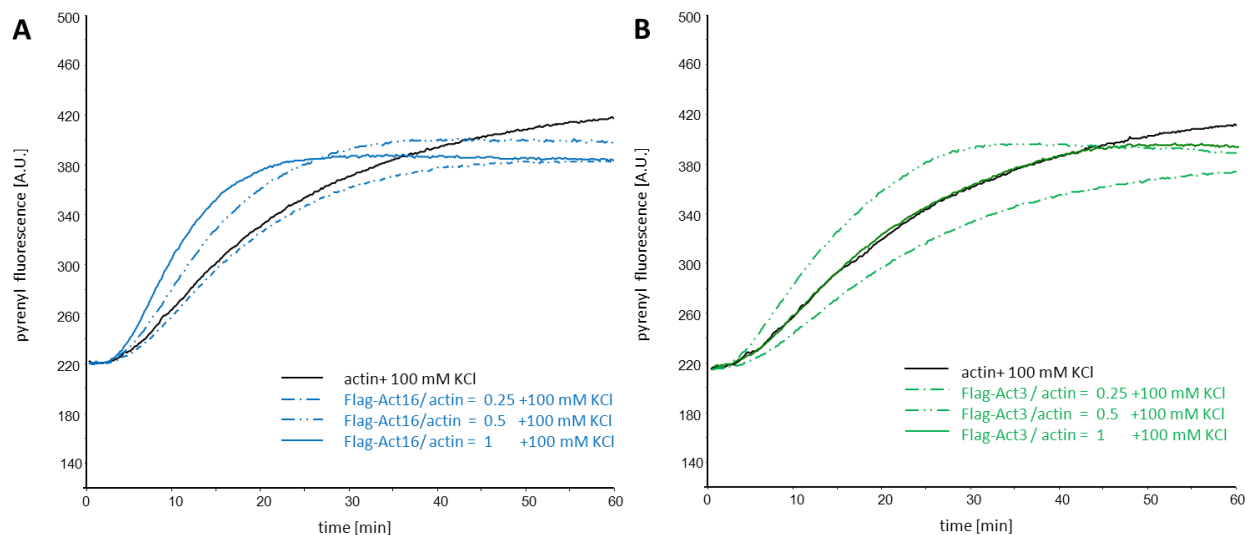


Figure 14: Fluorometric analysis of the influence of 100mM KCl on actin polymerization. We incubated in the presence of 100mM KCl Flag-Act16, respectively Flag-Act3, with rabbit actin under polymerizing conditions. As pyrene-labeled actin raises the fluorometric spectrum during polymerization, we measured the signals with the fluorescence spectrometer LS55 (365nm excitation). A) Adding 100mM KCl to Flag-Act16 and rabbit actin abolished the nucleating activity of Flag-Act16 on rabbit actin polymerization. B) If we applied 100mM KCl to a mixture of Flag-Act3 and rabbit actin, promotion of actin polymerization was abolished.

3.2.2 Influences of Flag-actin variants on actin filaments

When actin filaments are long enough to become entangled, the viscosity of an actin solution increases, which is measurable as a gain of time a mini steel ball needs to pass a certain distance (MacLean-Fletcher & Pollard, 1980). To check the role of Flag-tagged Act16, Act3, Act18 and Act31 in a network of actin filaments, we incubated 0.165 μ M, 0.183 μ M, 0.206 μ M, 0.236 μ M, 0.275 μ M, 0.33 μ M, 0.413 μ M, 0.55 μ M, 0.825 μ M, 1.65 μ M and 3.3 μ M of Flag-Act16, Flag-Act3, Flag-Act18, respectively Flag-Act31 with 16.5 μ M rabbit actin. Afterwards we filled the solution into a capillary and allowed polymerization for 15 minutes. Subsequently the apparent viscosity was measured. 16.5 μ M polymerized rabbit actin was set as reference. We could show that with increasing concentrations of Flag-Act16, respectively Flag-Act3, the viscosity of the actin polymer solution decreased drastically. When we applied a molar ratio of Flag-Act16/ actin = 0.11, respectively Flag-Act3/ actin = 0.11, the recorded time was reduced down to 5%, in comparison to the reference.

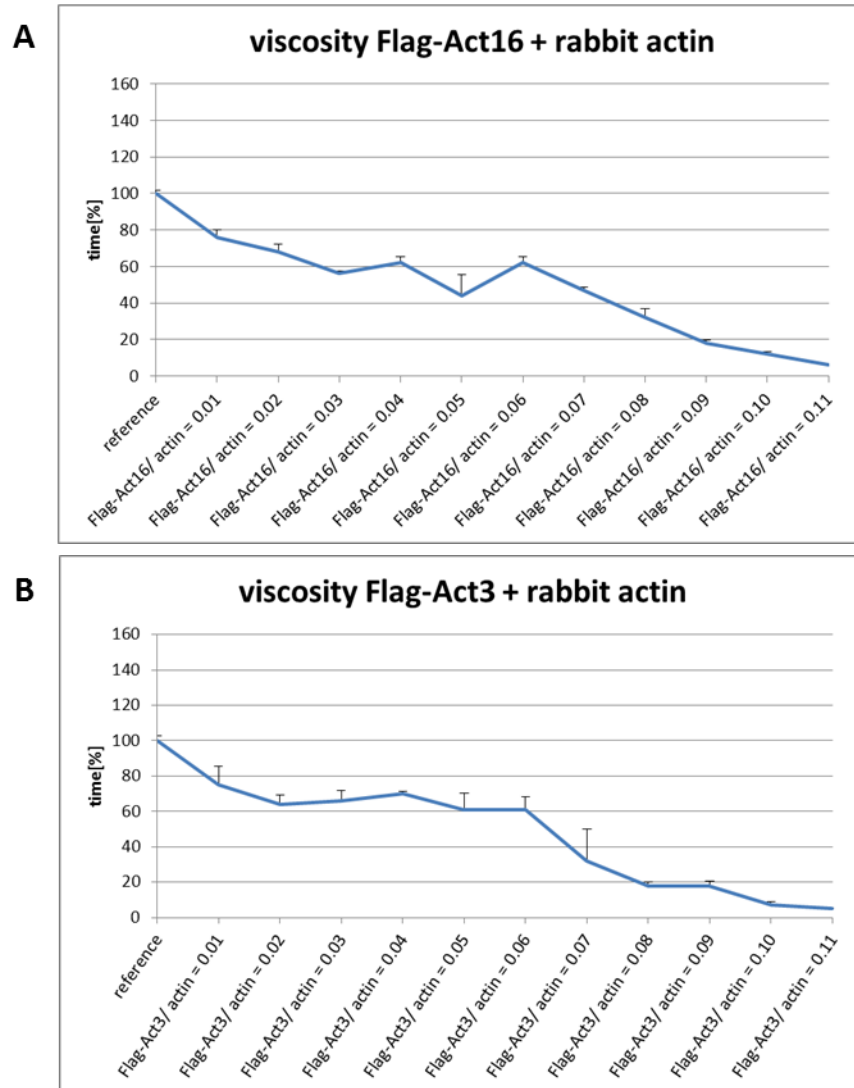


Figure 15: Viscometric analysis of the effects of Flag-Act16 and Flag-Act3. We incubated $16.5\mu\text{M}$ rabbit actin with different concentrations of Flag-Act16, respectively Flag-Act3, and induced polymerization within a capillary. Three independent experiments were conducted. A) With increasing amounts of Flag-Act16 in the polymerizing actin solution, the viscosity declined strongly. At a molar ratio of 0.11, the recorded time was reduced to 5% in comparison to the reference. B) Performing the low shear viscosity assay with increasing ratios of Flag-Act3, the viscosity decreased gradually. Adding a molar ratio of 0.11 of Flag-Act3 minimizes as well the measured time down to 5%, in comparison to the reference.

The influence of Flag-Act18 and Flag-Act31 on polymerized rabbit actin was much less dramatic, with Flag-Act18 even neglectable. This suggests that the dramatically reduced viscosity with Act16 and Act3 is a rather specific activity.

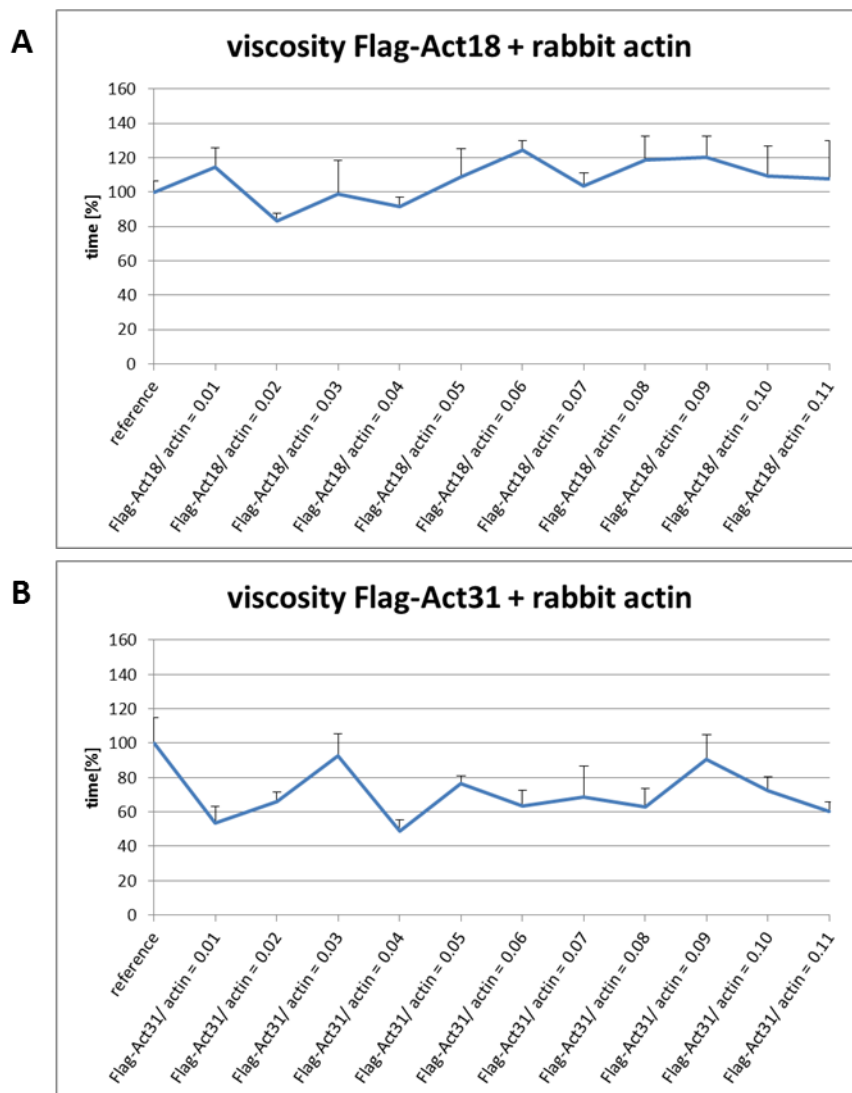


Figure 16: Viscometric analysis of Flag-Act18 and Flag-Act31 activities. We incubated 16.5 μ M rabbit actin with different concentrations of Flag-Act18, respectively Flag-Act31 and induced polymerization within a capillary. Three independent experiments were conducted. A) The viscosity of polymerized rabbit actin was not affected when we applied different concentrations of Flag-Act18. B) Performing the low shear viscosity assay with increasing ratios of Flag-Act31, the viscosity of polymerized rabbit actin seemed not to be significantly affected.

3.2.3 Depolymerization of F-actin

To further investigate the decline of viscosity observed in the low shear viscometry assays, the Flag-actin variants were checked for capping activities in the F-actin network. As a control we measured prepolymerized 0.1 μ M rabbit actin (100% pyrenylated) with 0.0075 μ M Cap32/34 (molar ratio 0.075). Prepolymerized 0.1 μ M rabbit actin depolymerized fast below the critical concentration.

We could show that with a molar ratio of 0.075 Cap32/34, the prepolymerized F-actin network was prevented from disassembly, even at the critical concentration of $0.1\mu\text{M}$ F-actin. When we applied our Flag-tagged actin variants Flag-Act16, Flag-Act3, Flag-Act18 and Flag-Act31 to prepolymerized $0.1\mu\text{M}$ rabbit actin, the rapid depolymerization of the F-actin network did not change, independent from the applied concentrations. In every conducted measurement we also checked potential effects of the elution buffer. As the depolymerization was not affected when we added appropriate volumes, buffer-based effects could be excluded.

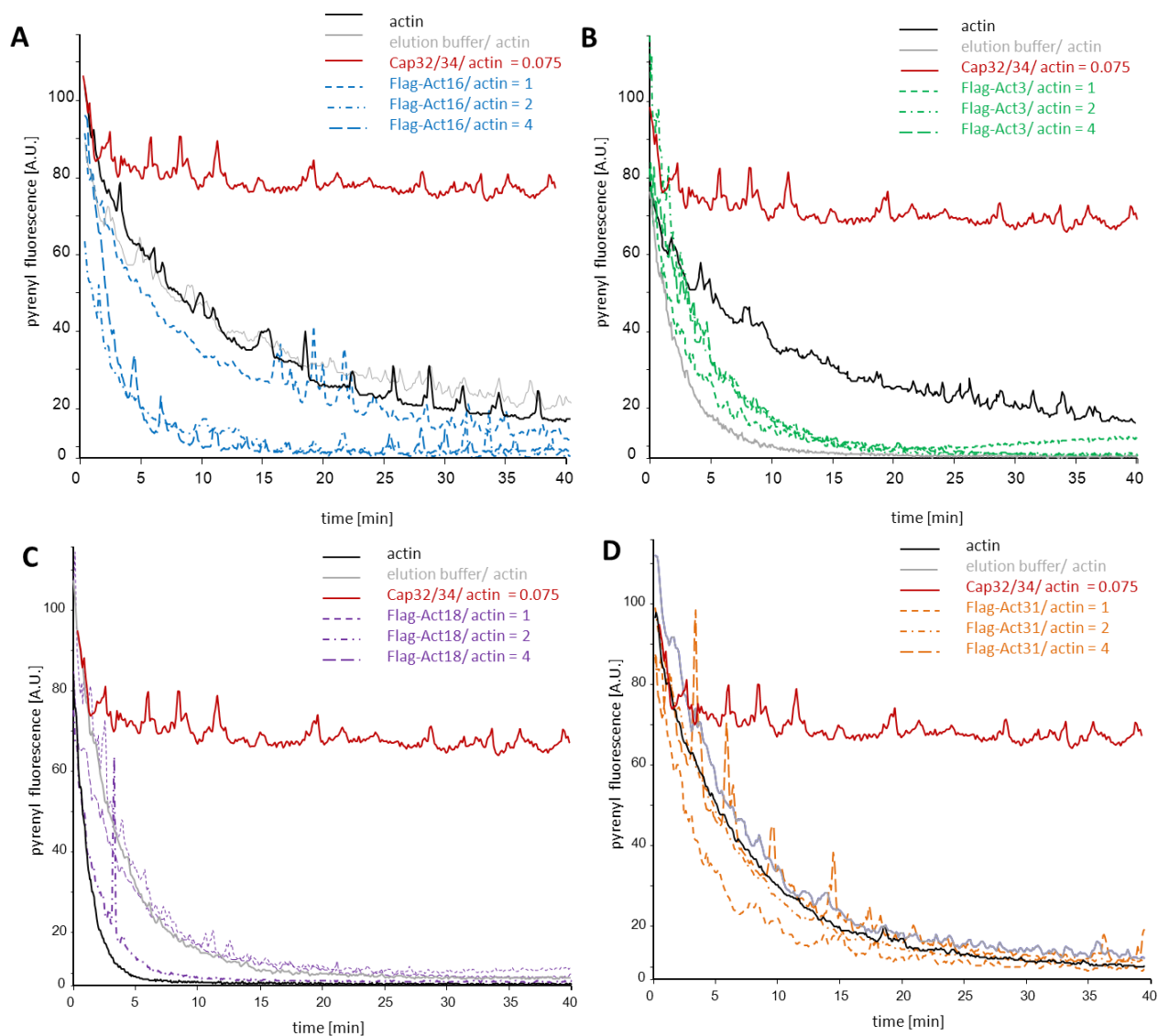


Figure 17: Fluorometric analysis of putative capping activities of Flag-Act16, Flag-Act3, Flag-Act18 and Flag-Act31. We incubated prepolymerized rabbit actin (100% pyrenylated) with Flag-Act16, Flag-Act3, Flag-Act18 and Flag-Act31. As a control we measured prepolymerized $0.1\mu\text{M}$ rabbit actin plus $0.0075\mu\text{M}$ Cap32/34 in every approach. Measurements of the fluorescence signal were conducted with the fluorescence spectrometer LS55 (365nm excitation). A)-D) The application of different concentrations of actin variants did not prevent $0.1\mu\text{M}$ F-actin from disassembly. The elution buffer had no effect.

3.2.4 Sedimentation assays

Besides fluorescence spectroscopy and low shear viscometry, sedimentation assays are also helpful tools to analyze actin polymerization. The basis of the sedimentation assay is the ability to pellet F-actin, but not G-actin. Therefore, Flag-actin variants which were associated with rabbit actin could be detected in the pellet. 2 μ M rabbit actin (42.0kDa) was used as reference. After a short 10.000g centrifugational step to remove short oligomers and byproducts, we incubated 2 μ M of Flag-Act16, Flag-Act3, Flag-Act18 and Flag-Act31 with 5 μ M rabbit actin under polymerizing conditions and centrifuged them at 100.000g. For exact detection of proteins, silver staining of the SDS-gel was conducted. Concomitantly as in previous experiments, about 60% of Flag-Act16 and Flag-Act3 (both 42.7kDa) seemed to be associated with rabbit F-actin, whereas the remaining 40% were detectable in the supernatant. In contrast, Flag-Act18 (43.5kDa) could not be pelleted at all and was found exclusively in the supernatant after ultracentrifugation. Surprisingly, about 40% of Flag-Act31 (40.9kDa) were found in the pellet after ultracentrifugation. The remaining 60% seemed to be in the supernatant.

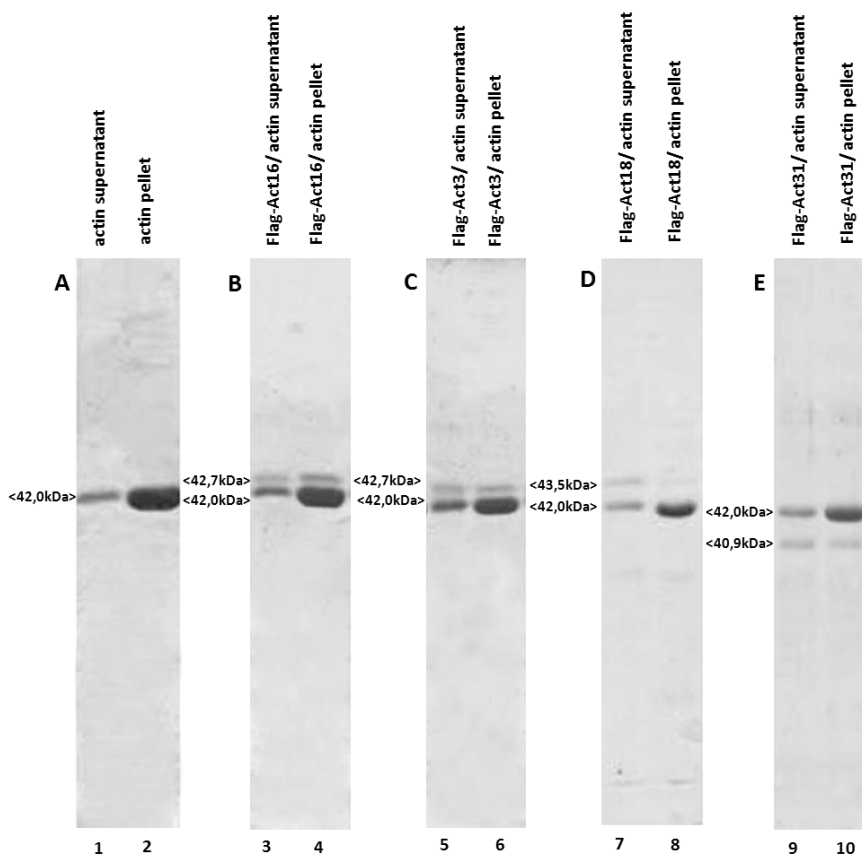


Figure 18: Sedimentation assay to study if Flag-Act16, Flag-Act3, Flag-Act18 and Flag-Act31 bind to rabbit F-actin. We incubated 2 μ M of the respective Flag-actin variant with 5 μ M rabbit actin under polymerizing conditions and pelleted the mixture at 100.000g. The analysis was done by silver staining the SDS-gel. Rabbit actin alone was used as reference. A) About 80% of the applied rabbit actin (42.0kDa) could be detected in the pellet. B) According to the signal in the pellet, about 60% of Flag-Act16 (42.7kDa) seemed to be associated with rabbit actin. C) Comparable to Flag-Act16, about 60% of Flag-Act3 (42.7kDa) are present in the 100.000g pellet. D) FlagAct18 (43.5kDa) was apparently not copolymerizing with rabbit actin. E) Concomitantly with previous experiments, about 40% of Flag-Act31 (40.9kDa) occurred in the 100.000g pellet.

3.2.5 Phalloidin stabilized F-actin

Phalloidin poisons a cell by preventing actin filaments from depolymerizing. Isolated from *Amanita phalloides* (a mushroom commonly known as the 'death cap'), phalloidin binds at the interface between subunits in F-actin and locks adjacent subunits together. Even when actin is diluted below its critical concentration, phalloidin-stabilized filaments will not depolymerize (Lodish et al., 2000). Hence we incubated 2 μ M of Flag-Act16, Flag-Act3, Flag-Act18 and Flag-Act31 with 4 μ M phalloidin (molar ratios 0.5) to check if the Flag-tagged actin variants were able to form filaments without rabbit actin. Analysis was done by silver staining the SDS-gel. As a control, 2 μ M rabbit actin were polymerized together with 4 μ M phalloidin (molar ratio 0.5). Flag-Act16 (42.7kDa) was not able to form sedimentable filaments stabilized with phalloidin, as it was detectable only in the supernatant. 50% of Flag-Act3 (42.7kDa) remained in the supernatant. About 70% of Flag-Act18 (43.5kDa) remained unassembled in the supernatant. According to the presented silver stain, Flag-Act31 (40.9kDa) remained exclusively in the supernatant.

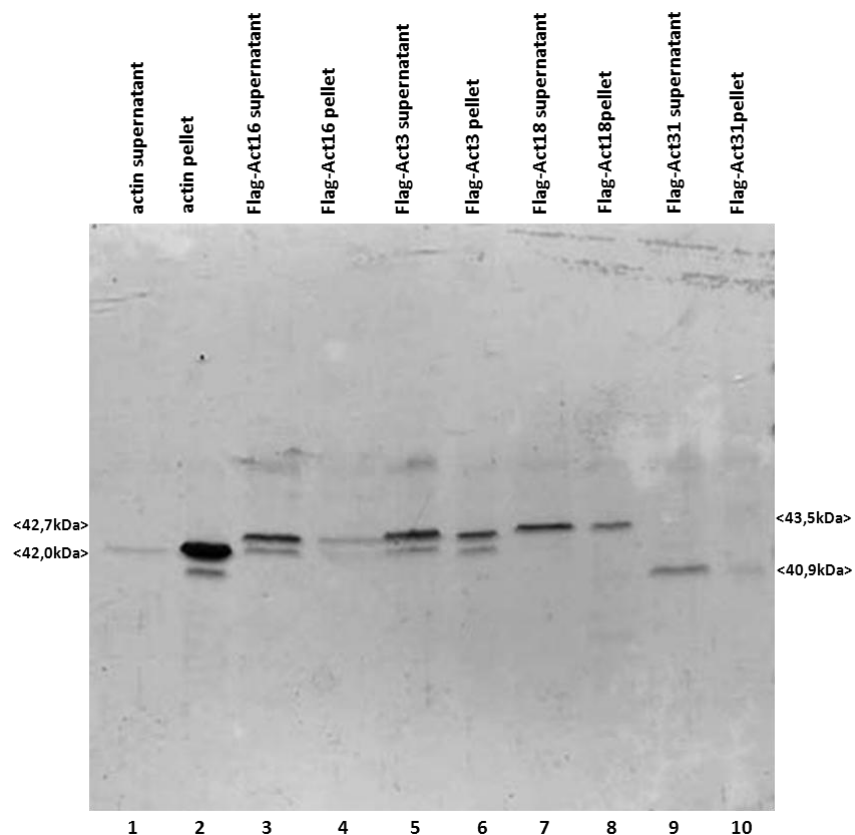


Figure 19: Sedimentation of Flag-Act16, Flag-Act3, Flag-Act18 and Flag-Act31 in the presence of phalloidin.

The Flag-actin variants have been incubated with a two-fold molar excess of phalloidin and centrifuged at 100.000g. 2 μ M rabbit actin was used as reference. Proteins were visualized by silver staining. Rabbit actin (42.0kDa) formed stable and sedimentable F-actin. Among the actin variants only Flag-Act3 and Flag-Act18 showed significant amounts of protein in the pellets.

To observe a potential formation of actin filaments 1 μ M Flag-Act16, Flag-Act3, Flag-Act18 and respectively Flag-Act31, were incubated with 6 μ M TRITC-labelled phalloidin under polymerizing conditions. 1 μ M rabbit actin was used as reference. For better orientation of the focus plane, single *D. discoideum* cells (AX2-GFP) were added. Explicit actin filaments could be observed in polymerized rabbit actin, whereas Flag-Act16, Flag-Act18 and Flag-Act31 were not able to form a visible actin network. We could observe, however, small elongated structures of Flag-Act3.

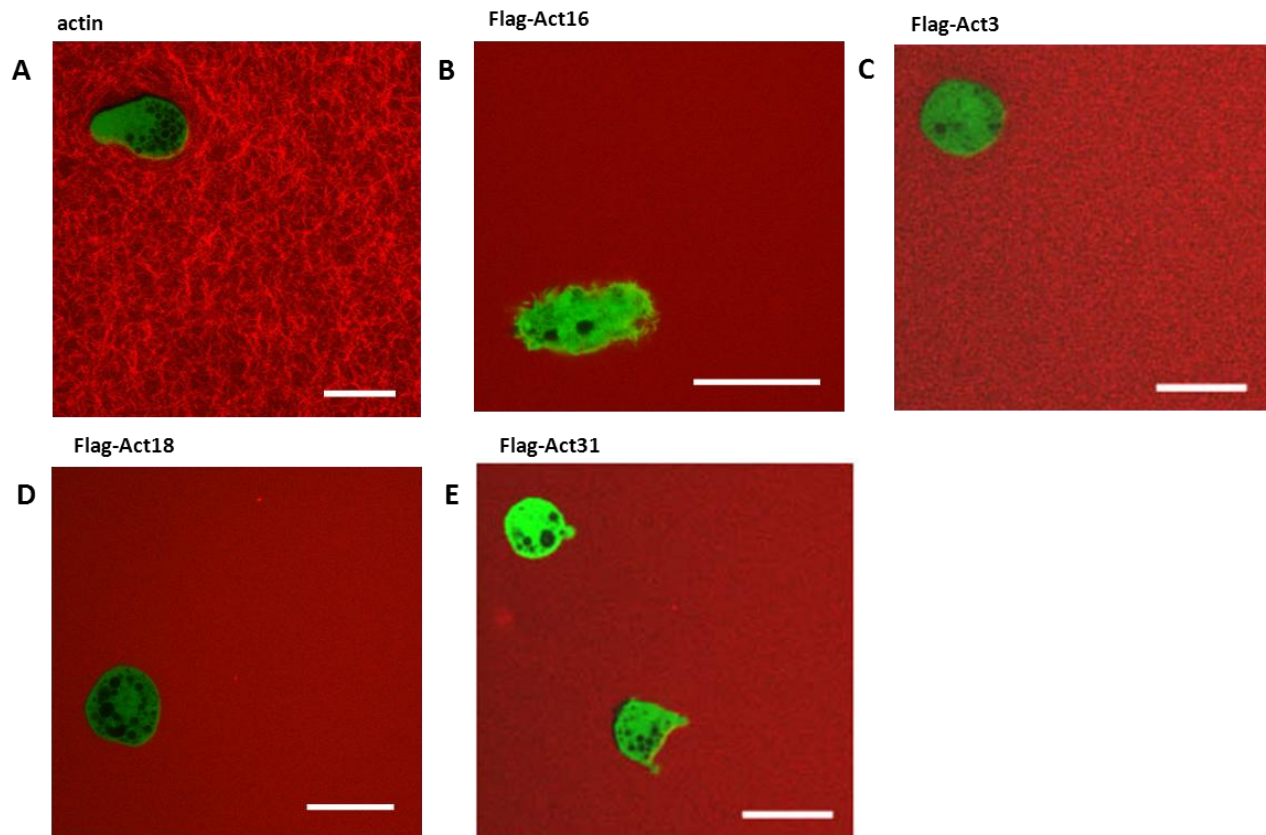


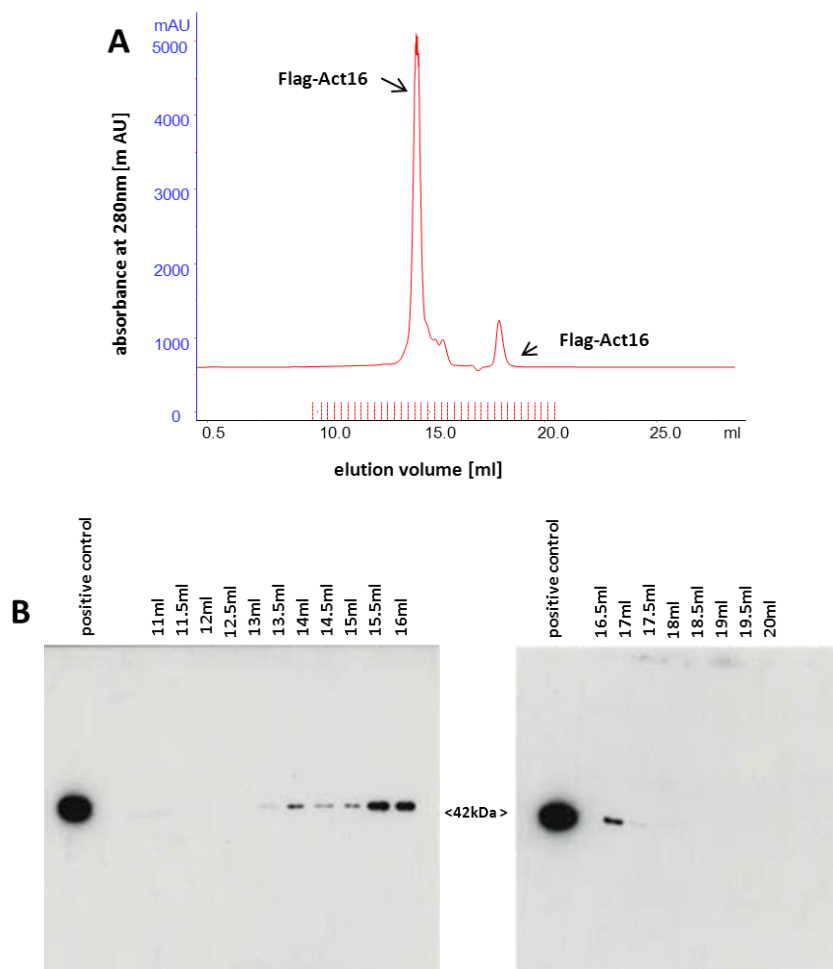
Figure 20: Potential filament formation of Flag-Act16, Flag-Act3, Flag-Act18 and Flag-Act31.

1 μ M of the respective Flag-actin variant and 6 μ M TRITC-labelled phalloidin were incubated under polymerizing conditions and pictures were taken using the 100x Neofluar 1.3 oil immersion objective (488nm, 543nm excitation). Single *D. discoideum* cells (AX2-GFP; green) were applied for better orientation on the focus plane. Scale bar 10 μ m. A) Rabbit actin exhibited clearly visible actin. B)-E) Except Flag-Act3 (C), none of the other actin variants showed supramolecular structures.

3.2.6 FPLC analysis of Flag-actin variants

Flag-Act16, Flag-Act3, Flag-Act18 and Flag-Act31 were analyzed on an AEKTA superose 6 gel filtration column to check the potential oligomerization of the Flag-actin variants under non-polymerizing conditions. All tested Flag-actin variants have a size of about 42kDa. To estimate the molecular mass of the applied Flag-actin variants, standard calibration curves were generated in advance, by applying catalase (240kDa), thyroglobulin (669kDa), bovine serum albumin (BSA; 67kDa), ribonuclease (13.7kDa), cytochrome C (12kDa) and ATP (553Da; data not shown).

Interestingly, the elution profile of 0.4mg/ml Flag-Act16 showed two peaks at 13.5ml and 16.5ml. When we analyzed the collected 0.5ml fractions in western blot analysis with the Flag antibody Flag 6F7, it became clear that Flag-Act16 could be eluted reproducibly in a range from 13.5 to 16.5ml. According to the standard calibration curves short oligomers from Flag-Act16 monomers up to tetramers could be possible.



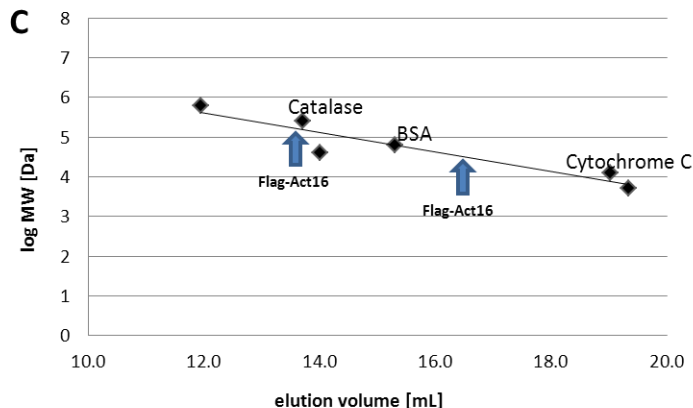


Figure 21: The oligomerization of Flag-Act16 was studied by using the AEKTA FPLC column. 0.4mg/ml purified Flag-Act16 was diluted in IEDANBP buffer and applied onto the FPLC column AEKTA superpose 6. The upper panel shows the elution profile. The middle panel shows the analysis of collected fractions of 0.5ml each via western blot analysis, using the primary Flag antibody Flag-6F7. The lower panel displays the correlation of the elution volume of Flag-Act16 and the calibration runs.

The same approach was used for the other actin variants (data not shown). All eluted as *bona fide* monomers. Only a small fraction of Flag-Act3 eluted also close to the excluded volume and consisted most likely of denatured aggregates.

3.2.7 Purified actin variants in a transmission electron microscope

For the visualization of potential filaments we used also a transmission electron microscope. Performing a negative stain, proteins and protein complexes from 100kDa onwards can be visualized. G-actin monomers with a size of about 42kDa are supposed to appear only as background noise. Freshly purified Flag-Act16, Flag-Act3, Flag-Act18 and Flag-Act31 (5 μ M) were centrifuged at 100.000g to remove preformed aggregates and byproducts. Freshly prepared rabbit actin served as reference. We tested the ability of Flag-Act16, Flag-Act3, Flag-Act18 and Flag-Act31 to polymerize without and with rabbit actin. The actin samples were incubated under polymerizing conditions and copper grids were placed upside down on 10 μ l of each polymerized sample for 1min. After washing, 2% uranyl acetate was used for negative staining. Pictures were taken with the JEM-1200 EX II Electron microscope.

Freshly prepared rabbit actin formed clearly visible actin filaments under polymerizing conditions. In contrast, Flag-Act16, Flag-Act3, Flag-Act18 and Flag-Act31 without additional rabbit actin, were not able to assemble into polymers. Aggregates of different sizes and shapes occurred, as well as background noise, probably caused by monomers. Finally, we incubated 5 μ M rabbit actin with 2.5 μ M Flag-Act16, Flag-Act3, Flag-Act18, respectively Flag-Act31, under polymerizing conditions. Precise actin filaments could be observed, as well as aggregates of different sizes and shapes that were partly attached to the actin filaments. Background noise was also detectable.

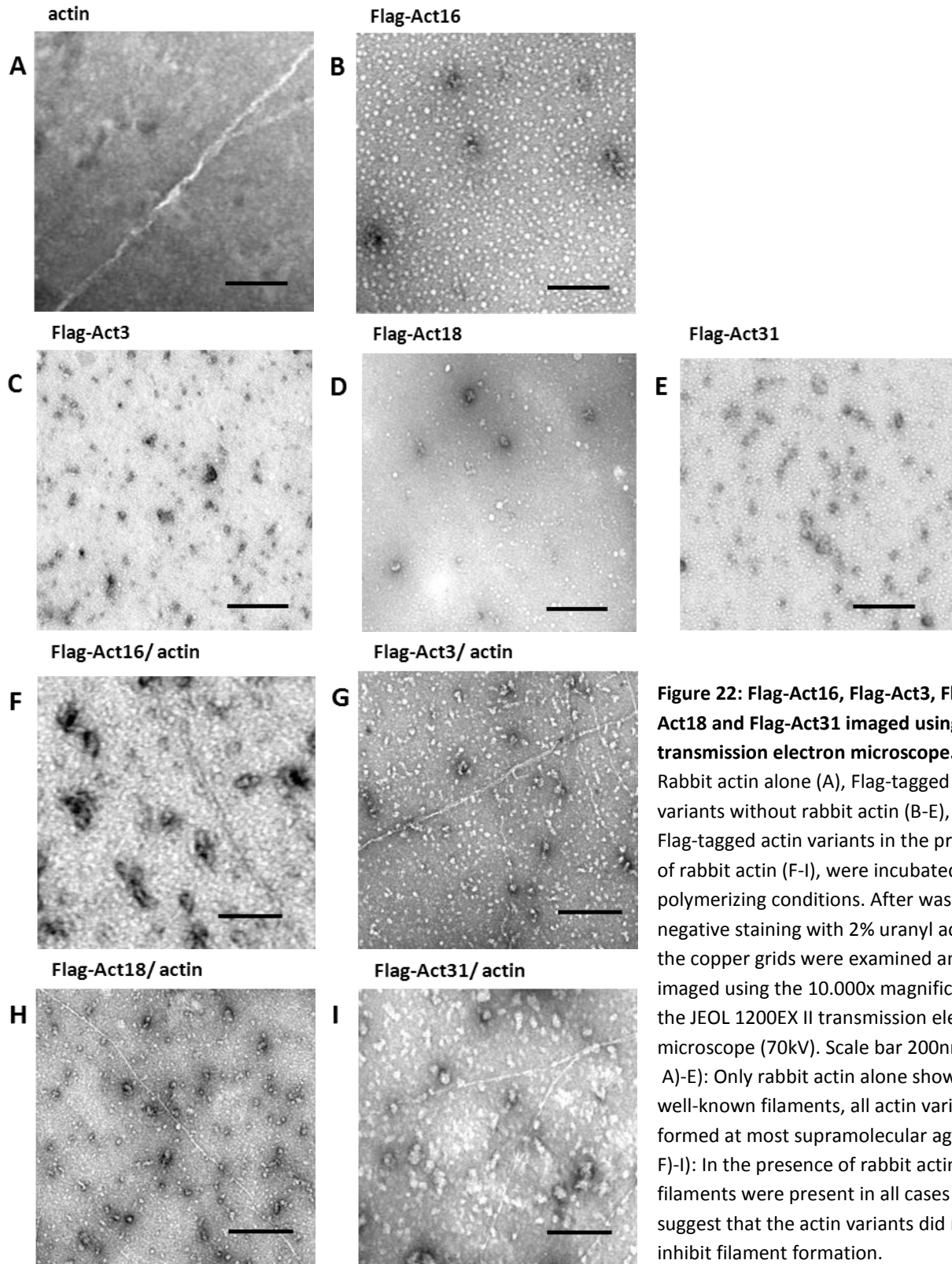


Figure 22: Flag-Act16, Flag-Act3, Flag-Act18 and Flag-Act31 imaged using a transmission electron microscope. Rabbit actin alone (A), Flag-tagged actin variants without rabbit actin (B-E), and Flag-tagged actin variants in the presence of rabbit actin (F-I), were incubated under polymerizing conditions. After washing and negative staining with 2% uranyl acetate, the copper grids were examined and imaged using the 10.000x magnifications at the JEOL 1200EX II transmission electron microscope (70kV). Scale bar 200nm. A)-E): Only rabbit actin alone showed the well-known filaments, all actin variants formed at most supramolecular aggregates. F)-I): In the presence of rabbit actin, filaments were present in all cases which suggest that the actin variants did not inhibit filament formation.

3.2.8 Interaction studies with severin

To identify potential interaction partners of Act16, Act3, Act18 and Act31, GFP-Traps (Chromotek) were performed with GFP-Act16, GFP-Act3, GFP-Act18 and GFP-Act31 cells from *D. discoideum*. The GFP-fusion proteins bind to beads coated with the GFP-antibody and can be pulled down together with their putative interaction partners. In mass spectrometry analysis, the actin binding protein severin was reproducibly detected to interact with GFP-Act31. As the severin that was available in the laboratory was His-tagged, beaded agarose derivatized with the nitrilotriacetic acid (NTA) chelation moiety and loaded with divalent nickel ions (Ni^{2+}) could be used for detection of severin. When we performed a western blot analysis by using the monoclonal Flag antibody 6F7, we could show that all tested Flag-tagged actin interacted in a Ca^{2+} -dependent manner with severin.

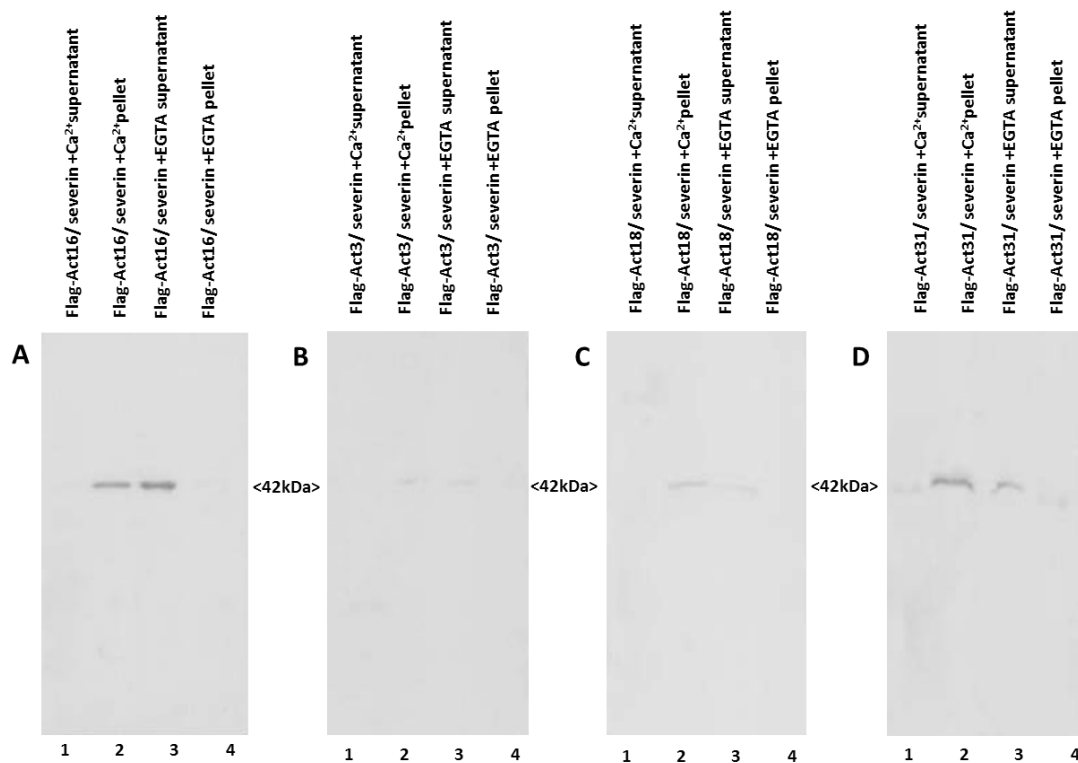


Figure 23: Interaction studies of Flag-Act16, Flag-Act3, Flag-Act18 and Flag-Act31 with severin.

We mixed Flag-Act16, Flag-Act3, Flag-Act18 and Flag-Act31 with severin (molar ratios 1) and added 1mM Ca^{2+} , respectively 1mM EGTA. These approaches were incubated with Ni^{2+} -NTA beaded agarose for 90 minutes at 4°C and subsequently centrifuged. Western blots were performed by using the monoclonal Flag antibody 6F7.

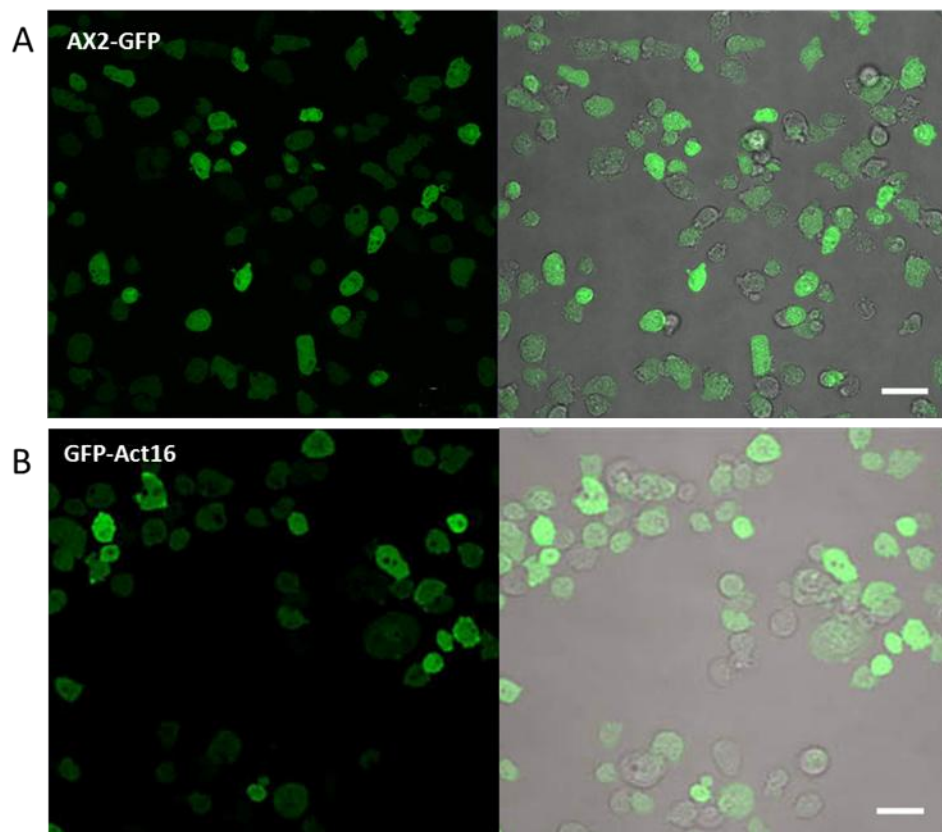
A)-D): All Flag-tagged actin variants interacted Ca^{2+} -dependent with severin, as they could be pulled down with Ni^{2+} -NTA beaded agarose. Adding EGTA, no interaction of the Flag-tag actin variants and severin occurred as the Flag-actin variants remained in the supernatant.

3.3 GFP-actin variant overexpressors

To analyze the function of Act16, Act3, Act18 and Act31 *in vivo*, we transferred the respective genes into a construct with a blasticidin/ or geneticin resistance cassette and a GFP-tag. As the alkaline C-terminus of actin is essential for the polymerization of actin, we decided to add the GFP-tag to the acidic N-terminus. In doing so, dysfunctions in actin dynamics can be minimized (Kim et al., 2007). The GFP-tag was attached to determine the expression levels and localizations of the overexpressed actin variants. All constructs contained the act15 promotor and the act8 terminator.

3.3.1 Expression of the fusion proteins

Expression of GFP-coupled actin variants in transformed *D. discoideum* cells were checked by taking pictures of living cells. They showed that 90% of the AX2-GFP cells and GFP-Act16 cells significantly expressed the fusion proteins, whereas in the GFP-Act3 cell line about 70% of the cell population showed clearly a green signal. The weakest expression frequency was detected in GFP-Act18 cells with 3-5% positive transformants. In the GFP-Act31 cells, an 80% ratio of positive transformants could be detected.



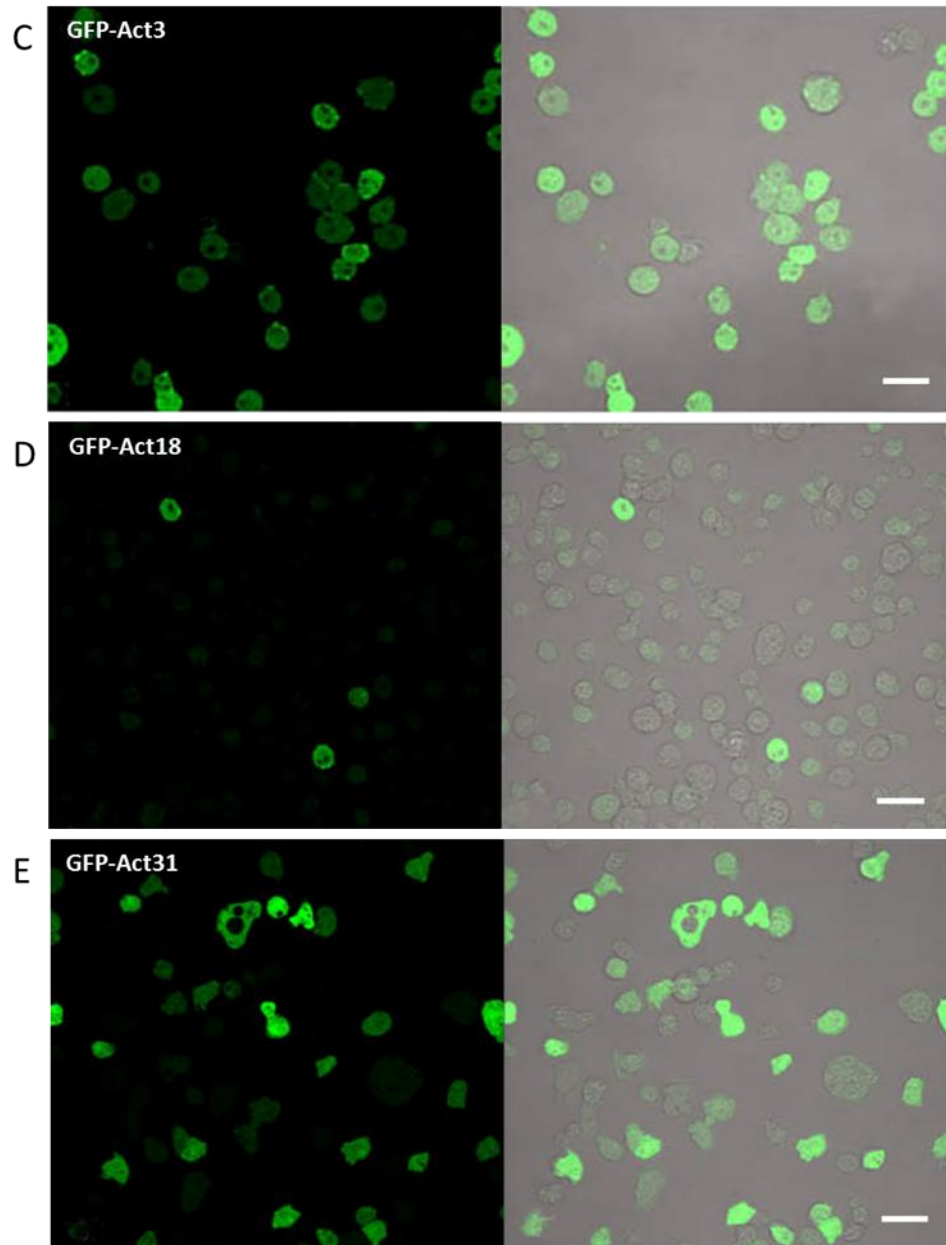


Figure 24: Different expression of GFP-actin variants in transformed *D. discoideum* cells.

The ratio of GFP-positive to unlabeled cells within the transformed cell lines was documented using the 40x LDA-Plan 0.50 Ph2 (488nm excitation) of the LSM 510 confocal microscope. The left panel shows the fluorescence picture. The right panel visualizes a merge of the bright-field illumination and the GFP-signal. Scale bar 10 μ m.

A) The GFP control was detectable in 90% of the AX2-GFP cells. B) GFP-Act16 was expressed in 90% of the transformed cells. C) GFP-Act3 was detectable in about 70% of the transformed cells. D) GFP-Act18 was detectable in 3-5% of the cells. E) GFP-Act31 occurred in 90% of the transformed cells.

We checked the expression levels biochemically in western blots using the monoclonal GFP-antibody K3-184-2 and detected the GFP control in AX2-GFP cells (27kDa) as well as the GFP-coupled actin variants (70kDa).

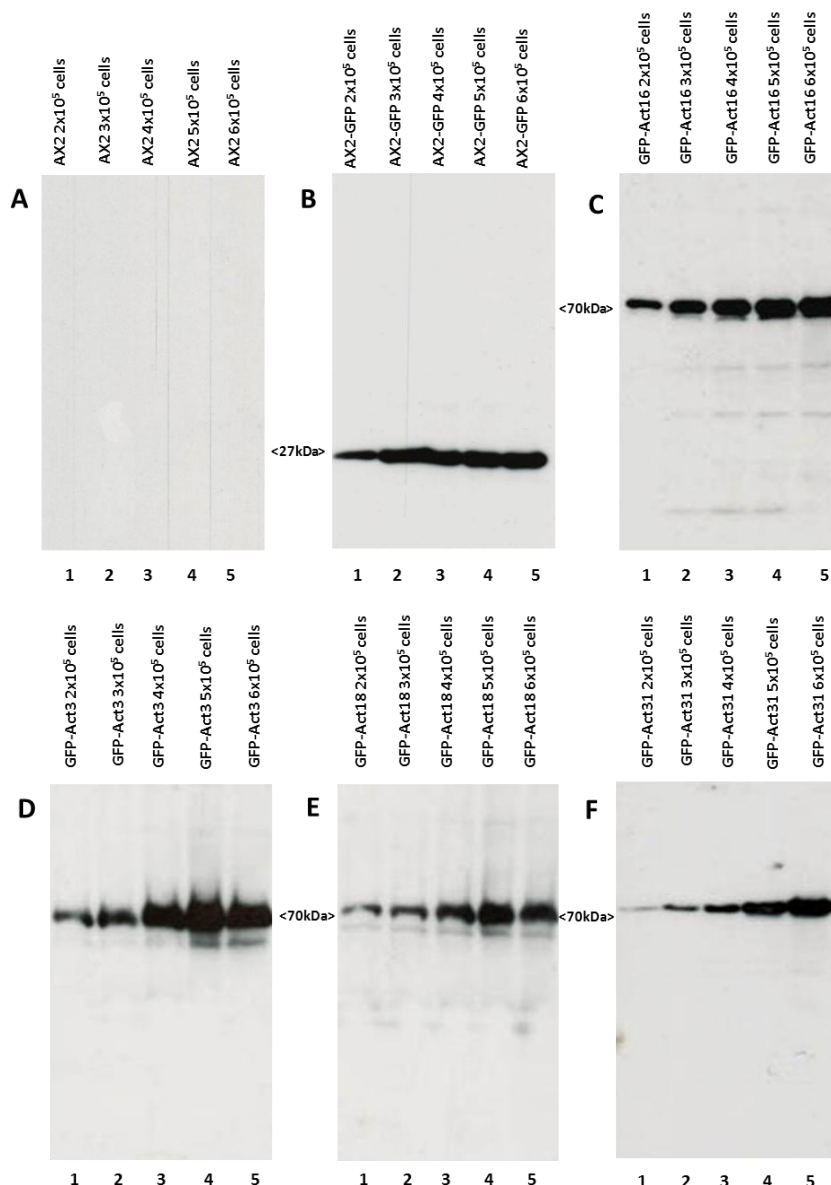


Figure 25: The monoclonal GFP antibody K3-184-2 was used to quantify the expression of the GFP-actin variants. Western blots using the monoclonal GFP antibody K3-184-2 to test the expression levels of endogenous actin in a dilution series of *D. discoideum* cells (2×10^5 - 6×10^5 cells/lane respectively lane 1-5). The antibody interacted with soluble GFP of the AX2-GFP cells (27kDa) and detected all GFP-coupled actin variants (70kDa).

Endogenous actin (42kDa) was proved in all cell types with the monoclonal actin antibody Act-1, as well as the GFP-tagged conventional actin variant GFP-Act16 (70kDa). No cross-reaction with any of the other tested GFP-coupled actin variants was detected.

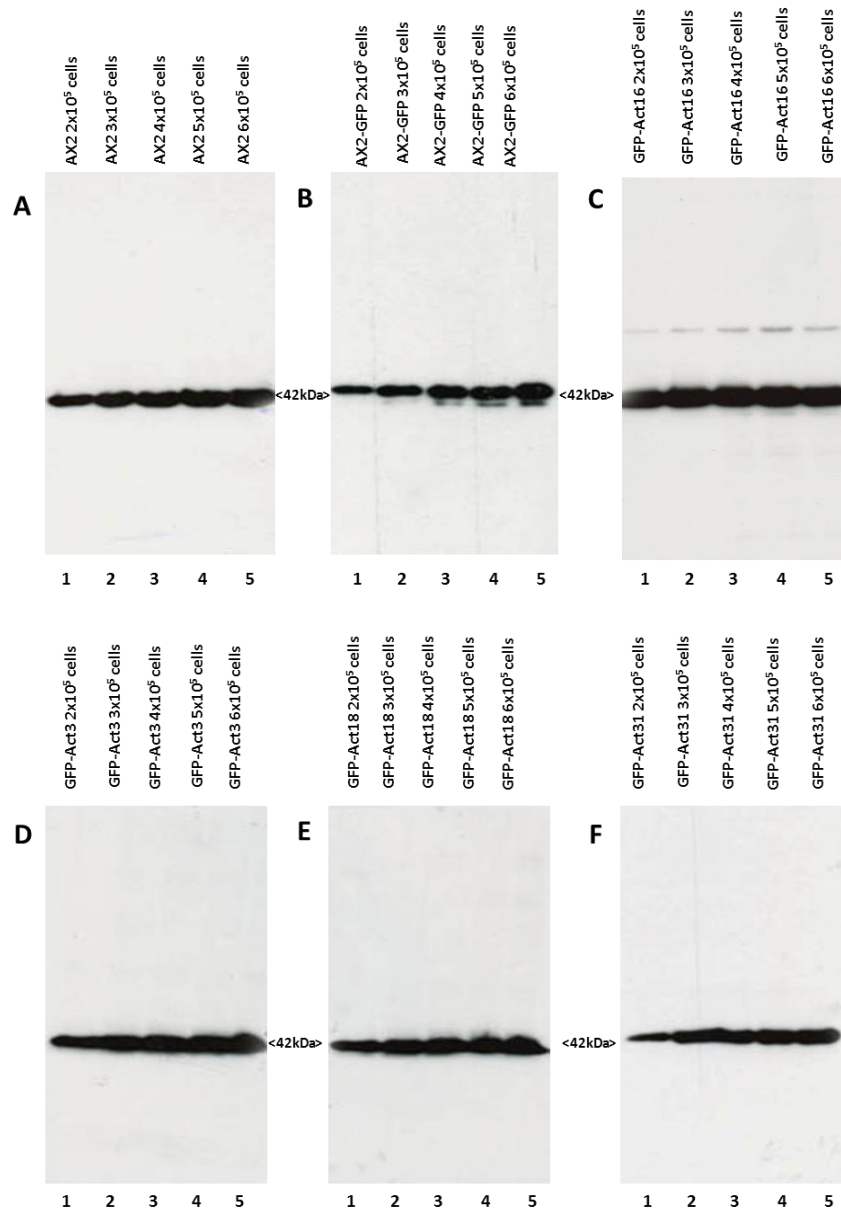


Figure 26: The monoclonal actin antibody Act-1 was used to quantify the expression of endogenous actin and to study cross-reactions with Act16, Act3, Act18 and Act31. Western blots using the monoclonal actin antibody Act-1 to test the expression levels of endogenous actin in a dilution series of *D. discoideum* cells (2x10⁵-6x10⁵ cells/lane, respectively lane 1-5). The signal of endogenous actin (42kDa) became gradually stronger with higher quantities of cells. The monoclonal antibody Act-1 detected endogenous actin (42kDa) in all tested cell lines and GFP-Act16 (70kDa). In contrast, GFP-Act3, GFP-Act18 and GFP-Act31 did not exhibit the appropriate signal.

Furthermore we applied the monoclonal actin antibody 224-236-1 to define its binding epitope and to study possible cross-reactions with our actin variants of interest. The antibody recognized endogenous actin (42kDa) in all tested cell lines and exhibited a distinct cross-reaction with GFP-Act16 (70kDa). No interaction with GFP-Act3, GFP-Act18 or GFP-Act31 was detected.

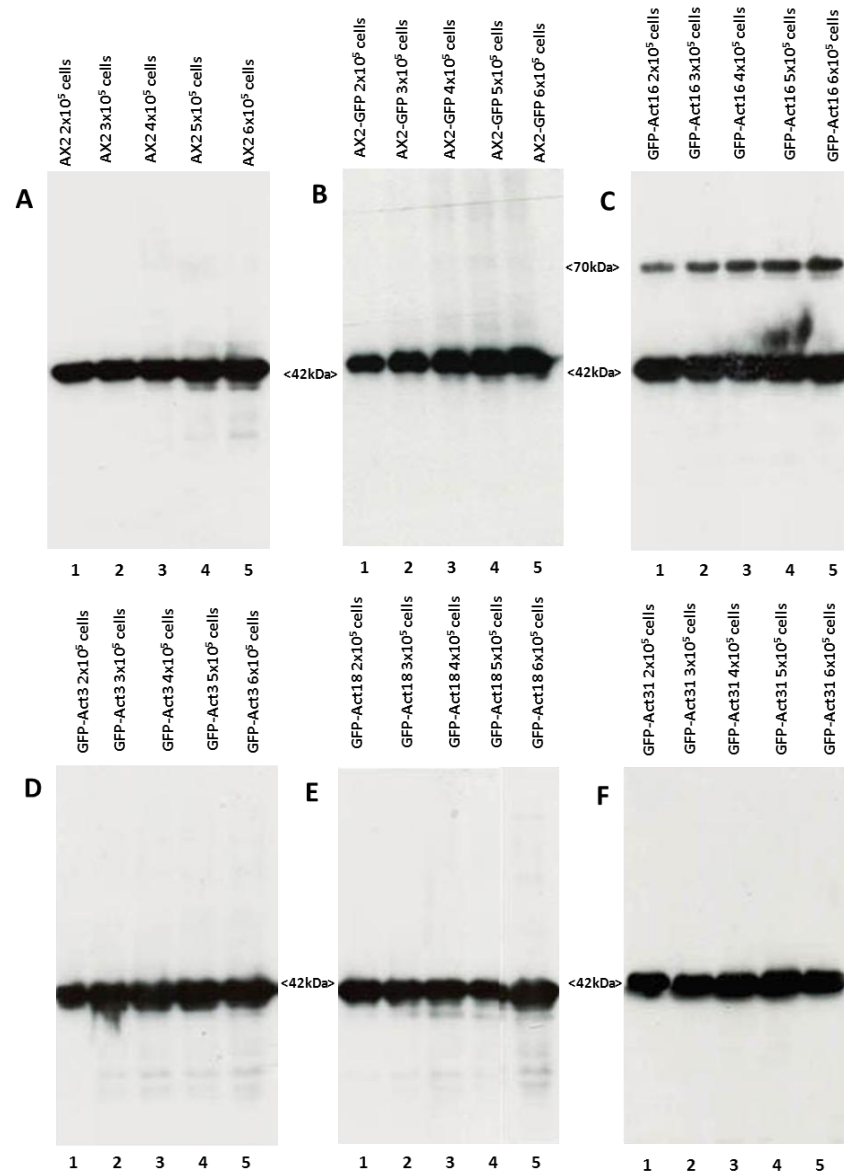


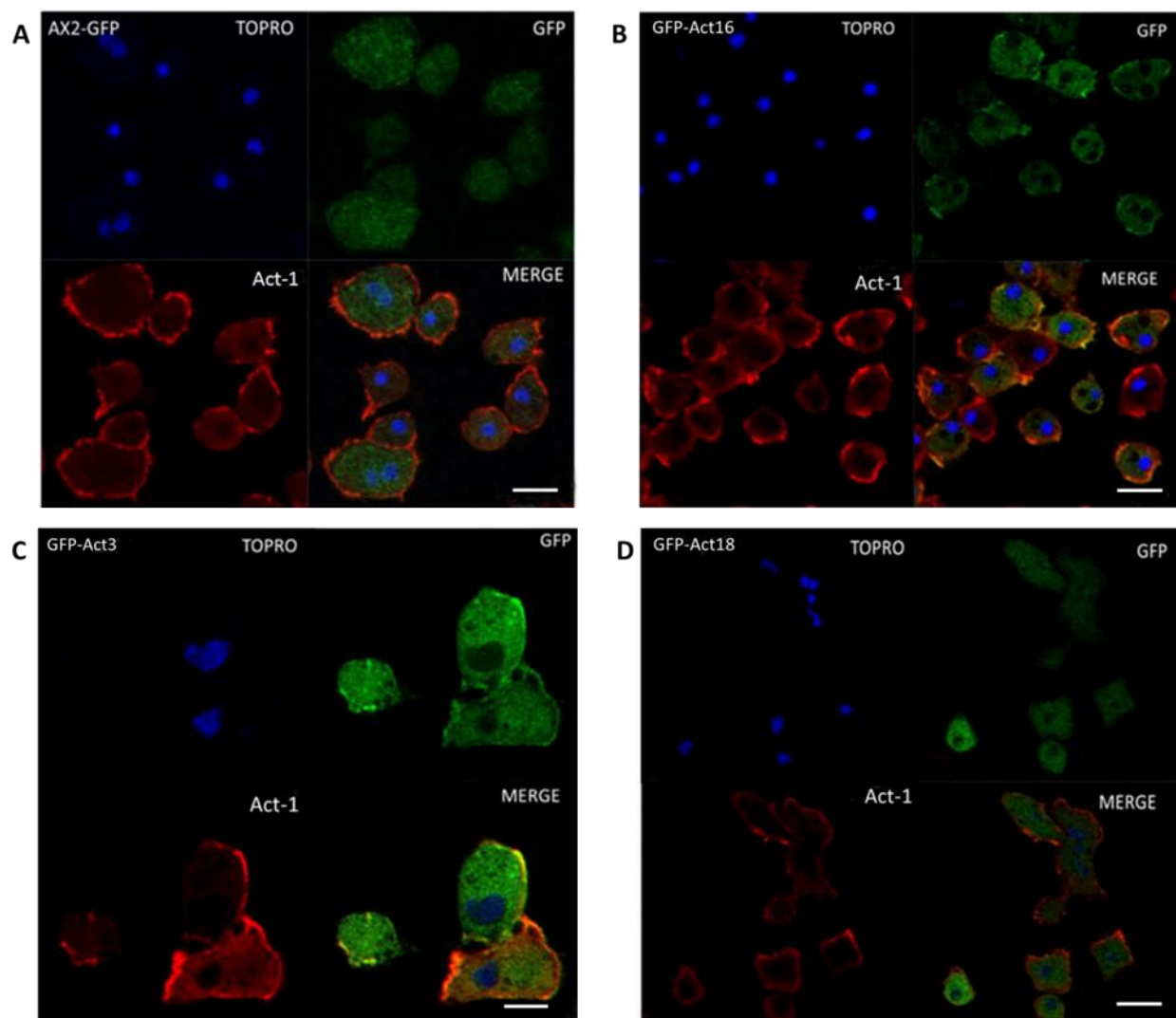
Figure 27: The monoclonal actin antibody 224-263-1 was used to define its binding epitope and to study cross-reactions with Act16, Act3, Act18 and Act31. Western blots using the monoclonal actin antibody 224-236-1 to study its binding epitope and possible cross-reactions with Act16, Act3, Act18 and Act31. The expression level of endogenous actin (42kDa) increased according to the dilution series of *D. discoideum* cells (2×10^5 - 6×10^5 cells/lane, respectively lane 1-5). The antibody also interacted with GFP-Act16 (70kDa), whereas GFP-Act3, GFP-Act18 and GFP-Act31 could not be detected with the monoclonal antibody 224-236-1.

The application of the monoclonal filactin antibody 4S-59-4 in western blot analysis showed that the tested cell lines AX2, AX2-GFP, GFP-Act16, GFP-Act3, GFP-Act18 and GFP-Act31 expressed filactin (105kDa; data not shown). Expected interactions with endogenous actin (42kDa) could be observed in all tested cells, whereas no interaction with Act16, Act3, Act18 and Act31 occurred (Gallinger, 2013).

3.3.2 Analyzing the F-actin cytoskeleton

3.3.2.1 Localization studies of actin variants in *D. discoideum* using fluorescence microscopy

To study the localization of GFP-Act16, GFP-Act3, GFP-Act18 and GFP-Act31 within the transformed *D. discoideum* cells, fixed cells were examined under the LSM 510 confocal microscope. GFP-Act16 and GFP-Act3 colocalized predominantly with endogenous actin at the cell cortex and were also detectable in the cytoplasm. GFP-Act18 and GFP-Act31 could not be visualized in the cell cortex, but were distributed throughout the cytoplasm. The GFP of the AX2-GFP cells was not associated with actin and was, as expected, spread homogenously in the cytoplasm of the dedicated cells.



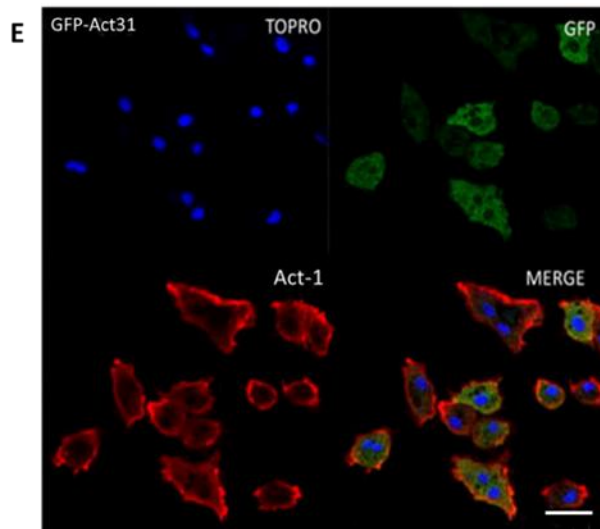


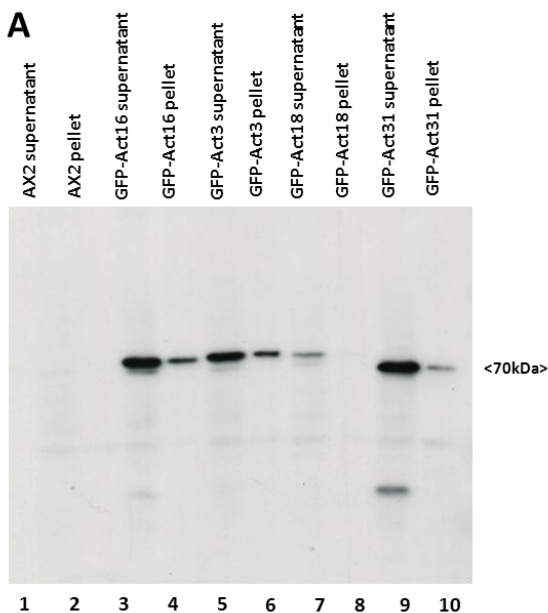
Figure 28: Immunofluorescence images were taken to visualize the GFP-actin variants. After fixation with methanol (-20°C) the cells were incubated with the primary actin antibody Act-1, the secondary Cy3-conjugated antibody goat-anti-mouse and the nucleic acid stain TOPRO. Images were taken using the 63x Neofluar oil immersion objective (488nm, 543nm and 633nm excitation) at the LSM 510 confocal microscope. The nucleus could be imaged using TOPRO (blue), actin variants were fused with GFP (green), endogenous actin was detected with the monoclonal antibody Act-1 (red). Scale bar 5µm. A) GFP of AX2-GFP cells was found in the cytoplasm. B) GFP-Act16 colocalized with endogenous actin in the cell cortex and in the cytoplasm. C) GFP-Act3 was part of the cell cortex and the cytoplasm. D) GFP-Act18 occurred within the cytoplasm. E) GFP-Act31 was also localized in the cytoplasm.

3.3.2.2 The Triton-insoluble cytoskeleton and differential spin downs for the detection of additional cytoskeletal components

To investigate whether the GFP-actin variants are associated with F-actin in *D. discoideum* cells, we used a biochemical approach and carried out two different assays: (1) analysis of the Triton-insoluble cytoskeleton and, (2) analysis of differential centrifugation. The Triton-insoluble cytoskeleton assay was performed essentially as described (McRobbie & Newell, 1983). Western blot analysis of the Triton insoluble cytoskeleton assay showed that GFP-Act16 and GFP-Act3 were allocated with the insoluble F-actin network in the pellet. A clear signal in the supernatant indicated an additional cytoplasmic occurrence. Immunofluorescence studies suggested that GFP-Act18 and GFP-Act31 were soluble proteins of the cytoplasm. This could be confirmed by the clear signal of GFP-Act18 and GFP-Act31 in the supernatant. The weak signal in the supernatant of GFP-Act18 was a consequence of the low expression of this GFP-coupled actin variant within the cells. When we executed the differential spin down, first we eliminated cells that could not be lysed by repeated freezing and thawing. Therefore, the first centrifugation step was performed at 800g. Vesicles, peroxisomes, mitochondria, ER and similar cellular components were present in the 10.000g pellet.

As the GFP signals of all tested actin variants were detected in this fraction, the association of GFP-Act16, GFP-Act3, GFP-Act18 and GFP-Act31 with these cell organelles was assumed. At 100.000g actin filaments of the F-actin network were sedimented. Only GFP-Act16 and GFP-Act3 could be detected in these pellets. As the final supernatants showed, GFP-Act16, GFP-Act3, GFP-Act18 and GFP-Act31 were localized in the cytoplasm. The weak signal of GFP-Act18 reflected again the low expression of this actin variant in the transformed cells.

(1) Triton-insoluble cytoskeleton



(2) Differential centrifugation

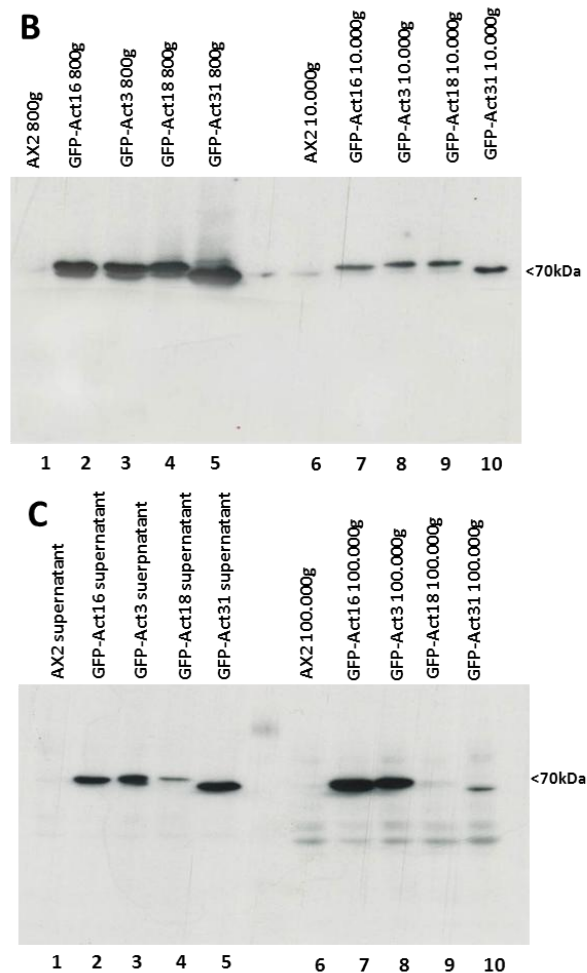
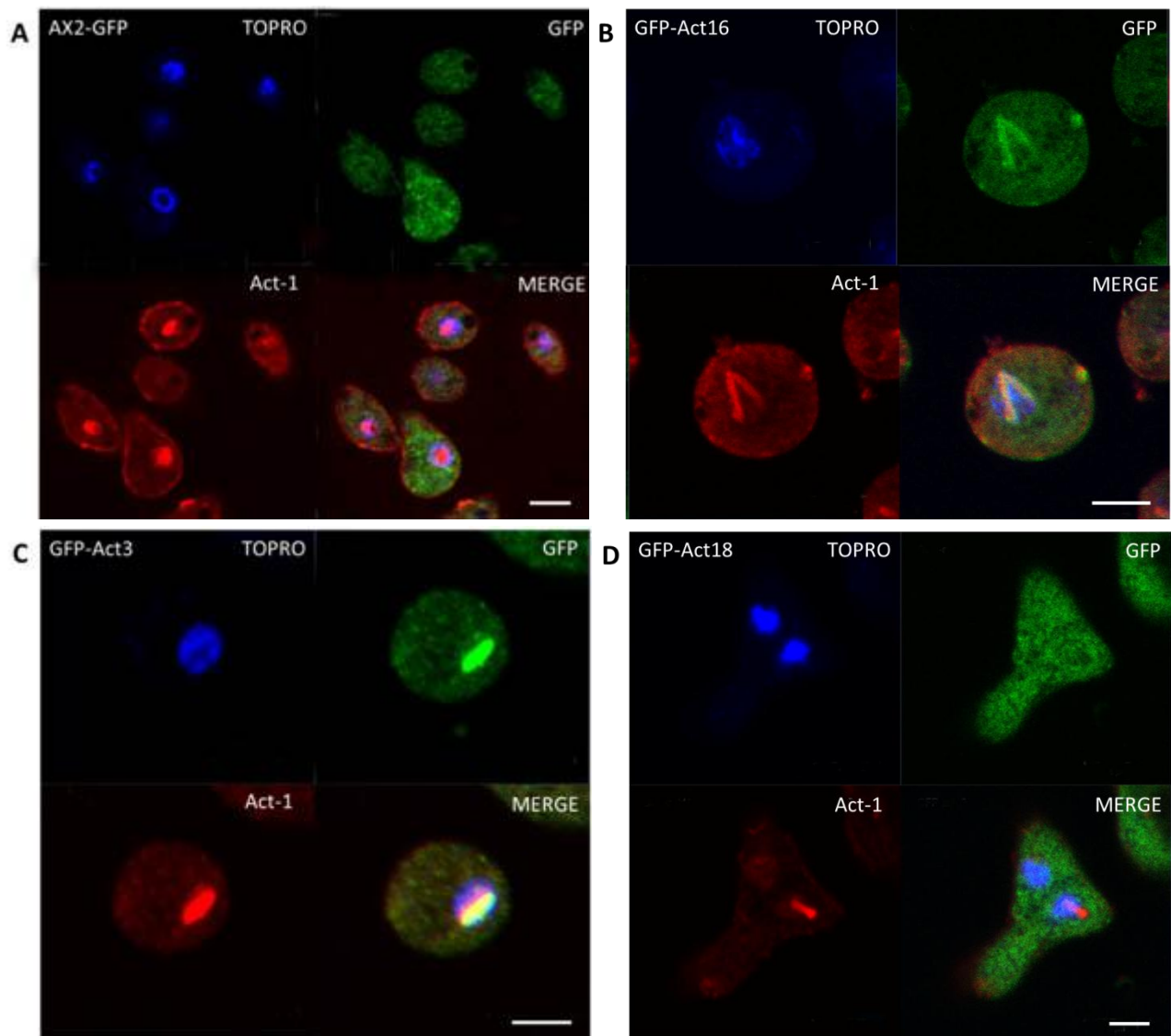


Figure 29: The Triton-insoluble cytoskeleton assay and the differential spin down were performed to localize the GFP-actin variants biochemically. Western blots were incubated with the monoclonal GFP antibody K3-184-2 for the detection of the GFP-actin variants (70kDa). A) The Triton-insoluble cytoskeleton (1.5×10^5 cells/lane) indicated that GFP-Act16 and GFP-Act3 were associated with the F-actin network, as they were detectable in the pellets. GFP-Act18 and GFP-Act31 were preferably found in the supernatant, which suggested a cytoplasmic localization. B) The differential spin down assay (5×10^5 cells/lane) showed comparable signals after the 800g and 10.000g centrifugation steps. An association of all tested GFP-actin variants with vesicles, peroxisomes, mitochondria, ER or similar cellular components cannot be excluded. C) After centrifugation at 100.000g (5×10^5 cells/lane) GFP-Act16 and GFP-Act3 occurred in the pellet. Accordingly, they were associated with F-actin. The final supernatants showed that GFP-Act16, GFP-Act3, GFP-Act18 and GFP-Act31 occurred also in the cytoplasm of the transformed cells.

3.3.3 Rod formation in GFP-actin overexpressors

3.3.3.1 Nuclear actin rods

Nuclear actin rods are present in *D. discoideum* spores and can be induced in vegetative cells under stress conditions (Sameshima et al., 2000). These rod-shaped paracrystals are formed if cells are treated with DMSO or increased temperatures (Osborn & Weber, 1984). Subsequently actin migrates into the nucleus. These rods consist of actin and a set of actin binding proteins, including cofilin, actin interactin protein 1 (Aip1) and coronin (Minamide et al., 2010). Consequently, the primary actin antibody Act-1 was used to visualize nuclear rods in fixed cells. All tested cell lines were able to form nuclear rods. Interestingly, GFP-Act16 and GFP-Act3 were part of these rods, whereas GFP, GFP-Act18 and GFP-Act31 were not associated with the nuclear rods.



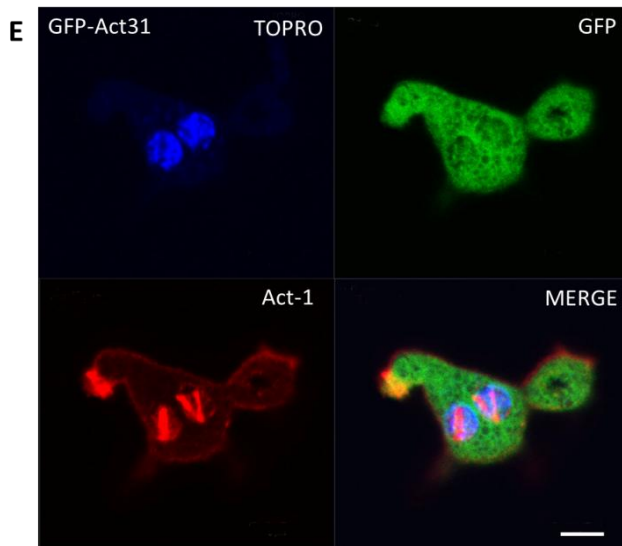
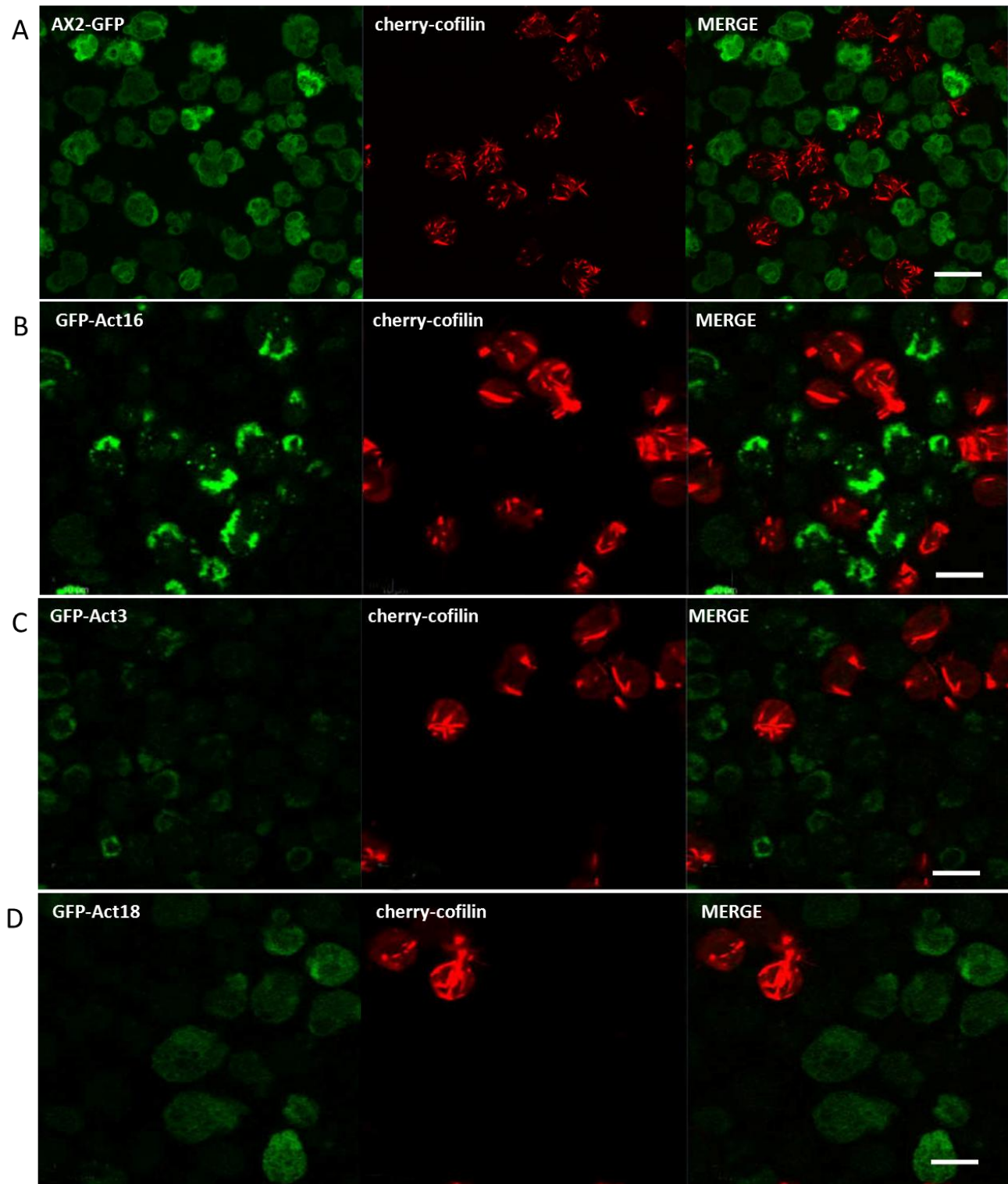


Figure 30: Nuclear rods in GFP-actin variant overexpressors. After treatment with 5% DMSO for one hour at 28°C *D. discoideum* cells were fixed with methanol (-20°C), incubated with the primary actin antibody Act-1, the secondary antibody Cy3-conjugated goat-anti-mouse IgG and the nucleic acid stain TOPRO. Images were taken using the 63x Neofluar 1.4 oil immersion objective (488nm, 543nm and 633nm excitation) at the LSM 510 confocal microscope. The nucleus could be imaged via TOPRO (blue), actin variants were fused to GFP (green), endogenous actin was detected with Act-1 (red). Scale bar 5µm. A) AX2-GFP cells formed nuclear rods, but GFP was not part of these rods. B) GFP-Act16 cells formed nuclear rods and GFP-Act16 was part of these rods. C) GFP-Act3 cells formed nuclear actin rods and GFP-Act3 was part of these rods. D) GFP-Act18 cells formed nuclear rods, but GFP-Act18 is not part of these rods. E) GFP-Act31 cells showed clear rods, but GFP-Act31 was not part of these rods.

3.3.3.2 The role of Act16, Act3, Act18 and Act31 in cytoplasmic rods

If vegetative cells are exposed to stress conditions like poisonous NaN_3 , stretched bundles in the cytoplasm can be observed. Rods can be fragmented by pressure, indicating that the rods may be effective in absorbing physical pressure. Whereas just a few cofilin molecules are included in the nuclear rods, cofilin is an important component of cytoplasmic rods (Nishida et al., 1987). Therefore cherry-cofilin cells were used as reference.

Live cell images showed that, after treatment with 10mM NaN_3 , cytoplasmic rods appeared in cherry-cofilin cells, but in none of the tested GFP-actin overexpressors. Instead of cytoplasmic rods, crescent-shaped aggregations occurred in GFP-Act16 and GFP-Act3 cells. Cells overexpressing GFP-Act18 or GFP-Act31 did not exhibit cytoplasmic rods or comparable structures.



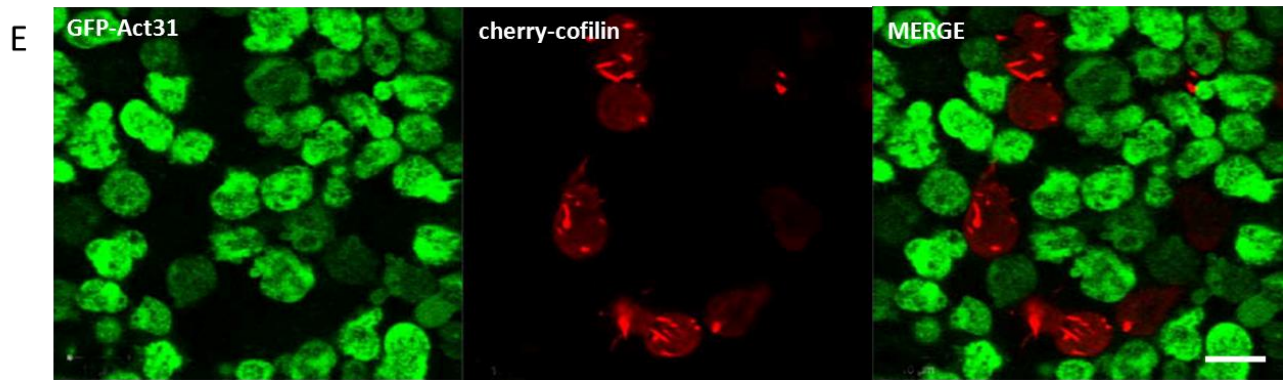


Figure 31: Cytoplasmic rods in GFP-actin overexpressors. After treatment with 10mM NaN_3 at 28°C for one hour, living cells were imaged using the 40x LDA-Plan 0.50 Ph2 objective (488nm and 543nm excitation) at the LSM 510 confocal microscope. The left panel shows the GFP-actin variants (green), the middle panel displayed cherry-cofilin cells (red) as reference and the right panel visualizes the merge. Scale bar 10 μm . A) No cytoplasmic rods could be observed in AX2-GFP cells. B) GFP-Act16 cells formed crescent shaped aggregates. C) GFP-Act3 cells showed crescent shaped aggregates. D) GFP-Act18 did not show cytoplasmic rods. E) GFP-Act31 cells did not exhibit cytoplasmic rods.

3.3.4 Germination and viability of spores

To survive unfavorable environmental conditions, vegetative cells aggregate to become a multicellular form of organization and subsequently a large number of cells differentiates into dormant spores within a fruiting body. Dormant spores are morphologically static. The actin cytoskeleton is inactive in spores, which correlates with high levels of actin phosphorylation (Kishi et al. 1998). After the germination of spores is induced, actin is dephosphorylated and nuclear rods are denatured (Sameshima et al., 2000).

To check the viability of spores from the GFP-actin overexpressors, 100 spores were plated together with *K. aerogenes* onto SM-agar plates. Germination begins immediately in the presence of food, induced by polysaccharides originated from the bacterial cell wall, which work as spore germination promoters (Ihara et al., 1990). After 96h the number of plaques was counted. The wild type strain AX2 was used as reference and showed a high viability of spores, with 91.2% germinating spores. AX2-GFP spores (47.4%), GFP-Act18 spores (77.6%) and GFP-Act31 spores (57.0%) exhibited a reduced ability for germination. In the GFP-Act16 cells the viability of the dormant spores seemed to be significantly strong affected, hence just 7.4% of the plated spores germinated. Also GFP-Act3 spores showed a reduced viability, as just 4.8% of the plated spores were able to germinate. Consequently, a GFP-induced influence could not be excluded.

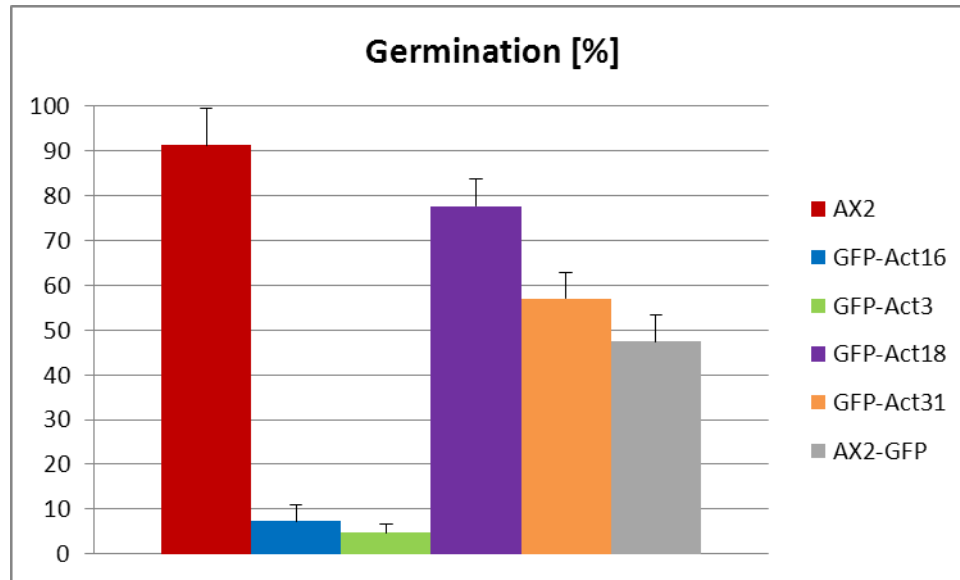


Figure 32: Germination of spores in GFP-actin variant overexpressors. 100 spores of each tested GFP-overexpressing cell line were plated together with *K. aerogenes* onto SM-agar plates. After 96h the number of plaques was counted. Five independent experiments were performed. The wild type strain AX2 was used as reference. The germination was reduced in all tested cell lines. A significant strong decrease up to 95% occurred in GFP-Act16 and GFP-Act3 overexpressing cells, whereas GFP-Act18, GFP-Act3 and AX2-GFP cells showed a reduction up to 51%. A GFP-induced influence could not be excluded.

GFP-actin variant spores could feature a defective round shape, if only dot-like structures instead of actinrods are formed in the cells (Sameshima et al., 2000). Therefore the size of 50 single spores of the cell lines AX2, AX2-GFP, GFP-Act16, GFP-Act3, GFP-Act18 and GFP-Act31 was determined in length and width using the 100x Neofluar 1.3 oil immersion objective (bright field illumination) at the LSM 510 confocal microscope. We could prove that the spores from the compared cell lines did not exhibit any differences concerning length and width, and all the strains developed the typical elliptic spore shape (data not shown).

3.3.5 Growth rates in *D. discoideum* mutants

The growth of *D. discoideum* can be divided into four different phases: first of all, the cells adapt themselves to growth conditions during the lag-phase. Secondly, the log-phase or exponential phase, which is a period that is characterized by fast cell doubling and terminated by a decrease of nutrients and accumulation of waste. The third phase is the stationary phase, which is often due to a growth-limiting factor such as the depletion of an essential nutrient, and/or the formation of inhibitory products such as an organic acid. Growth rate and death rate are equal during the stationary phase. At death phase cells run out of nutrients and die (dictybase.org).

To investigate deviations in growth rates of GFP-Act16, GFP-Act3, GFP-Act18 and GFP-Act31 overexpressors in comparison to the wild type, cells were grown under standard conditions (HL5 nutrient rich medium, 21°C, 160rpm) in shaking cultures and counted twice daily.

A shortened lag-phase of overexpressing GFP-Act16 and GFP-Act3 mutants and a high doubling rate especially at the beginning of the growth period could be observed. Both mutants reached the stationary phase more quickly than the wild type and died earlier, which was indicated by round cells. In contrast, GFP-Act18 and GFP-Act31 had an extended lag-phase and reached the stationary phase later than the wild type cells. The growth rate of AX2-GFP cells was consistent with the increase of AX2 cells. A GFP-based effect could therefore be excluded.

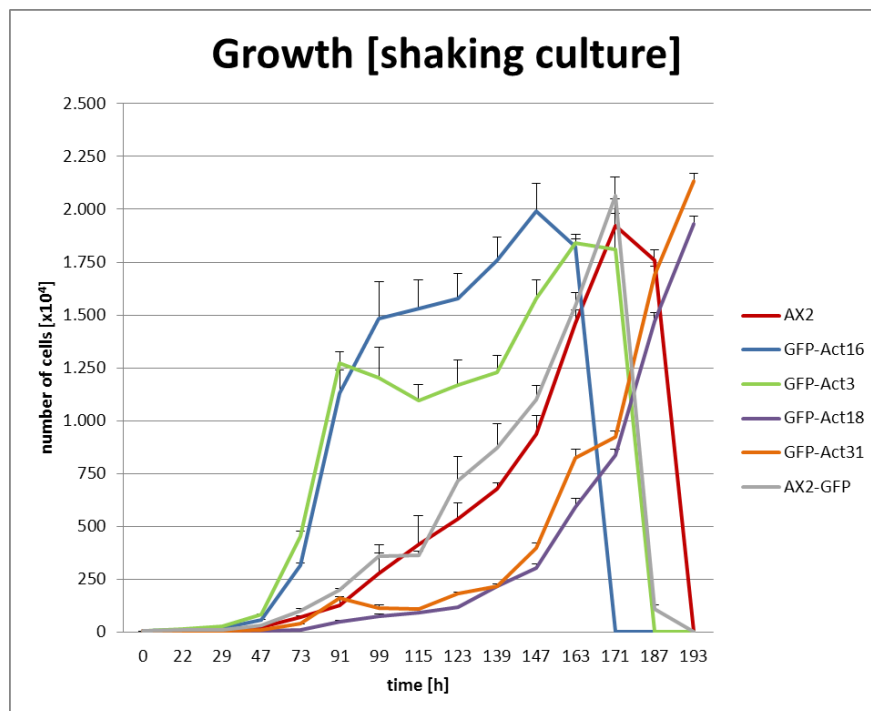
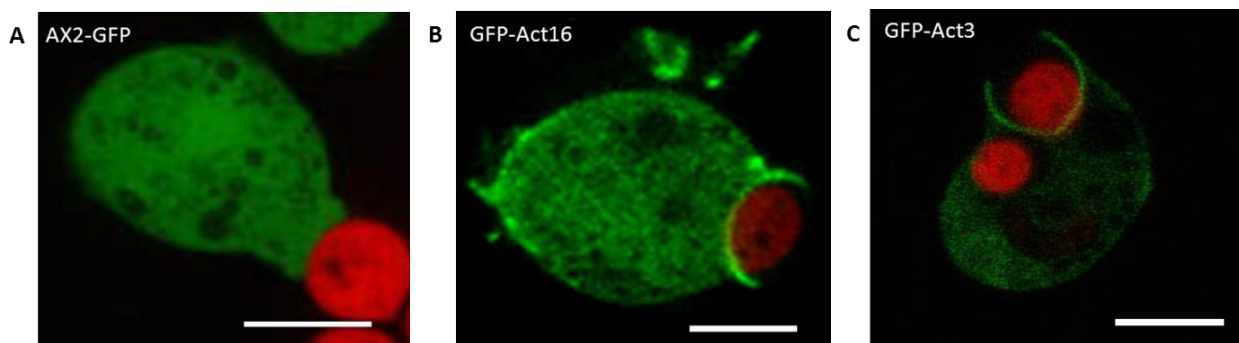


Figure 33: Growth rates of GFP-actin mutants. Cells were seeded at a density of 5×10^4 cells/ml. The cells were incubated in a shaking culture at 21°C and 160rpm. Twice a day the cell density was determined. Three independent experiments were performed. GFP-Act16 cells and GFP-Act3 cells were characterized by a shortened lag-phase and a high doubling rate. In comparison to the wild type AX2, GFP-Act18 cells and GFP-Act31 cells had an extended lag-phase and reached the stationary phase later. No GFP-induced influence occurred.

3.3.6 The role of Act16, Act3, Act18 and Act31 in phagocytosis

The plasma membrane segregates the cytoplasm from the extracellular environment by regulating and coordinating the entry and exit of small and large molecules. Whereas small molecules can transverse the plasma membrane through pumps or channels, macromolecules and particles must be carried into the cell via endocytosis. Endocytosis occurs by multiple mechanisms that fall into two broad categories, 'phagocytosis' (uptake of large particles) and 'pinocytosis' (uptake of small particles and fluids; Conner & Schmid, 2003). The lower eukaryote *D. discoideum*, that internalizes microorganisms as a food source, is known to be a 'professional phagocyte' (Bozzaro & Eichinger, 2011). Accordingly, the particle uptake, sequestering and maturation into phagosomes of *D. discoideum* resembles in many ways the events observed in macrophages, neutrophils or dendritic cells of mammals. The major endocytic process can be differentiated into five steps, all of them involving the actin cytoskeleton: membrane invagination, coated pit formation, coated pit sequestration, detachment of the newly formed vesicle and movement of this new endocytic compartment away from the plasma membrane into the cytosol (Qualmann et al. 2000). During endocytosis of large particles like yeast cells, the composition of the plasma membrane is altered at the specialized area immediately below the target particle, which is known as the phagocytic cup.

To investigate if any of the actin variants are localized in the phagocytic cup during endocytosis, the GFP-overexpressing cell lines were fed with TRITC-labeled yeast and pictures were taken with the LSM 510 confocal microscope. The GFP signal of the AX2-GFP cells was detected in the cytoplasm, but not in the phagocytic cup. In contrast, a clear signal of GFP-Act16 and GFP-Act3 occurred in the phagocytic cup of the respective cells. GFP-Act18 and GFP-Act31 could not be determined in the phagocytic cup of the overexpressors. These proteins were homogenously distributed in the cytoplasm.



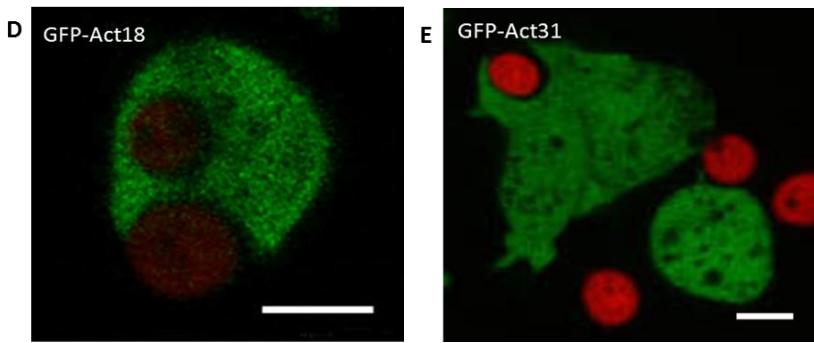


Figure 34: The localization of GFP-actin variants during phagocytosis. 2×10^6 cells/ml of every tested cell line were starved one hour in nutrient deficient medium and challenged with $1/10$ of TRITC-labeled yeast cells. Images were taken by using a 100x Neofluar 1.3 oil immersion objective (488nm and 543nm excitation) at the LSM 510 confocal microscope. Scale bar $2 \mu\text{m}$ A) In AX2-GFP cells, GFP was spread within the cytoplasm, but not enriched in the phagocytic cup. B) GFP-Act16 accumulated in the phagocytic cup during the uptake of yeast cells. C) Also GFP-Act3 was concentrated in the phagocytic cup during phagocytosis. D) In GFP-Act18 cells, the GFP-signal occurred in the cytoplasm, but not enriched in the phagocytic cup. E) GFP-Act31 occurred in the cytoplasm, but not accumulated in the phagocytic cup.

Given that GFP-Act16 and GFP-Act3 were enriched in the phagocytic cup during phagocytosis, whereas an accumulation of GFP-Act18 and GFP-Act31 could not be detected in the phagocytic cup, the uptake of TRITC-labeled yeast was measured at the fluorescence spectrometer LS55. Surprisingly, all mutants showed a disturbed uptake of yeast and had only about 50% of the phagocytosis capacity compared to the wild type. As the uptake of the AX2-GFP cell line was equally low, an influence of GFP could not be excluded.

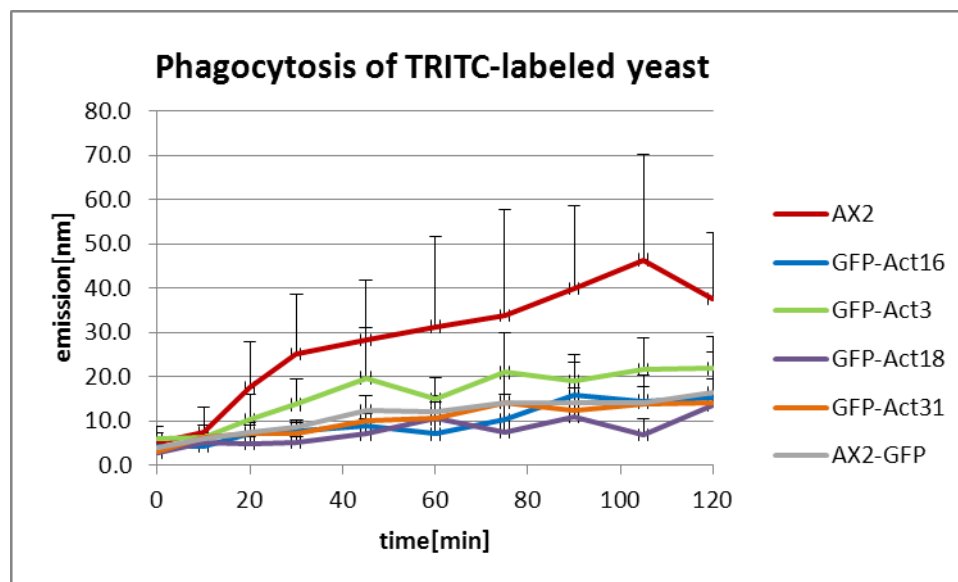


Figure 35: Phagocytosis of TRITC-labeled yeast. 2×10^6 cells/ml were starved one hour in nutrient deficient medium and fed with $1/10$ of fluorescent yeast cells. Fluorescence from internalized yeasts was measured at the fluorescence spectrometer LS55 (544nm excitation) every ten minutes. Three independent experiments were performed. In all mutants the uptake of yeast was reduced up to 50%. GFP-induced effects are possible, as the uptake was also reduced to 50% in AX2-GFP cells.

Thereupon, we picked single clones of every GFP-actin variant cell line and transferred them on plated *K. aerogenes* (SM-agar plates). The purpose was to check if GFP-Act16, GFP-Act3, GFP-Act18 and GFP-Act31 were also implicated in the phagocytosis of smaller particles like bacteria. As we measured the diameter of the plaques daily, we did not observe any significant alterations. No GFP-induced influence could be detected.

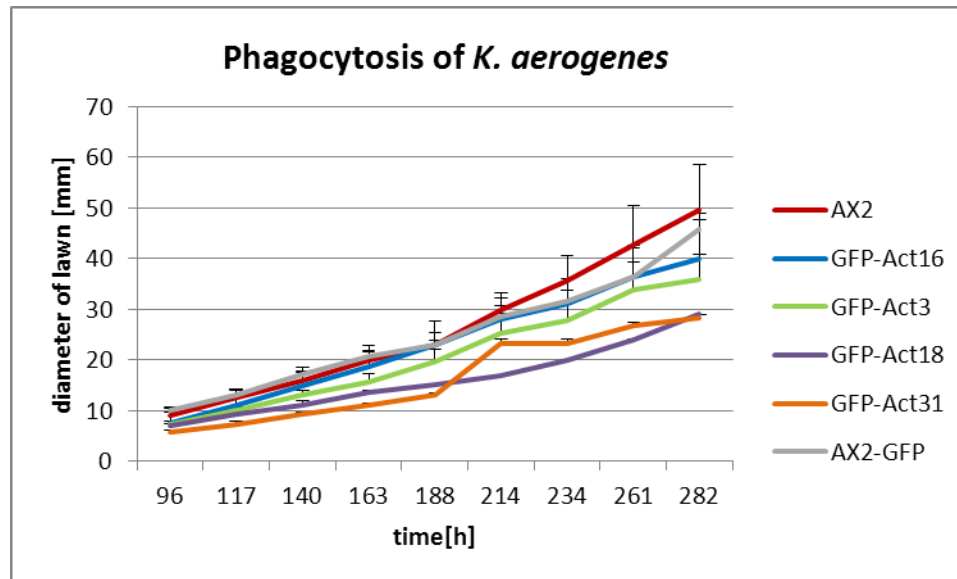


Figure 36: Phagocytosis of plated non-pathogenic *K. aerogenes*. Single clones of *D. discoideum* were put onto a lawn of non-pathogenic *K. aerogenes* on SM nutrient agar plates. Incubation at 21°C for 12 days. The diameter of the plaques was measured daily. Five independent experiments were performed. Phagocytosis of bacteria was not significantly affected. No GFP-induced influence occurred.

3.3.7 Phototaxis and development of GFP-actin mutants

D. discoideum cells differentiate into complex multicellular slugs which are able to migrate phototactically towards a light source to reach environments with more favorable conditions. To investigate whether GFP-Act16, GFP-Act3, GFP-Act18 and GFP-Act31 are implicated in the control of slug-movement or development, we performed phototaxis assays and developmental courses. To analyse phototaxis, cells were transferred onto water agar plates and wrapped in a dark colored box with an opening for the entry of light. After 48 hours of incubation, the tracks of the slugs after migration did not show any alterations concerning the distances or directions of movements in comparison to the AX2 wild type strain. GFP-induced effects could be also excluded.

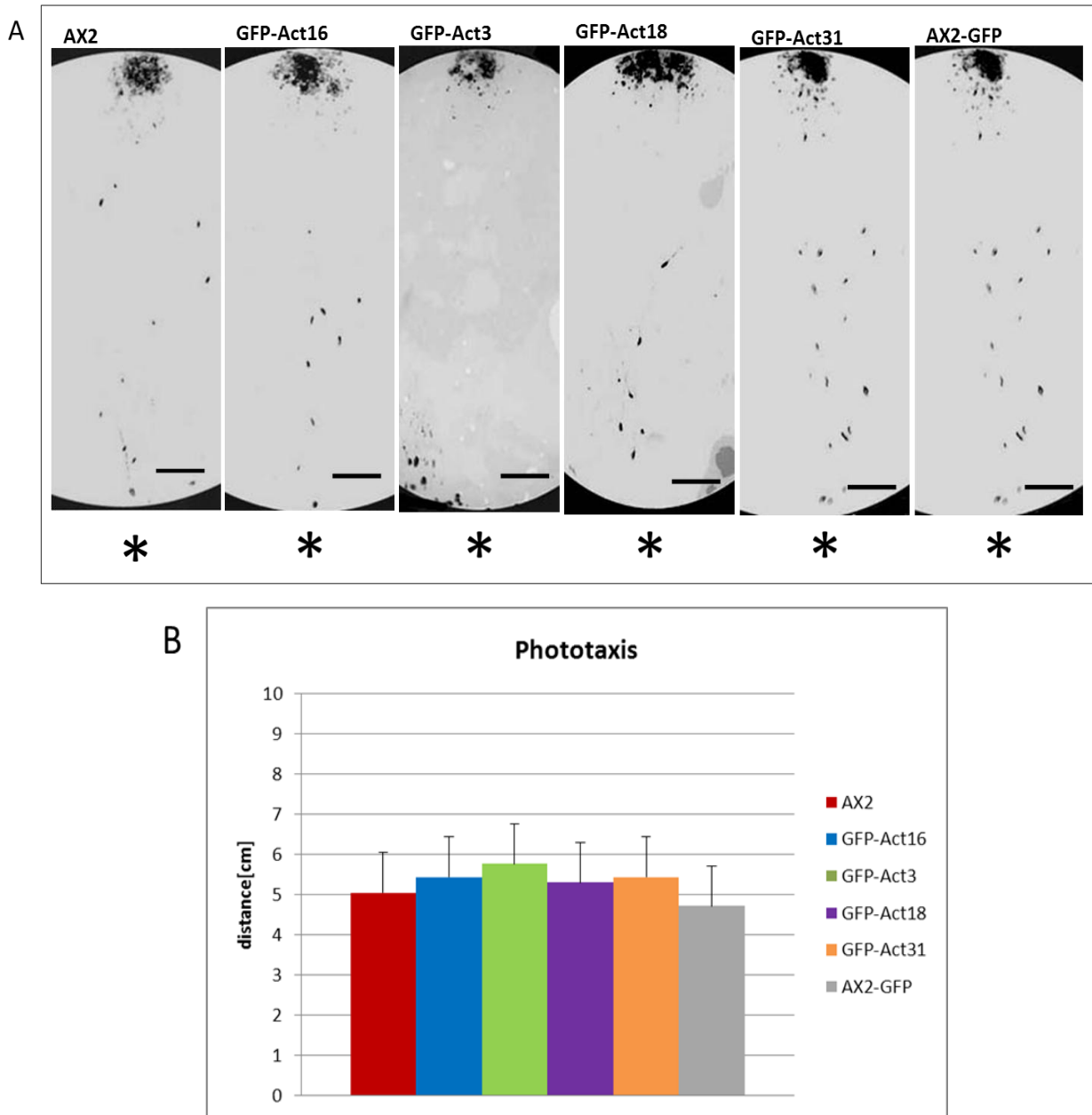
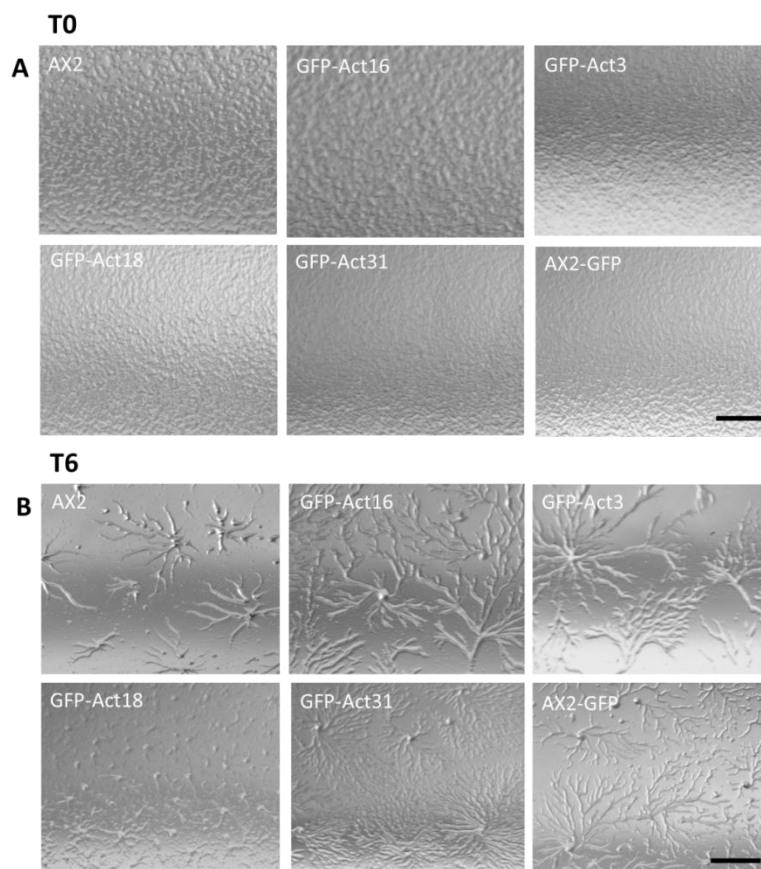


Figure 37: Phototaxis of GFP-actin variant overexpressing cells. *D. discoideum* cells were transferred onto water-agar plates and incubated in a dark colored box with a 2mm wide opening for the light source (*). After 48 hours the tracks of the migrated slugs could be visualized via amido black staining. Five independent experiments were performed. Scale bar 1cm. A) No alterations in distance and direction occurred in the GFP-actin overexpressors in comparison to the AX2 wild type strain. No GFP-induced effects could be observed. B) Measured distances did not show any significant differences between the tested cell lines.

To study the development of GFP-Act16, GFP-Act3, GFP-Act18 and GFP-Act31, cells from shaking cultures were adjusted to 5×10^6 cells/ml, washed and transferred onto phosphate-agar plates for starvation. The complete cell cycle was documented for 24 hours (one picture every ten minutes) by using the binocular microscope Stereo Discovery.V8.

In the beginning of the cell cycle all cell lines streamed towards an aggregation center, as it was expected for the first six hours of starvation (Chisholm & Firtel, 2004). When we compared the cohorts after six hours it became obvious that GFP-Act18 cells formed smaller clusters. As a consequence, the resulting fruiting bodies were smaller and more fruiting bodies per area occurred, in comparison to the other cell lines. Nonetheless, all studied cell lines completed the entire developmental cycle within 24 hours.



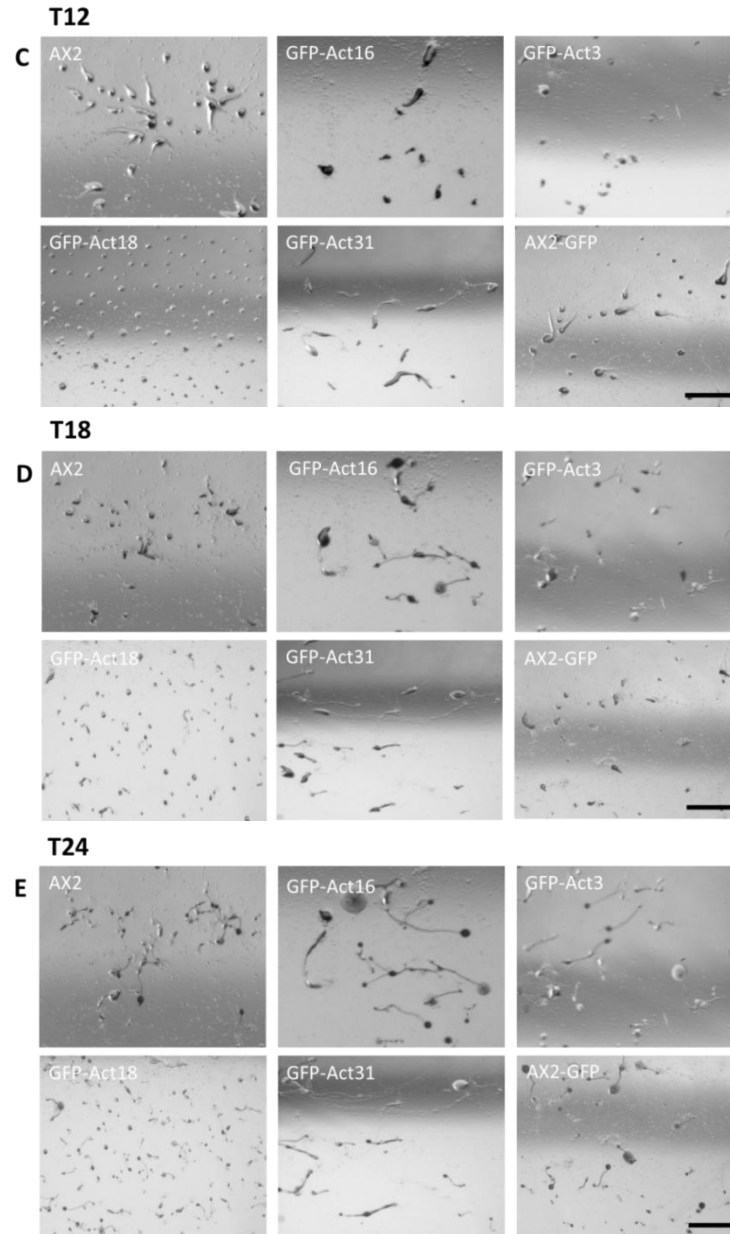


Figure 38: Studying the 24 hours life cycle of GFP-Act16, GFP-Act3, GFP-Act18 and GFP-Act31 overexpressing cells. 5×10^6 cells/ml of *D. discoideum* cells from shaking cultures were transferred onto phosphate-agar plates for starvation. Cell cycles were documented by using the Achromat S 0.63x FWS 115mm objective (bright field) at the Stereo Discovery.V8 binocular microscope. Pictures were taken every 10 minutes for 24 hours (T0=start, T6=6 hours, T12=12 hours, T18=18 hours, T24=24 hours). Three independent experiments were performed. Scale bar 1cm. A) Identical densities of vegetative cells were transferred onto the phosphate agar plates. B) The cells streamed towards an aggregation center. GFP-Act18 overexpressing cells formed smaller cohorts. C) AX2, GFP-Act16, GFP-Act3, GFP-Act31 and AX2-GFP cells developed migrating slugs, whereas GFP-Act18 cells did not exhibit typical slugs, but aggregates of cells. D) AX2, GFP-Act16, GFP-Act3, GFP-Act31 and AX2-GFP slugs culminated into fruiting bodies. GFP-Act18 cells developed slugs and fruiting bodies more slowly. E) AX2, GFP-Act16, GFP-Act3, GFP-Act31 and AX2-GFP showed fruiting bodies of comparable sizes and densities. GFP-Act18 cells formed smaller fruiting bodies with a higher density per area.

To address the issue, if the differences monitored in the developmental cycle could also be shown biochemically, a western blot analysis for contact site glycoprotein A (CsA) was performed. CsA is a cell adhesion protein of aggregating *D. discoideum* cells (Stadler et al. 1989). The protein (70kDa) is involved in intercellular adhesion that is characteristic for the aggregation of competent cells (Müller & Gerisch, 1978). AX2, GFP-Act16, GFP-Act3, GFP-Act18, GFP-Act31 and AX2-GFP cells from shaking cultures were adjusted to 5×10^6 cells/ml, washed and starved for six hours in nutrient deficient Soerensen buffer. By using the monoclonal CsA antibody 33-294-17, we detected the cell adhesion protein in all tested cell lines with comparable intensities. In GFP-Act18 overexpressing cells, the signal was slightly reduced. The corresponding Coomassie staining showed that equal quantities of cells were applied in the assay.

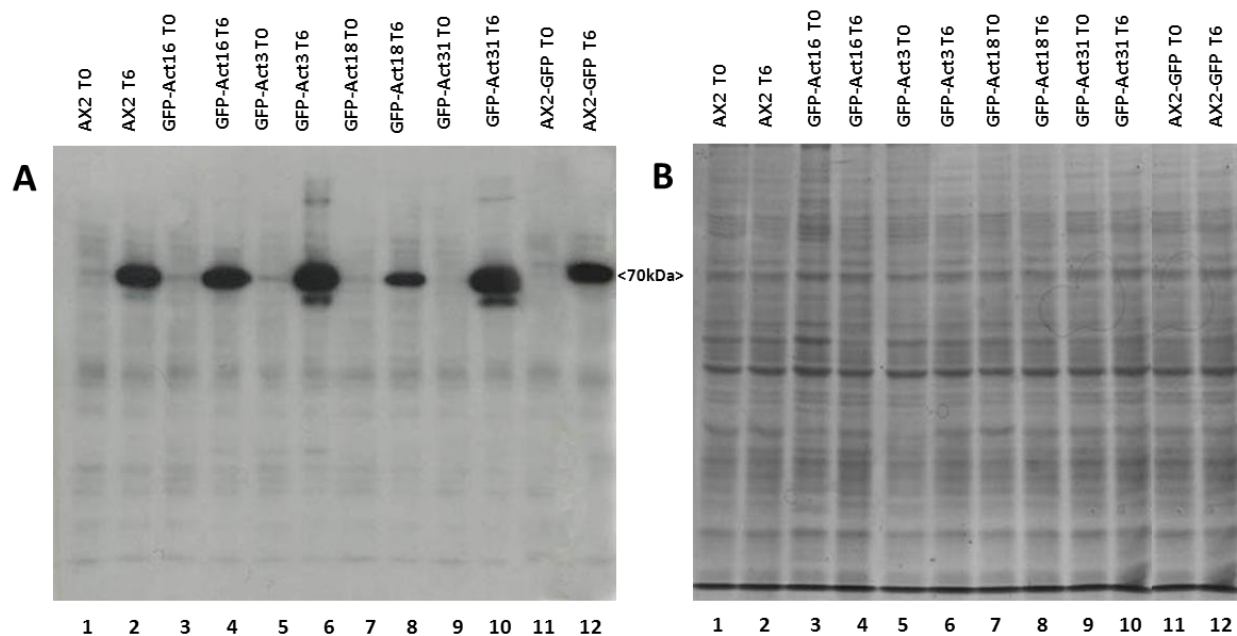


Figure 39: Expression of the contact site A glycoprotein in GFP-actin mutants after six hours starvation.

Western blot analysis using the monoclonal CsA antibody 33-294-1. We adjusted the cells from shaking cultures to 5×10^6 cells/ml and starved them in nutrient deficient Soerensen buffer for six hours. A) The CsA glycoprotein (70kDa) could be detected in all tested cell lines (5×10^6 cells/lane). The signal seemed to be reduced in the GFP-Act18 cells after six hours starvation. B) Coomassie staining demonstrated that comparable protein concentrations were applied in the assay (5×10^6 cells/lane).

3.3.8 The *in vivo* effects of GFP-Act16, GFP-Act3, GFP-Act18 and GFP-Act31

To analyze the functions of the actin isoforms Act16, Act3, Act18 and Act31 in *D. discoideum* cells, the actin variants were GFP-tagged and overexpressed. First of all, we studied cross-reactions with the actin antibodies Act-1 and 224-236-1. The colocalization with F-actin was determined visually via immunofluorescence images that could be approved biochemically by performing the Triton-insoluble cytoskeleton and differential spin down assay. We figured out the role of the GFP-actin variants in induced nuclear and cytoplasmic rods. Subsequently, classical cell biological assays were conducted, as we monitored the germination of spores and the growth rates in shaking cultures. The influence of GFP-Act16, GFP-Act3, GFP-Act18 and GFP-Act31 on phagocytosis was investigated at the LSM 510 confocal microscope, when we took images of the phagocytic cups. The uptake of TRITC-labeled yeast was measured and compared to the endocytosis of *K. aerogenes* bacteria. To characterize the phototaxis of GFP-actin mutants, we determined the covered distance and directionality of GFP-actin overexpressing slugs for 48 hours. These results were completed by developmental assays that recorded the cell cycles for 24 hours.

Table 2: Short summary of the effects of GFP-Act16, GFP-Act3, GFP-Act18 and GFP-Act31 that could be observed in the conducted cell biological assays.

| | GFP-Act16 | GFP-Act3 | GFP-Act18 | GFP-Act31 |
|--|-----------|----------|-----------|-----------|
| cross-reaction with actin antibody Act-1 | √ | – | – | – |
| cross-reaction with actin antibody 224-236-1 | √ | – | – | – |
| colocalization with F-actin | √ | √ | – | – |
| part of nuclear rods | √ | √ | – | – |
| forming 'cytoplasmic-rod-like' aggregates | √ | √ | – | – |
| reduced regermination | √ | √ | – | – |
| affected growth rate | √ | √ | √ | √ |
| localized in the phagocytic cup | √ | √ | – | – |
| phagocytosis of TRITC-labeled yeast reduced | √ | √ | √ | √ |
| phagocytosis of <i>K.aerogenes</i> affected | – | – | – | – |
| 24 hours cell cycle affected | – | – | √ | – |
| phototaxis affected | – | – | – | – |

4. Discussion

The major goal of this work was to analyze the functions of selected actin variants in actin dynamics in the model organism *D. discoideum* *in vitro* and *in vivo*. Although the compared actin variants show different levels of similarity, the basic structure of the proteins is strongly conserved. Analysis of the studied proteins revealed that Flag-Act16 and Flag-Act3 might be part of the actin cytoskeleton, due to their ability to promote actin polymerization. Together with rabbit actin both actin variants are able to enhance the formation of short actin filaments. In contrast, effects of Flag-Act18 and Flag-Act31 on actin polymerization could not be observed. *In vivo* characterization suggested that GFP-Act16 and GFP-Act3 are associated with F-actin. The overexpression might support the organization of the F-actin network during growth and could disturb the activation of the actin cytoskeleton in the process of regermination. The association of the GFP-actin variants with cellular organelles might impair the phagocytic capacity of *D. discoideum* cells. Furthermore, GFP-Act18 mutants exhibit a reduced expression of CsA, which seems to affect the cellular development.

4.1 Evolution of the actinome

Sequence analysis showed that the actinome of *D. discoideum* can be divided into three sections: actins, actin variants and ARPs (Joseph et al., 2008). Therefore it was a prerequisite for further *in vitro* and *in vivo* studies to perform thorough bioinformatic comparisons. The phylogenetic analysis involving all members of the *D. discoideum* actinome revealed the evolutionary relation of the different actins to each other in correlation to the bacterial ancestor MreB. The conventional actins, also named the Act8 group, are assumed to be the tip of a series of duplication events on chromosome 2, as 20% of all proteins in *D. discoideum* have arisen by a relatively recent duplication (Eichinger et al., 2005). When members of a protein family are clustered on one chromosome, the physical distance between family members often correlates strongly with their evolutionary divergence. Another example of putative tandem duplication events in *D. discoideum* is to be found on chromosome 5, where either single genes or blocks containing several consecutive genes are repeated. Prime examples for this event are Act3 (coordinates 2884652 to 2885782, Watson strand) and Act18 (coordinates 2886806 to 2887948, Watson strand), which share 88% identity on the protein level (dictybase.org; NCBI blastp). In contrast, Act31 is localized on chromosome 1 (coordinates 2844541 to 2845608, Watson strand) and does not belong to an actin gene cluster (Joseph et al., 2008). Like the ARPs, Act31 did not branch off from any *D. discoideum* actin and was not related to any other actin in this tree. It must have taken its separate track way before the evolution of *D. discoideum*. Therefore, Act31 is also called 'orphan ARP' (Joseph et al., 2008).

When we performed protein sequence alignments of the phosphate binding motif 1 (Ph1), the connecting motif 2 (C2), the phosphate motif 2 (Ph2), the adenosine motif (Ad), and the connecting motif 1 (C1) of human β -actin (P60709), rabbit muscle actin (P68135), Act16 (DDB_G0272248), Act3 (DDB_G0289487), Act18 (DDB_G0289489) and Act31 (DDB_G0269476), it became obvious that the sequence motifs were highly conserved within the analyzed actin variants. Although the amino acid sequences of the compared actins variants show different levels of similarity, the proclaimed ribbon models suggested that the general three-dimensional forms of the biopolymers human β -actin (P60709), rabbit muscle actin (P68135), Act16 (DDB_G027224), Act3 (DDB_G0289487), Act18 (DDB_G0289489) and Act31 (DDB_G0269476) are almost identical with Act8 (P07830) in the ADP-state. This suggests that the actins were apparently under huge pressure in terms of structure and function to keep this perfect molecular design.

The presence of the Act8 group in *D. discoideum* is still a mystery. There are 17 genes (Act8 group) which have distinct DNA coding sequences, they have complete promoters and terminators, they are all expressed, some of them are even developmentally regulated, but they code for identical proteins, the conventional actin (Joseph et al., 2008). One knows since years that on the protein level more than 95% of actin in *D. discoideum* represent conventional actin and the remaining 5% were just a careful calculation about the limits of detectability (Vandekerckhove & Weber, 1980). Why keeps *D. discoideum* an obviously luxurious actin cytoskeleton that is guaranteed up to 17 fold throughout evolution? It is certainly very difficult, if not presently impossibly, to analyze this via gene disruptions. Perhaps one should shed light on the presence of distinct mRNAs and putative RNA complexes at different times during development. In view of the overwhelming amount of conventional actin, the actin variants cover apparently only a tiny niche in the actinome of a *D. discoideum* cell.

4.2 The influence of Flag-tagged actin variants on *in vitro* actin dynamics

We used the baculoviral expression system of the Sf9 cells to express the Flag-tagged actin variants Flag-Act16, Flag-Act3, Flag-Act18 and Flag-Act31. The indigenous chaperones of insect cells are necessary for correct folding and oligomerization of recombinant proteins. Many chaperones are heat shock proteins (for example HSP40, HSP60 and HSP70) and are needed to prevent aggregation and misfolding during the folding of newly synthesized chains, to prevent nonproductive interactions with other cell components, to direct the assembly of larger proteins and multi-protein complexes, and to protect previously folded proteins from unfolding due to stress exposition (Fink, 1999). As the Sf9 expression system is eukaryotic, posttranslational modifications are possible and engineered polypeptides with many domains can be fold by sequential and cotranslational folding of their domains, whereas in prokaryotic cells proteins usually are folded posttranslationally, which could lead to an intramolecular misfolding (Netzer & Hartl, 1997).

In addition, differences between the *in vivo* and *in vitro* nature of the interactions of chaperones with actin have been reported (Frydman & Hartl, 1996).

Flag-Act16 and Flag-Act3 promoted the polymerization of rabbit actin as the lag-phase during the polymerization assay measured at the fluorometer was significantly shortened. This effect was intensified with increasing concentrations of Flag-Act16 and Flag-Act3. In contrast, Flag-Act18 and Flag-Act31 did not affect the polymerization of rabbit actin.

One can assume that the used Flag-Act16 and Flag-Act3 samples contained already short oligomers that could not be removed by the previous clear spin. These short aggregates could act as nucleators to overcome the energetically unfavorable lag-phase and induce the actin polymerization. The application of 100mM KCl to the actin polymerization assays abolished the observed effects. Higher salt concentrations *in vitro* seemed to lower the affinity of Flag-Act16 and Flag-Act3 for rabbit actin. The viscosity of an actin solution was gradually reduced when we incubated rabbit actin with increasing concentrations of Flag-Act16 and Flag-Act3 under polymerizing conditions. In contrast, the incubation of rabbit actin with different concentrations of Flag-Act18 and Flag-Act31 did not affect the viscosity of the polymerized samples. The disassembly of F-actin at the critical concentration of 0.1 μ M was not altered under the application of different concentrations of Flag-Act16, Flag-Act3, Flag-Act18 and Flag-Act31. A role as potential capping proteins could be therefore excluded for all tested actin variants. To sum up, the incubation of rabbit actin with increasing shares of Flag-Act16 and Flag-Act3 promoted the polymerization of actin on one hand and lowered the viscosity of the polymerized samples on the other hand. One possible explanation could be that Flag-Act16 and Flag-Act3 induce the formation of short actin filaments. The elongation of actin filaments would lead to an amplification of the fluorescence signal, whereas the viscosity of the actin solution would decrease, as the actin filaments are shorter under the influence of Flag-Act16 and Flag-Act3, than actin filaments of conventional actin with or without Flag-Act18 and Flag-Act31.

Cosedimentation studies showed that about 60% of Flag-Act16 and Flag-Act3 were associated with polymerized rabbit actin, whereas Flag-Act18 was not part of the sedimented actin fraction. About 40% of Flag-Act31 could be detected together with rabbit F-actin in the pellet. Without rabbit actin, Flag-Act16 and Flag-Act31 were not able to form stable actin filaments, not even under the application of stabilizing phalloidin. 40 % of Flag-Act3 and 30% of Flag-Act18 assembled under polymerizing conditions when we added phalloidin. These observations could be partly confirmed, when we checked the formation of TRITC-phalloidin stabilized Flag-actin filaments microscopically. Here, Flag-Act3 was the only Flag-actin variant which exhibited stable patches. When we checked the oligomerization of the Flag-tagged actin variants, Flag-Act16 was measurable in a range of 40-160kDa, meaning that a polymerization of Flag-Act16 up to a tetramer is indicated. Denatured aggregates of Flag-Act3 were detectable, whereas an ordered oligomerization of Flag-Act18 and Flag-Act31 could be excluded.

Images taken at the transmission electron microscope visualized that no polymerization of Flag-Act16, Flag-Act3, Flag-Act18 and Flag-Act31 was possible without the supplementation of freshly prepared rabbit actin. Aggregates of different sizes and shapes occurred, but the precise number of assembled G-actin monomers could not be identified. Incubation of freshly prepared rabbit actin with Flag-Act16, Flag-Act3, Flag-Act18 and Flag-Act31 under polymerizing conditions proved that the formation of filamentous rabbit actin was not disturbed by the Flag-actin variants.

Severin is a conserved, Ca^{2+} -dependent, well studied actin binding protein and therefore a good marker for the activity and integrity of actin itself. It consists of three domains which all have different actin binding activities: domain 1 binds to G-actin and caps actin filaments at the barbed end, domain 2 binds to the side of actin filaments, domain 3 binds to G-actin as well and thus can sever filaments in combination with domain 1, the three domains share very similar three dimensional structures (Andre et al., 1988; Eichinger & Schleicher, 1992; Schnuchel et al., 1995). The *D. discoideum* protein is a homolog of human gelsolin (Yin et al. 1990). Severin could be confirmed as a binding partner for all studied Flag-actin variants in immunoprecipitation analysis and mass spectrometry. The binding of severin to actin requires micromolar concentrations of Ca^{2+} which also induces its severing activity. Severin binds to other conformational species of actin like high speed supernatant actin (HSS-actin) or fluorescein isothiocyanate labeled actin as well (Giffard et al., 1984). Therefore, one can conclude that the expression of actin variants in Sf9 cells leads to at least partially folded recombinant proteins. This is not a trivial assumption because it is after decades of intensive experimental approaches still impossible to purify a fully recombinant actin.

Consequently, Flag-Act16 did not show all the characteristics of conventional actin, although Act16 is part of the Act8 group and exhibits the identical amino acid sequence as the other 17 actins. For the detection and purification of proteins in a wide variety of settings, affinity tags have become essential tools for the production of recombinant proteins. The Flag-tag structure has been optimized for compatibility with other proteins it is attached to, in that it is more hydrophilic than other common epitope tags and therefore less likely to denature or inactivate proteins to which it is appended (Joel et al., 2004). To determine potential influences of the Flag-tag concerning actin dynamics *in vitro*, we tried to remove the Flag-peptide (1012 Da). Freshly purified Flag-Act16 was incubated with a specific recombinant enterokinase (Novagen) that should bind to the amino acid sequence of the Flag-tag for subsequent removal. After numerous trials under different conditions we came to the conclusion that the removal of the N-terminal Flag-tag was not successful. The inability of a protease to cleave a fusion protein may have been caused by sterical hindrance. For example, the cleavage site may have been too close to the ordered structure in the target protein (Joel et al., 2004).

Results obtained using tagged proteins should be carefully controlled and interpreted with caution, taking into consideration changes to the proteins natural state upon addition of a fusion tag. Additionally, some proteins need to be activated by certain conditions or factors, therefore *in vitro* assays are just significant to a limited extend. Furthermore, the interactions of the actin variants in the cytoskeleton of *D. discoideum* are extremely specific and the use of rabbit muscle actin for the in vitro actin polymerization assays could be unfavorable. Hence, the *in vitro* assays should be repeated with purified conventional actin from *D. discoideum*.

4.3 GFP-Act16, GFP-Act3, GFP-Act18, GFP-Act31 and their cellular functions in *D. discoideum*

Generating the GFP-overexpressors was quite a challenge and expression levels of the GFP-tagged actin variants varied drastically. As Act16 belongs to the Act8 group, GFP-Act16 could be detected with both monoclonal actin antibodies Act-1 and 224-236-1. The respective epitopes are very short and specific for conventional actin (Simpson et al., 1984; Westphal et al., 1997). Consequently, also endogenous actin of the cell lysates could be detected easily. In contrast, GFP-Act3, GFP-Act18 and GFP-Act31 could not be recognized by using Act-1 and 224-236-1, although e.g. Act3 had only 11 different amino acids as compared to the conventional actin Act16. To draw a conclusion, the binding epitopes in the actin variants GFP-Act3, GFP-Act18 and GFP-Act31 might have been too divergent or possibly, the different amino acids in the actin variants caused an antigenic change at a topologically different site within the protein.

With regard to the actin cytoskeleton of *D. discoideum*, we analyzed the localization of GFP-Act16, GFP-Act3, GFP-Act18 and GFP-Act31 by conducting microscopical and biochemical approaches. GFP-Act16 and GFP-Act3 colocalized in immunofluorescence studies with endogenous actin in the cell cortex, and to some extent in the cytoplasm. Keeping in mind that Act18 and Act31 differ rather drastically from actins of the Act8 group, the predominant localization of GFP-Act18 and GFP-Act31 within the cytoplasm was after all not surprising. These observations were confirmed biochemically by performing the Triton insoluble cytoskeleton assay and the differential spin downs. Also in these approaches Act18 and Act31 behaved like soluble proteins without any interactions with conventional actin in and/or on microfilaments.

Interestingly, GFP-Act16 and GFP-Act3 were part of the DMSO induced nuclear actin rods, which is another clear indication that these actin variants are part of the actin cytoskeleton.

Also in this case one cannot unequivocally show whether these actin variants are intrinsic parts of the filaments, because binding along filaments would be sufficient to detect these proteins in nuclear rods. In principle, the designation 'actin rods' is somewhat misleading because other cytoskeletal proteins were identified in the rods as well, such as cofilin, Aip1 and coronin (Vandebrouck et al., 2010).

Many of these proteins are rather large (50kDa and more) and cannot simply pass the nuclear membrane through the pores without a specific transporting system. The GFP-tagged actin variants Act16 and Act3 have a size of about 70kDa and also need to be imported or exported by a transporter system (Gerace & Burke, 1988).

There exist also cytoplasmic rods and cofilin can be taken as a marker for both nuclear rods, and cytoplasmic rods as well. Cytoplasmic rods can be induced via inhibition of ATP synthesis by NaN_3 (Minamide et al., 2010). The tested GFP-actin variant overexpressors were not able to form typical needle-shaped cytoplasmic rods, but GFP-Act16 and GFP-Act3 seemed to be part of crescent-shaped aggregates within the cytoplasm.

During unfavorable environmental conditions, cells and spores of *D. discoideum* and their intracellular particles remain in an immobile state. After the germination of spores is induced, the actin synthesis is activated until actin constitutes 2-3% of the germinating spore (MacLeod et al., 1980). But spore cells retain only two of the actin mRNA sequences initially present in the pseudoplasmodium and it is still unclear whether these actin mRNA sequences encode identical actin proteins (Tsang et al., 1982). The viability of GFP-Act16 and GFP-Act3 spores was significantly reduced, whereas the regermination of GFP-Act18 and GFP-Act31 spores was just slightly decreased. The size and shape of the tested spores was not affected in our experiments. Expression of GFP-actin can affect the morphology and function of *D. discoideum* cells severely, possibly as a result of the large increase in the number of actin monomers that occurs during overexpression of GFP-actin fusion proteins (Aizawa et al., 1997). As a result the excess of GFP-actin variant monomers could sequester actin binding proteins that are not available anymore for the actin proteins that were synthesized constitutively during germination, which could result in a disturbed activation of the actin cytoskeleton. Furthermore, there remains the inevitable problem that whenever we label *in vivo*, we will always interfere with the biology of the labeled structures. As a central structure, the actin cytoskeleton interacts with numerous molecules that regulate its dynamics. Any marker will interfere with those biological processes by occupying the limited binding sites along the actin cytoskeleton. If those binding sites are saturated with markers, they will not bind the factors that regulate actin structure (Du & Ren, 2011).

In shaking culture experiments GFP-Act16 and GFP-Act3 overexpressors reproducibly showed a reduced lag-phase. In contrast, GFP-Act18 and GFP-Act31 mutants exhibited a delayed lag-phase in comparison to the AX2 or AX2-GFP cells. It is known that at reduced densities *D. discoideum* cells grow slower, as the cells have to adapt to their new environment, before the synthesis of actin increases and cell doubling starts (dictybase.org). As GFP-Act16 and GFP-Act3 seems to be part of the F-actin fraction in the cell cortex it could be involved in the F-actin organization during growth, which seems to promote the entry into the log-phase.

GFP-Act18 and GFP-Act31 are assumed to be part of the cytoplasm with no association to the F-actin network. A large increase in the number of GFP-Act18 and GFP-Act31 monomers might disturb the organization and regulation of the F-actin network. The cytokinesis of the GFP-actin variant overexpressors was not affected.

During phagocytosis of TRITC-labeled yeast cells GFP-Act16 and GFP-Act3 accumulated in the phagocytic cup, whereas GFP-Act18 and GFP-Act31 were spread homogeneously in the cytoplasm. As the phagocytic cup is a surface protuberance, the F-actin associated proteins GFP-Act16 and GFP-Act3 are concentrated in this structure, whereas the cytoplasmic proteins GFP-Act18 and GFP-Act31 are not enriched in the phagocytic cup. When we measured the uptake of TRITC-labeled yeast at the fluorometer, a reduced uptake down to 50% in comparison to the wild type was detected in all cell lines. For phagocytosis of large particles, the membrane of a phagocytic cup has to be remodeled extensively by the actin cytoskeleton and its stimulated polymerization (Lee et al., 2007; Griffin et al., 1975). Intracellular compartments like recycling endosomes or the ER are necessary for the contribution of extra membrane to completely surround the particles (Gagnon et al., 2002). As we proved in differential spin downs, the GFP-Act16, GFP-Act3, GFP-Act18 and GFP-Act31 are associated with cell organelles like vesicles, mitochondria and ER. The recruitment of extra membrane could be disturbed consequently, which influences the phagocytic capacity. Furthermore, the phagocytosis is also reduced in AX2-GFP cells, so that the interference of the GFP-tag with general biological processes has to be considered again.

The need for insertion of endomembrane to completely surround the particles also explains why large particles are more susceptible to inhibition than their smaller counterparts (Lee et al., 2007). For the uptake of smaller particles, the actin driven formation of membrane protrusions do not 'zipper up' along a ligand-coated particle, but instead they collapse to fuse with the plasma membrane (Connor & Schmid, 2003). Consequently, the phagocytosis of plated *K. aerogenes* was not influenced by the overexpression of the GFP-actin variants.

The overexpression of the GFP-actin variants had no significant effect on the covered distance or the directionality in the performed phototaxis assay. Imaging the cell cycle of the GFP-actin variants for 24 hours proved that GFP-Act18 overexpressing cells produced smaller fruiting bodies and a higher density of fruiting bodies per area, in comparison to the other tested cell lines. In parallel, the expression of the early aggregation marker CsA was delayed in the GFP-Act18 cells after six hours of starvation. It can be assumed that if the formation of stable intercellular contacts is restricted, due to a reduced expression of CsA, fewer cells aggregate to form a single fruiting body. As the 24 hours cell cycle assay was performed with the same number of vegetative cells for every cell line, a higher density of fruiting bodies per area occurred.

As the *in vivo* assays showed, GFP-actin overexpressors are useful to characterize possible functions of different actin variants in the model organism *D. discoideum*. Nonetheless, it has to be considered that besides the discussed fundamental limitations due to the GFP-labeling of actin, the overexpression of a specific protein often leads to inconsistencies concerning the observed phenotype. Overexpression can influence different organelles of the cell at the same time, though it is not uncommon for an overexpressing strain to display lethality or to show no phenotype at all. Consequently, to analyze the roles of Act16, Act3, Act18 and Act31 *in vivo* precisely, it might be worthwhile to create knock-out mutants for further characterization.

5. References

- Aizawa H, Sameshima M, Yahara I (1997): A green fluorescent protein-actin fusion protein dominantly inhibits cytokinesis, cell spreading and locomotion in *Dictyostelium*. *Cell Structure and Function* 22: 335-345.
- Andre E, Lottspeich F, Schleicher M, Noegel A (1988): Severin, gelsolin and villin share homologues sequence in regions presumed to contain F-actin severing domains. *The Journal of Biological Chemistry* 263: 722-727.
- Andre E, Brink M, Gerisch G, Isenberg G, Noegel A, Schleicher M, Segall JE, Wallraff E (1989): A *Dictyostelium* mutant deficient in severin, an F-actin fragmenting protein, shows normal motility and chemotaxis. *The Journal of Cell Biology* 108: 985-995.
- Alberts B, Johnson A, Lewis J, Raff M, Roberts K, Walter P (2004): *Molecular biology of the cell*. Wiley-VCH Verlag GmbH & Co KgaA; ISBN 3-527-30492-4.
- Bertholdt G, Stadler J, Bozzaro S, Fichtner B, Gerisch G (1985). Carbohydrate and other epitopes of the contact site A glycoprotein of *Dictyostelium discoideum* as characterized by monoclonal antibodies. *Cell Differentiation* 16: 187-202.
- Bork P, Sander C, Valencia A (1992): An ATPase domain common to prokaryotic cell cycle proteins, sugar kinases, actin and HSP70 heat shock proteins. *Proceedings of the National Academy of Sciences USA* 89: 7290-7294.
- Bozzaro S & Eichinger L (2011): The professional phagocyte *Dictyostelium discoideum* as a model host for bacterial pathogens. *Current Drug Targets* 12: 942–954.
- Carballido-Lopez R (2006): The bacterial actin-like cytoskeleton. *Microbiology and Molecular Biology Reviews* 70: 888-909.
- Carlier MF (1990): Actin polymerization and ATP hydrolysis. *Advances in Biophysics* 26: 51-73.
- Cleuren YT & Boonstra J (2012): Actin: structure, functions and disease. Consuelas VA, Minas DJ (eds), Chapter 2: 61-96. Nova Publishers.
- Chisholm RL & Firtel RA (2004): Insights into morphogenesis from a simple developmental system. *Nature Reviews Molecular Cell Biology* 5: 531-41.
- Conner SD & Schmid SL (2003): Regulated portals of entry into the cell. *Nature* 422: 37-44.
- Csete ME & Doyle JC (2002): Reverse engineering of biological complexity. *Science* 295: 1664-1669.

Dickinson RB, Southwick FS, Purich DL (2002): A direct-transfer polymerization model explains how the multiple profilin-binding sites in the actoclampin motor promote rapid actin-based motility. *Archives of Biochemistry and Biophysics* 406: 296-301.

Domazetovska A, Ilkovski B, Cooper ST, Ghoddusi M, Haderman EC, Minamide LS, Gunning PW, Bamburg JR, North KN (2007): Mechanisms underlying intranuclear rod formation. *Brain* 130: 3275-3284.

Doolittle RF & York AL (2002): Bacterial actins? An evolutionary perspective. *Bioessays* 24: 293-296.

Du F & Ren H (2010): Development and application of probes for labeling the actin cytoskeleton in living plant cells. *Protoplasma* 248: 239-250.

Eichinger L & Schleicher M (1992): Characterization of actin- and lipid-binding domains in severin, a Ca^{2+} -dependent F-actin fragmenting protein. *Biochemistry* 31: 4779-4787.

Eichinger L, Pachebat JA, Glöckner G, Rajandream MA, Sucgang R, Berriman M, Song J, Olsen R, Szafranski K, Xu Q, Tunggal B, Kummerfeld S, Madera M, Konfortov BA, Rivero F, Bankier AT, Lehmann R, Hamlin N, Davies R, Gaudet P, Fey P, Pilcher K, Chen G, Saunders D, Sodergren E, Davis P, Kerhornou A, Nie X, Hall N, Anjard C, Hemphill L, Bason N, Farbrother P, Desany B, Just E, Morio T, Rost R, Churcher C, Cooper J, Haydock S, van Driessche N, Cronin A, Goodhead I, Muzny D, Mourier T, Pain A, Lu M, Harper D, Lindsay R, Hauser H, James K, Quiles M, Madan Babu M, Saito T, Buchrieser C, Wardroper A, Felder M, Thangavelu M, Johnson D, Knights A, Louseged H, Mungall K, Oliver K, Price C, Quail MA, Urushihara H, Hernandez J, Rabbinowitsch E, Steffen D, Sanders M, Ma J, Kohara Y, Sharp S, Simmonds M, Spiegler S, Tivey A, Sugano S, White B, Walker D, Woodward J, Winckler T, Tanaka Y, Shaulsky G, Schleicher M, Weinstock G, Rosenthal A, Cox EC, Chisholm RL, Gibbs R, Loomis WF, Platzer M, Kay RR, Williams J, Dear PH, Noegel AA, Barrell B, Kuspa A. (2005): The genome of the social amoebae *Dictyostelium discoideum*. *Nature* 435: 43-57.

Fink A (1999): Chaperone-mediated protein folding. *Physiological reviews* 79: 425-442.

Frydman J & Hartl FU (1996): Principles of chaperone-assisted protein folding: differences between *in vitro* and *in vivo* mechanisms. *Science* 272: 1497-1502.

Gagnon E, Duclos S, Rondeau C, Chevet E, Cameron PH, Steele-Mortimer O, Paiement J, Bergeron JJM, Desjardins M (2002): Endoplasmic reticulum-mediated phagocytosis is a mechanism of entry into macrophages. *Cell* 110: 119-131.

-
- Gallinger J (2013): WH2 domains and actin variants as multifunctional organizers of the actin cytoskeleton. PhD Thesis, Ludwig-Maximilians-Universität München.
- Gerace L & Burke B (1988): Functional organization of the nuclear envelope. *Annual Review of Cell and Developmental Biology* 4: 335-74.
- Gerisch G (1962): Cell functions and cell function changes in the development of *Dictyostelium discoideum*. Inhibitors of aggregation, their effects on cellular contact formation and morphogenetic movements. *Experimental Cell Research* 26: 462-484.
- Giffard RG, Weeds AG, Spudich JA (1984): Ca^{2+} -dependent binding of severin to actin: a one-to-one complex is formed. *The Journal of Cell Biology* 98: 1796-1803.
- Griffin FM, Griffin JA, Leider JE, Silverstein SC (1975): Studies on the mechanism of phagocytosis. Requirements for circumferential attachment of particle-bound ligands to specific receptors on the macrophage plasma membrane. *The Journal of Experimental Medicine* 142: 1263-1282.
- Haus U, Hartmann H, Trommler P, Noegel A, Schleicher M (1991): F-actin capping by Cap32/34 requires heterodimeric conformation and can be inhibited by PIP2. *Biochemical and Biophysical Research Communications* 181: 833-839.
- Ihara M, Tanaka Y, Hashimoto Y, Yanagisawa K (1990): Partial purification and some properties of spore germination promotor(s) for *Dictyostelium discoideum* excreted by *Klebsiella aerogenes*. *Agricultural and Biological Chemistry* 54: 2619-2627.
- Israel L (2002): Domänenanalyse des Cyclase-assoziierten Proteins (CAP) und Charakterisierung von Filactin, einem neuartigen actinähnlichen Protein aus *Dictyostelium discoideum*. PhD Thesis, Ludwig-Maximilians-Universität München.
- Joel PB, Fagnant PM, Trybus KM (2004): Expression of a nonpolymerizable actin mutant in Sf9 cells. *Biochemistry* 43: 11554-11559.
- Joseph JM, Fey P, Ramalingam N, Liu XI, Rohlf M (2008): The actinome of *Dictyostelium discoideum* in comparison to actins and actin-related proteins from other organisms. *PlosOne* 3: e2654.
- Kaimaktchiev V, Goebel H, Laing N, Narus M, Weeks D, Nixon R (2006): Intracellular nemaline rod myopathy. *Muscle Nerve* 34: 369-372.

-
- Kim DJ, Kim SH, Kim SM, Bae JI, Ahnn JJ, Song WK (2007): F-actin binding region of SPIN90 C-terminus is essential for actin polymerization and lamellipodia formation. *Cell Communication and Adhesion* 14: 33-43.
- Kishi Y, Clements C, Mahadeo DC, Cotter DA, Sameshima M (1998): High levels of actin tyrosine phosphorylation: correlation with the dormant state of *Dictyostelium* spores. *Journal of Cell Science* 111: 2923-2932.
- Kouyama T & Mihashi K (1981): Fluorimetry study of N-(1-pyrenyl)iodoacetamide-labelled F-actin. Local structural change of actin protomer both on polymerization and on binding of heavy meromyosin. *European Journal of Biochemistry* 114: 33-38.
- Laemmli UK (1970): Cleavage of structural proteins during the assembly of the head of bacteriophage T4. *Nature* 227: 680-685.
- Lee WL, Mason D, Schreiber AD, Grinstein S (2007): Quantitative analysis of membrane remodeling at the phagocytic cup. *Molecular Biology of the Cell* 18: 2883-2892.
- Lodish H, Berk A, Zipursky SL, Matsudaira P, Baltimore D, Darnell J (2000): *Molecular cell biology* 4th edition New York: W. H. Freeman; 2000. ISBN-10: 0-7167-3136-3.
- MacLean-Fletcher SD & Pollard TS (1980): Viscometric analysis of the gelation of *Acanthamoeba* extracts and purification of two gelation factors. *Journal of Cell Biology* 85: 414-428.
- MacLeod C, Firtel RA, Papkoff J (1980): Regulation of actin gene expression during spore germination in *Dictyostelium discoideum*. *Developmental Biology* 76: 263-274.
- McRobbie SJ & Newell PC (1983): Changes in actin associated with the cytoskeleton following chemotactic stimulation of *Dictyostelium discoideum*. *Biochemical and Biophysical Research Communications* 115: 351-359.
- Minamide LS, Maiti S, Boyle JA, Davis RC, Coppinger JA, Bao Y, Huang TY, Yates J, Bockoch GM, Bamburg JR (2010): Isolation and characterization of cytoplasmic cofilin-actin rods. *The Journal of Biological Chemistry* 285: 5450-5460.
- Müller K & Gerisch G (1978): A specific glycoprotein as the target site of adhesion blocking fab in aggregating *Dictyostelium* cells. *Nature* 274: 445-449.
- Muller J, Oma Y, Vallar L, Friedrich E, Poch O, Winsor B (2005): Sequence and comparative genomic analysis of actin-related proteins. *Molecular Biology of the Cell* 16: 5736-5748.

-
- Mullins RD, Heuser JA, Pollard TD (1998): The interaction of ARP2/3 complex with actin: nucleation, high affinity pointed end capping, and formation of branching networks of filaments. *Proceedings of the National Academy of Sciences USA* 95: 6181-6186.
- Netzer WJ & Hartl FU (1997): Recombination of protein domains facilitated by co-translational folding in eukaryotes. *Nature* 388: 343-349.
- Nishida E, Iida K, Yonezawa N, Koyasu S, Yahara I, Sakai H (1987): Cofilin is a component of intranuclear and cytoplasmic actin rods induced in cultured cells. *Proceedings of the National Academy of Sciences USA* 84: 5262-5266.
- Noegel AA, Blau-Wasser R, Sultana H, Müller R, Israel L, Schleicher M, Patel H, Weijer CJ (2004): The cyclase-associated protein CAP as regulator of cell polarity and cAMP signaling in *Dictyostelium*. *Molecular Biology of the Cell* 15: 934-945.
- Osborn M & Weber K (1984): Actin paracrystal induction by forskolin and by db-cAMP in CHO cells. *Experimental Cell Research* 150: 408-418.
- O'Connell KL & Stults JT (1997): Identification of mouse liver proteins in two-dimensional electrophoresis gels by matrix-assisted laser desorption/ionization mass spectrometry of *in situ* enzymatic digests. *Electrophoresis* 18: 349-359.
- Poch O & Winsor B: Who's who among the *Saccharomyces cerevisiae* actin-related proteins? A classification and nomenclature proposal for a large family. *Yeast* 13: 1053-1058.
- Pollard TD & Weeds AG (1984): The rate constant for ATP hydrolysis by polymerized actin. *Federation of European Biochemical Societies Letters* 170: 94-98.
- Pollard TD & Borisy GG (2003): Cellular motility driven by assembly and disassembly of actin filaments. *Cell* 112: 453-465.
- Pollard TD & Earnshaw WD (2004): *Cell Biology*, First Edition, Saunders, ISBN 1-4160-2388-7.
- Qualmann B, Kessels MM, Kelly RB (2000): Molecular links between endocytosis and the actin cytoskeleton. *Journal of Cell Biology* 150: 111-116.
- Raper KB (1935): *Dictyostelium discoideum*, a new species of slime mold from decaying forest leaves. *Journal of Agricultural Research* 50: 135-148.
- Sameshima M, Kishi Y, Osumi M, Mahadeo D, Cotter DA (2000): Novel actin cytoskeleton: actin tubules. *Cell Structure and Function* 25: 291-295.

-
- Sept D & McCammon JA (2001): Thermodynamics and kinetics of actin filament nucleation. *Biophysical journal* 81: 667-674.
- Schleicher M & Jockusch B (2008): Actin: its cumbersome pilgrimage through cellular compartments. *Histochemistry and Cell Biology* 129: 695-704.
- Schnuchel A, Wiltschek R, Eichinger L, Schleicher M, Holak TA (1995): Structure of severin domain 2 in solution. *Journal of Molecular Biology* 247: 21-27.
- Schwalb M & Roth R (1979): Axenic growth and development of the cellular slime mould *Dictyostelium discoideum*. *Journal of General Microbiology* 60: 283-286.
- Schüler H, Karlsson R, Schutt CE, Lindberg U (2006): The connection between actin ATPase and polymerization. *Advances in Molecular and Cell Biology* 37: 49-61.
- Simpson PA, Spudich JA, Parham P (1984): Monoclonal antibodies prepared against *Dictyostelium* actin: characterization and interactions with actin. *The Journal of Cell Biology* 99: 287-295.
- Sparrow JC, Nowak KJ, Durling HJ, Beggs AH, Wallgreen-Pettersson C, Romero N, Nonaka I, Laing NG (2003): Muscle diseases caused by mutations in the skeletal muscle alpha-actin gene (ACTA1). *Neuromuscular Disorders* 13: 519-531.
- Spudich JA & Watt S (1971): The regulation of rabbit skeletal muscle contraction. Biochemical studies of the interaction of the tropomyosin-troponin complex with actin and the proteolytic fragments of myosin. *The Journal of Biological Chemistry* 246: 4866-4871.
- Stadler J, Keenan TW, Bauer G, Gerisch G (1989): The contact site A glycoprotein of *Dictyostelium discoideum* carries a phospholipid anchor of a novel type. *The European Molecular Biology Organization Journal* 8: 371-377.
- Tsang AS, Mahbubani H, Williams JG (1982): Cell-type specific actin mRNA populations in *Dictyostelium discoideum*. *Cell* 31: 375-382.
- Vandebrouck A, Domazetovska A, Mokbel N, Cooper ST, Ilkovski B, North KN (2010): *In vitro* analysis of rod composition and actin dynamics in inherited myopathies. *Journal of Neuropathology and Experimental Neurology* 69: 429-441.
- Vandekerckhove J & Weber K (1980): Vegetative *Dictyostelium* cells containing 17 actin genes express a single major actin. *Nature* 284: 475-477.

-
- Wachi M, Doi M, Tamaki S, Park S, Nakajima-Iijima S, Matsubishi M (1987): Mutant isolation and molecular cloning of mre genes, which determine cell shape, sensitivity to mecillinam, and the amount of penicillin-binding proteins in *Escherichia coli* cell. *Journal of Bacteriology* 169: 4935-4940.
- Westphal M, Jungbluth A, Heidecker M, Mühlbauer B, Heizer C, Schwartz JM, Marriott G, Gerisch G (1997): Microfilament dynamics during cell movement and chemotaxis monitored using a GFP-actin fusion protein. *Current Biology* 7: 176-183.
- Williams KL & Newell PC: A genetic study of aggregation in the cellular slime mould *Dictyostelium discoideum* using complementation analysis. *Genetics* 82: 287-307.
- Winder SJ & Ayscough KR (2005): Actin-binding proteins. *Journal of Cell Science* 118: 651-654.
- Witke W, Schleicher M, Noegel A (1992): Redundancy in the microfilament system: abnormal development of *Dictyostelium* cells lacking two F-actin cross-linking proteins. *Cell* 68: 53-62.
- Yin HL, Janmey PA, Schleicher M (1990): Severin is a gelsolin prototype. *Federation of European Biochemical Societies Letters* 264: 78-80.
- Zolghadr K, Rothbauer U, Leonhardt H (2008): The fluorescent two-hybrid (F2H) assay for direct analysis of protein-protein interactions in living cells. *Methods of Molecular Biology* 812: 275-282.

List of figures

Figure 1: Life cycle of *D. discoideum* (Chisholm & Firtel, 2004).

Figure 2: Sequential arrangement of the five actin motifs.

Figure 3: Typical G-actin structure in the ADP-state.

Figure 4: The process of actin polymerization (after Gallinger, 2013).

Figure 5: Actin binding proteins.

Figure 6: The actinome of *D. discoideum* (after Joseph et al., 2008).

Figure 7: Alignment of the actin variants Act3, Act18 and Act31 with conventional actin.

Figure 8: Phylogenetic tree of the *D. discoideum* actinome.

Figure 9: Motif logos of human β -actin, rabbit actin, and the *D. discoideum* actins Act16, Act3, Act18 and Act31.

Figure 10: Ribbon-models of human β -actin, rabbit actin, and the *D. discoideum* actins Act16, Act3, Act18 and Act31.

Figure 11: Flag-tagged actin variants purified from Sf9 cells.

Figure 12: Fluorometric analysis of the influence of Flag-Act16 and Flag-Act3 on actin polymerization.

Figure 13: Fluorometric analysis of the influence of Flag-Act18 and Flag-Act31 on actin polymerization.

Figure 14: Fluorometric analysis of the influence of 100mM KCl on actin polymerization.

Figure 15: Viscometric analysis of the effects of Flag-Act16 and Flag-Act3.

Figure 16: Viscometric analysis of Flag-Act18 and Flag-Act31 activities.

Figure 17: Fluorometric analysis of putative capping activities of Flag-Act16, Flag-Act3, Flag-Act18 and Flag-Act31.

Figure 18: Sedimentation assay to study if Flag-Act16, Flag-Act3, Flag-Act18 and Flag-Act31 bind to rabbit F-actin.

Figure 19: Sedimentation of Flag-Act16, Flag-Act3, Flag-Act18 and Flag-Act31 in the presence of phalloidin.

Figure 20: Potential filament formation of Flag-Act16, Flag-Act3, Flag-Act18 and Flag-Act31.

Figure 21: The oligomerization of Flag-Act16 was studied by using the AEKTA FPLC column.

Figure 22: Flag-Act16, Flag-Act3, Flag-Act18 and Flag-Act31 imaged using a transmission electron microscope.

Figure 23: Interaction studies of Flag-Act16, Flag-Act3, Flag-Act18 and Flag-Act31 with severin.

Figure 24: Different expression of GFP-actin variants in transformed *D. discoideum* cells.

Figure 25: The monoclonal GFP antibody K3-184-2 was used to quantify the expression of the GFP-actin variants.

Figure 26: The monoclonal actin antibody Act-1 was used to quantify the expression of endogenous actin and to study cross-reactions with Act16, Act3, Act18 and Act31.

Figure 27: The monoclonal actin antibody 224-263-1 was used to define its binding epitope and to study cross-reactions with Act16, Act3, Act18 and Act31.

Figure 28: Immunofluorescence images were taken to visualize the GFP-actin variants.

Figure 29: The Triton-insoluble cytoskeleton assay and the differential spin down were performed to localize the GFP-actin variants biochemically.

Figure 30: Nuclear rods in GFP-actin variant overexpressors.

Figure 31: Cytoplasmic rods in GFP-actin overexpressors.

Figure 32: Germination of spores in GFP-actin variant overexpressors.

Figure 33: Growth rates of GFP-actin mutants.

Figure 34: The localization of GFP-actin variants during phagocytosis.

Figure 35: Phagocytosis of TRITC-labeled yeast.

Figure 36: Phagocytosis of plated non-pathogenic *K. aerogenes*.

Figure 37: Phototaxis of GFP-actin variant overexpressing cells.

Figure 38: Studying the 24 hours life cycle of GFP-Act16, GFP-Act3, GFP-Act18 and GFP-Act31 overexpressing cells.

Figure 39: Expression of the contact site A glycoprotein in GFP-actin mutants after six hours starvation.

List of tables

Table 1: Actin variants analyzed in this study.

Table 2: Short summary of the effects of GFP-Act16, GFP-Act3, GFP-Act18 and GFP-Act31 that could be observed in our conducted cell biological assays.

Acknowledgements

First of all, I want to thank *Prof. Michael Schleicher* for giving me the opportunity to do the experimental part of this work in his laboratory, for the stimulating discussions and the enormous support during my PhD time.

Many thanks go to *Prof. Dr. Wolfgang Baumeister* and *Oana Mihalache* for sharing precious reagents and expert knowledge. I thank *Prof. Dr. Kiebler* and *Dr. Bastian Popper* for supporting me with valuable materials, operational experience, scientific discussions and inspiration.

I want to thank all lab members for creating such a great working atmosphere where I found all sorts of help, support, motivation and friends. It was a great pleasure to work with you! Many thanks go to *PD Dr. Annette Müller-Taubenberger* for sharing advice, valuable reagents, cell lines and vectors. I sincerely thank *Daniela Rieger* for her professional and personal advice. I thank *Dr. Hellen Ishikawa Ankerhold* for great teamwork, scientific discussions and methodical support. I am grateful for technical and moral help from *Gudrun Trommler*, *Thi-Heu Ho*, *Stefanie Lindholz* and *Maria Beer*.

Very special thanks go to my colleagues and bench mates *Dr. Julia & Christoph Gallinger*, *Heike Roth*, *Dr. Matthias Samereier* and *Süleyman Kösem* for sharing the same problems with me and for having so much fun together inside and outside of the lab.

I want to thank Christoph for comments on this thesis, his personal and professional coaching and unforgettable moments during my PhD time.

I would like to thank *Dr. Peter Batsios*, *Dr. Dennis Zimmermann*, *Dr. Marija Vukajlovic* and *Angela Oberhofer* for stimulating scientific discussions and sharing leisure time together.

Finally, very special thanks go to my friends and family, who always supported me in my plans. Thanks for all your love, trust and patience throughout all the years of my studies.